Coherent and chaotic phenomena in nuclear matter

By

Alexander Volya

A DISSERTATION

Submitted to
Michigan State University
in partial fulfillment of the requirements
for the Degree of

DOCTOR OF PHILOSOPHY

Department of Physics and Astronomy

2000

ABSTRACT

Coherent and chaotic phenomena in nuclear matter

By

Alexander Volya

The interplay between coherence and chaos is often the key question in understanding the behavior of a complex many-body system. The research work presented here considers several topics from nuclear physics aiming to pose questions and search for answers in this unconquered area of many-body physics.

The first topic in this dissertation deals with pairing, which is responsible for superconductivity and superfluidity in macroscopic Fermi systems. The smallness of the nuclear system reduces the sharpness of this phase transition, making macroscopic methods inadequate. This fact calls for the development of other theoretical techniques to which this research work is dedicated.

Chaos, intrinsic to many-body systems, often complicates many solutions to nuclear physics problems. Nevertheless, as it is shown in the second research project, chaotic features can play a regularizing role and can be successfully used for extrapolating results of large-scale numerical work.

Pionic fusion is the process of pion production in the coalescence of two nuclei extremely close to the energetic threshold so that the coherent action of all nucleons is required for it to take place. This amazing reaction has been experimentally observed. The suggested theoretical treatment of pionic fusion successfully describes experimental results and can be used for future predictions.

In-medium pions may be considerably softened, and the reduction of the effective pion energy may open an unusual channel of photon "decay" into a pion and another

photon inside the nucleus. The possibility of using this reaction as a tool for probing the pionic mode, was investigated in detail.

Higher energies and densities make pionic features more pronounced. Squeezed states forming a pion condensate can be created in a heavy ion collision or in reactions with cosmic rays. The dynamical evolution of parametrically excited quantum pion fields is studied in the last chapter. The possibility of the appearance of an oriented chiral condensate is discussed along with the resulting charge fluctuations and particle multiplicities.

ACKNOWLEDGMENTS

I owe my deepest gratitude to my advisor Scott Pratt, whose careful guidance, patience and cheerful humor made my advances possible. Vladimir Zelevinsky played an essential role in my graduate career. His help and supervision in my research work were indispensable. I highly appreciate help and professional advice from W. Bauer, B.A. Brown, P. Danielewicz, M. Dykman and W. Repko. I am indebted to V. F. Dmitriev, K. Haglin, M. Horoi for joining my efforts in research work presented in this dissertation. I must thank G. Bertsch, D.A. Brown, F.M.Izrailev, M. Mostovoy, D. Mulhall and A. Sakharuk for all the constructive and motivating discussions with regard to my work. The atmosphere in the theory group and at the entire National Superconducting Cyclotron Lab is very stimulating, it was a privilege to work there. Finally, I would like to thank Shari Conroy for guiding me through the mazes of random paperwork and administrative chores that come with graduate school.

CONTENTS

LIST OF FIGURES

Chapter 1

Introduction

The complexity and chaos of the real world are not surprising to the modern day physicist or mathematician. It's long been known that most systems in nature are not integrable, furthermore the mathematical description of complex reality often results in an unstable solution. The order and coherence that we see in life is puzzling. Paradoxes such as the infinite growth of entropy or time reversibility in physical laws but not in nature, and concepts such as the anthropic principle are just a few of the issues that arose from our agelong preoccupation with this puzzle. There is a hope that a valuable insight to this may be gained from our experience and knowledge of small systems. The existence of coherent many-body effects such as hydrodynamical flow, sound waves, oscillations, rotations and phase transitions on the background of a completely chaotic and nonintegrable dynamics is known and has been reasonably well studied in the past century. Nuclear physics is one of those exciting sciences that spans a large variety of topics. Nuclear science straddles all regimes in physics, low and high energy, classical and quantum, micro and macroscopic, regular and chaotic. It is an excellent arena to unify our understanding of these diverse limits, and to understand the coexistence of things coherent and chaotic. This thesis is written as a "book of stories", or chapters, each of which can be read separately and presents

separate research, but at the same time all these chapters are strongly related by the amazing fact that these "stories" describe the same nuclear systems.

For most intents and purposes at low energies nuclei can be described as protons and neutrons that interact with some phenomenologically inspired forces. These collections of quantum "balls", mesoscopic in size, are perfect to explore the question of how the macro world is related to the micro world? From the beginning of the 20th century there has been clear experimental evidence that nuclei are somewhat similar to classical liquid drops. The success of the Weizacker mass formula which incorporates simple concepts of the volume energy, surface tension and Coulomb energy of a charged drop is a clear indication of this. However, this provides only a rough picture. Real-life quantum many-body effects are readily apparent.

One of the most important forces that remains after all bulk interactions, such as the mean field, are taken into account is the short-range pairing interaction. In fact at low excitation energies, i.e., at low temperatures, the nucleons are all in a special collective quantum state, so that the whole nucleus is a superfluid liquid drop, to use the condensed matter physics terminology. The experimental evidence for this along with the current theoretical understanding of nuclear pairing is discussed in chapter 2. Pairing in mesoscopic systems is theoretically challenging. Exact solutions are already too complicated to find and macroscopic methods are too approximate because they rely on the assumption of an infinite system. The last section of chapter 2 describes a method for treating the general pairing problem in a finite Fermi-system without violating particle number conservation.

Chaos is yet another interesting aspect of nuclear systems. The question of how the regular and collective nuclear features appear and exist in dynamical chaos is still open. Chaoticity in the nucleus is also conceptually important because there is hope to trace the path of classical many-body chaos into the quantum world. Signatures

of quantum chaos such as found in the level spacing and level density distribution are widely discussed and debated in the scientific community. In the work that is presented in chapter 3, we study how to utilize chaotic features in order to help solve the nuclear many-body problem. In this study we suggest that low-lying eigenvalues of realistic quantum many-body hamiltonians, given, as in the nuclear shell model, by large matrices, can be calculated by first diagonalizing small truncated matrices then exponentially extrapolating results, instead of performing full diagonalization. We consider a number of realistic and model examples where numerical data confirms this conjecture. Based on these results we argue that exponential convergence in an appropriate basis may be a generic feature of complicated ("chaotic") systems where the wave functions are localized in this basis.

Studies of nuclear systems are burdened by more fundamental considerations such as the choice of appropriate degrees of freedom. At low energies experience shows that protons and neutrons give a satisfactory set of variables, nevertheless it is not always true. Extreme collectivity may be the key for gathering enough energy to excite other modes such as pions. Recently observed rare heavy ion fusion processes, where the entire available energy is carried away by a single pion, is an example of such an unusual coherent behavior in nuclear reactions. Theoretical understanding of this process is challenging, because the usual methods used for heavy ion reactions must incorporate the precise features of the nuclear structure. In chapter 4 we calculate these cross sections in the sudden overlap approximation, modeling the initial and final nuclei as moving harmonic oscillator potentials. This allows for a fully quantum-mechanical treatment, exact conservation of linear and angular momenta and fulfillment of the Pauli principle. Our results are in satisfactory agreement with data. We also discuss general trends of the process and the mass number dependence.

The constitution of nuclear matter and the interplay between different degrees of

freedom is an intriguing question. For pions, the lightest species of mesons, depending on their coupling to nuclear matter, theory would predict a variety of possible interesting phenomena such as pion condensates or the existence of super-dense nuclei. Pion behavior in nuclear matter, discussed in chapter 5, is an investigation of the possibility of measuring pion dispersion through anomalous coupling in the reaction $\gamma \rightarrow \gamma' \pi_0$. If the pionic mode is softened in nuclear matter due to mixing with the delta-hole state, in-medium photon "decay" into pions becomes possible. This reaction, if observed, would give a tremendous contribution to our knowledge about pions in nuclei. Unfortunately, our calculations suggest that competing backgrounds are larger than the pionic channel of interest. We were therefore only able to conclude that the use of such a measurement to explore the pion dispersion relation might be untenable, although difficult exclusive measurements might allow one to conquer the background.

With higher energy, the number of different particle species grows considerably and non-nucleonic contributions become important, if not dominant. Pions in heavy ion reactions become not only the essential part of the overall picture, but also provide important detection probes for looking at different states of matter. The formation of coherent pion states, if not possible in normal matter, is still predicted at high energies and densities or in quark-gluon-plasma. The final chapter considers the "oriented" chiral condensate. It may be produced in high energy nuclear collisions. Unlike disoriented chiral condensates, previously considered in the literature i.e. a coherent state of pions with a disoriented in isospin source, we consider a squeezed state of pions produced in the frame of an effective field theory with time- and space-dependent pion masses. We discuss the general properties of the solution, identifying condensate modes and determining the resulting pion distributions. The implementation of the dynamics in the form of a sudden perturbation allows us to look for exact solutions.

In the region of condensation, a dramatic increase in pion production and charge fluctuations is demonstrated, which can serve as experimental evidence for the formation of a chiral condensate.

The main material of the dissertation was published and presented at various meetings: chapter 3 [1, 2], chapter 4 [3, 4, 5], chapter 5 [6, 7, 8], and chapter 6 [9, 10, 11].

Chapter 2

Particle number conserving description of pairing

2.1 Experimental evidence of paired collective states in nuclei

Pairing correlations play an important role in nuclear structure, determining an essential contribution to binding energy, odd-even effects, single-particle occupancies, quasiparticle excitation spectrum, radiation and beta-decay probabilities, transfer reaction amplitudes, and low-lying collective modes and moments of inertia [12, 13, 14]. The revival of interest in pairing correlations is related to studies of nuclei far from stability and predictions of exotic pairing modes [15]. Metal clusters, organic molecules and Fullerenes give another example of finite Fermi systems with possibilities of pairing correlations of superconducting type [16].

The experimental evidence of a paired superconducting state in nuclei is very rich. Direct observation of the gap and its variations with the size of the nucleus could be obtained simply by plotting the average energy shift between odd and even nuclei,

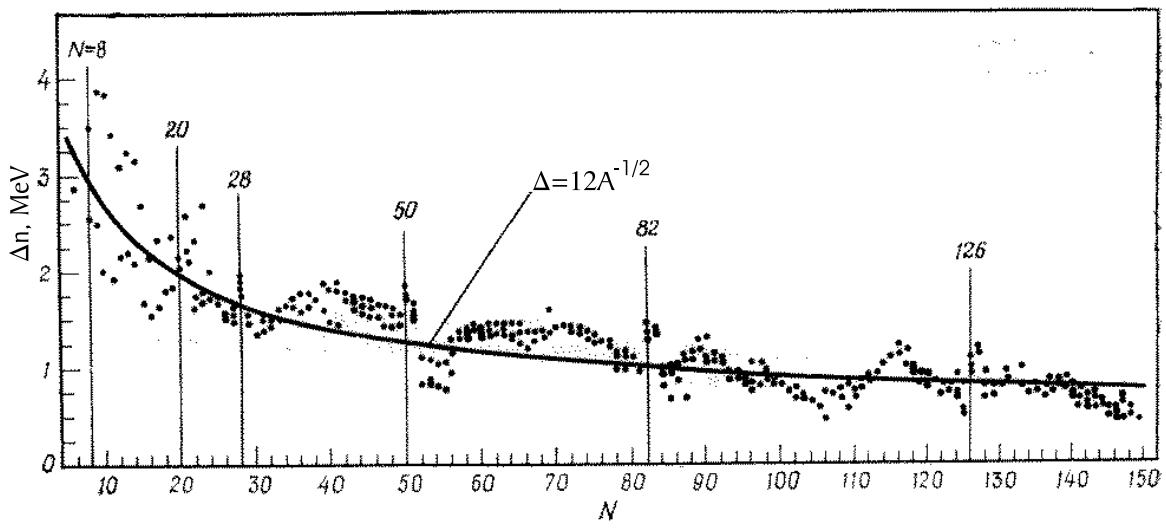

Figure 2.1: Observed fluctuation of the gap on the background of single particle energy.

which in the degenerate model approximation is directly related to the energy gap (see Eq.(2.11)). In Figure 2.1 obtained from [17] the energy difference of odd to even system is plotted, which is just a single particle excitation energy plus the gap. The behavior of the gap is easy to observe on the background of extra single particle energy.

Another interesting demonstration of nuclear superconductivity is in the rotational bands of nuclei. This example is important because of its analogy to the condensed matter systems where rotation causes the destruction of a superfluid state. Further, even some analogy could be drawn here to a magnetic field, or current flow as destructors of superconductivity. Every rotating system with angular momentum $\mathbf{J}$ possesses a term in its Hamiltonian $\hbar^2\mathbf{J}^2/2I$, where I is a moment of inertia defined by a particular configuration of contributing particles. If I is assumed to be constant the energy spectrum of rotation forms a band $\hbar^2 J(J+1)^2/2I$ with $J(J+1)$ being the eigenvalue of the operator $\mathbf{J}^2$. Observation of this rotational band allows experimental

determination of the moment of inertia. Theoretically, the moment of inertia could be obtained in the adiabatic approximation of a very slow rotation, cranking model, Ref.[18, 19, 20, 21]. The major idea of this model, in the context of superconducting states, is that particles form pairs not exactly of time conjugate orbits, i.e. spin projections of m and $-m$ for the same j, but with some extra coherent mixture of pairing between states with m and $-m \pm 1$ which creates a total rotational momentum along the axis perpendicular to the quantization axis. The amount of this mixing plays the perturbative role in this theory. The observed situation is again similar to the one in superfluids, where under the conditions of flow the pairing starts to shift from p and $-p$ paired momenta to $p + k/2$ and $-p + k/2$. The value of the moment of inertia in the cranking model is expressed by the following formula

$$I_x = \hbar^2 \sum_{\lambda,\lambda'} \frac{(u_\lambda v_{\lambda'} - u_{\lambda'} v_\lambda)^2}{E_\lambda + E_{\lambda'}} |(j_x)_{\lambda,\lambda'}|^2 \tag{2.1}$$

where the $(j_x)_{\lambda,\lambda'}$ is a momentum matrix element and the numerator forms a coherence factor, that could be substituted by occupation numbers using for example BCS results, see Eq.(2.14).

$$(u_\lambda v_{\lambda'} - u_{\lambda'} v_\lambda)^2 = n_\lambda(1 - n_{\lambda'}) + n_{\lambda'}(1 - n_\lambda)$$

With this formula one could show that for a perfect Fermi gas in a deformed container, the moment of inertia is close to that of a rigid body. Introduction of superconductivity causes the system to behave more fluid-like. The reason for this is that the energy denominator in (2.1) increases because of the influence of the gap; and because the coherence factor in the numerator is now a smaller number due to a smeared occupation in contrast to the steep jump in a Fermi gas. The decrease of strength due to the coherence factor could be observed in all single-particle nuclear transitions. This fluid-like behavior is characterized by a significant reduction of the moment of inertia. The systematics of the moment of inertia for different nuclei is presented in Fig

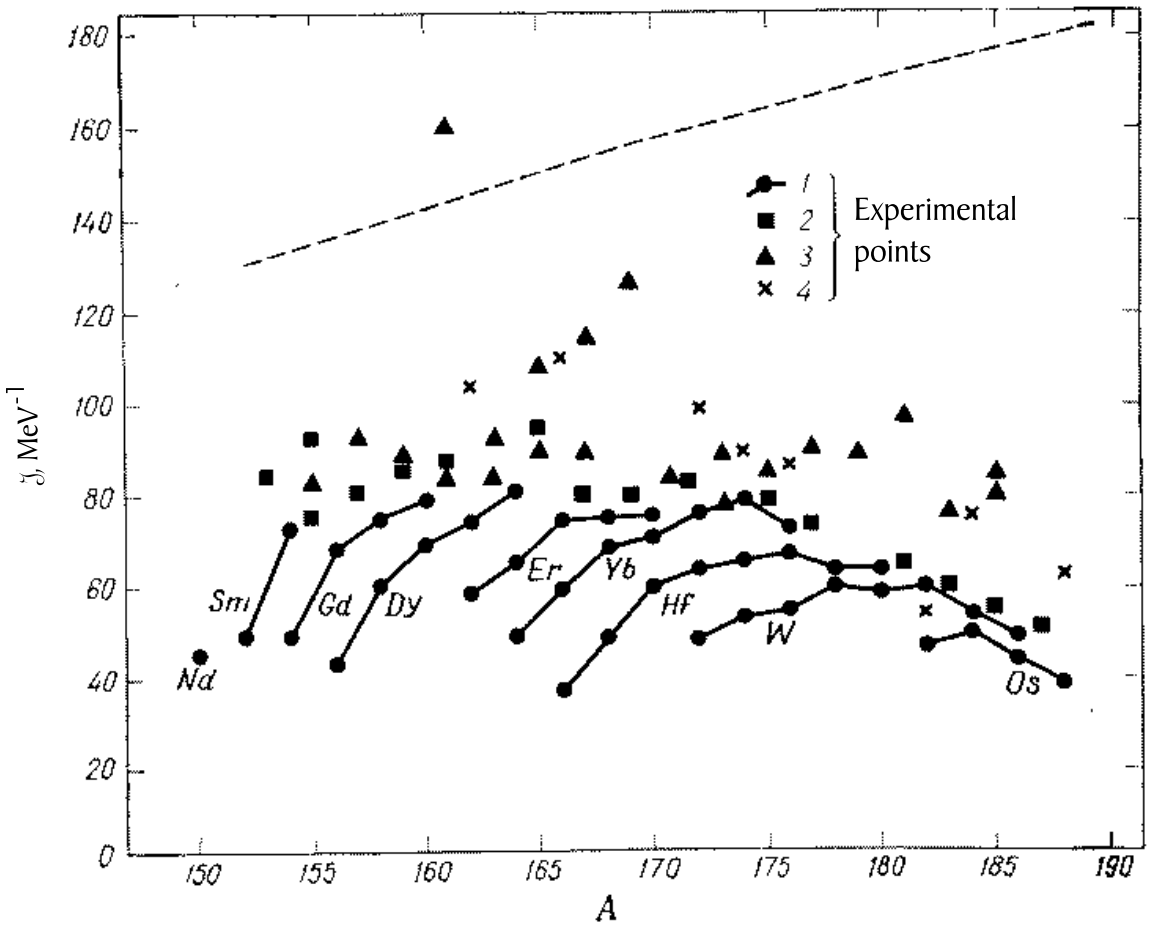

Figure 2.2: Moments of inertia for different nuclei are compared to the rigid body value (dashed line). 1: even-even systems, 2: odd Z, 3: odd N, 4: odd-odd systems.

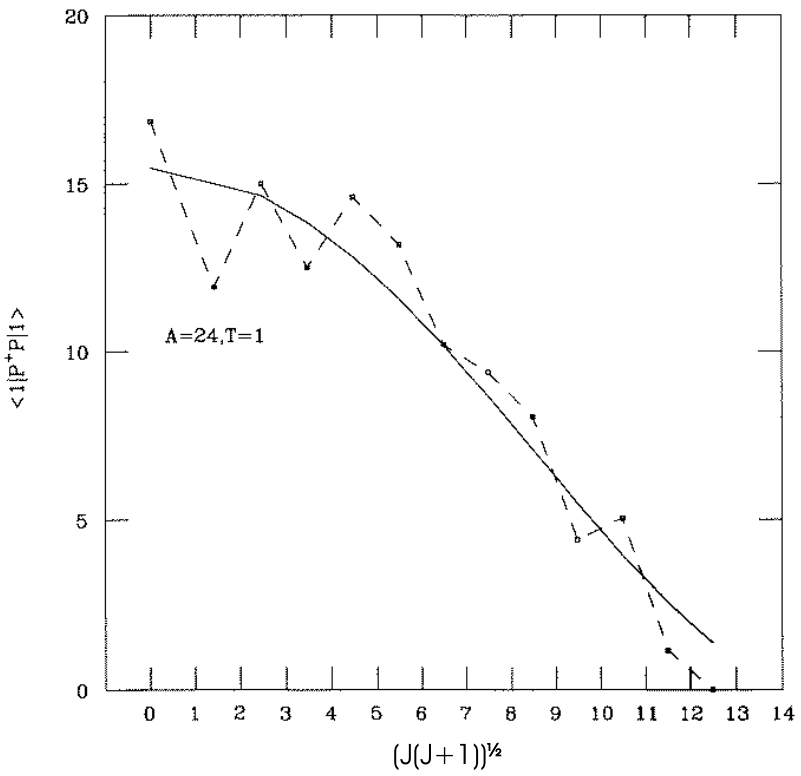

Figure 2.3: Gap size as a function of angular momentum, obtained with exact numerical calculations.

2.2 obtained from [17]. The rotational angular momentum is created by a coherent shift of all pairs. This shifting from the time conjugated pairing in turn leads to a reduction of the gap, which in nicely demonstrated [22] in Fig.2.3. This situation resembles a phase transition when it becomes energetically favorable to break pairs and re-align them for a higher total angular momentum.

2.2 Pairing forces

While the exact mechanisms of pairing remain ambiguous and widely discussed, their responsibility in creating microscopic effects is undeniable, as has been shown in the

previous section. Historically, pairing forces were first considered in nuclear physics, although their effects were not well understood until the development of BCS theory [24]. The mean field approximation used for the nuclear physics many-body problem leads to a shell model, a model where single particle energy levels could be grouped into shells that have a relatively high energy gap in between. It is not unreasonable to assume that some residual pairing interactions between nucleons still exist on the background of the mean field. Experiments show that the typical pairing force is a short range one, and that it is characterized by energies much smaller then a gap between shells. A good model of this force could be obtained by considering a δ-function as a pairing potential [25]

$$V = V_0\delta^3(\mathbf{x_1} - \mathbf{x_2}) = -\frac{V_0}{r_1 r_2}\delta(\mathbf{r_1} - \mathbf{r_2})\delta(\cos(\theta_1) - \cos(\theta_2))\delta(\phi_1 - \phi_2)\,.$$

The two-particle state can be written as the eigenstate of their total angular momentum

$$|J, M\rangle \quad = \sum_{m_1,m_2} C^{J,M}_{j_1,m_1,j_2,m_2}|j_1, m_1\rangle|j_2, m_2\rangle\,, \tag{2.2}$$

where

$$|j, m\rangle = [Y_l^m\chi_{1/2}]_{j,m}R_{n,l}(r)$$

is a single-particle wave function in the shell model. With some analytical work one could then compute the schematic level diagram of $< J, M|V|J, M >$, i.e. the energy of different paired states of a two particle system. This is shown in Figure 2.4 on the left. For comparison, the right side of the same picture displays experimentally determined energy levels of ^{210}Pb which has one pair of neutrons in the outer shell. Two identical particles in the same j-shell could couple only to an even total angular momentum.

This similarity between calculated and measured level structures, along with the fact that this picture is observed in basically all systems with one Cooper pair outside the main core, confirms that the residual nucleon-nucleon interaction is a short

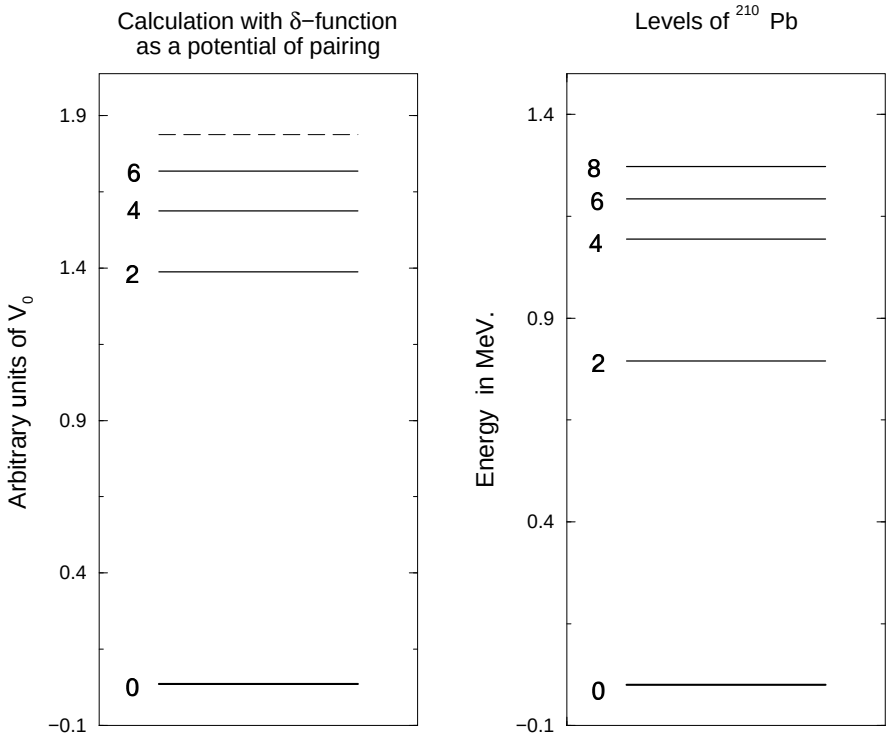

Figure 2.4: Paired states of a two particle system. Calculation with a δ-function-like potential is on the left; and on the right the energy levels of two neutrons in the $g_{9/2}$ shell in ^{210}Pb. Each level is labeled with the corresponding value of the angular momentum.

range one, for which a δ-function approximation was not a bad choice. Secondly, the effects of pairing could be only considered on unfilled shells in nuclei, just like in a Cooper model one electron pair is studied at the Fermi level. From the above considered case with a δ-function potential it is clear that most of the pairing strength would occur in those pairs that have the greatest single particle overlap, i.e., between time-conjugated states. This feature results in a preference of coupling to a total zero angular momentum, since $|j,m\rangle$ and $|j,-m\rangle$ are time conjugate, and leads to a considerably lower energy of the 0^+ ground state compared to the rest of the states. The analogy for an electron gas where coupling is strongest for the states with p and $-p$ could be emphasized at this point.

To complete this discussion about pairing forces in nuclei it would be interesting to mention the correlation length of time-conjugate pairs which, in contrast to usual superconductors, is normally much larger than the nuclear radius R.

$$\xi \approx \frac{\hbar p_{fermi}}{m\Delta} \approx RA^{1/3}$$

Another important parameter, correlation angle, is often introduced. Analytically it could be obtained with the use of $C^{0,0}_{l,m,l,-m} = \frac{(-1)^{l-m}}{\sqrt{2l+1}}$ and the formula for addition of Legendre polynomials applied to Eq. 2.2 which leads to:

$$|0,0>= R(r)(-1)^l \frac{\sqrt{2l+1}}{4\pi} P_l(\cos\theta_{12})$$

as a relative wave function. Its value is plotted in Fig. 2.5. Consequently, the above results lead to a correlation angle of the order $1/l$, which favors a short range interaction.

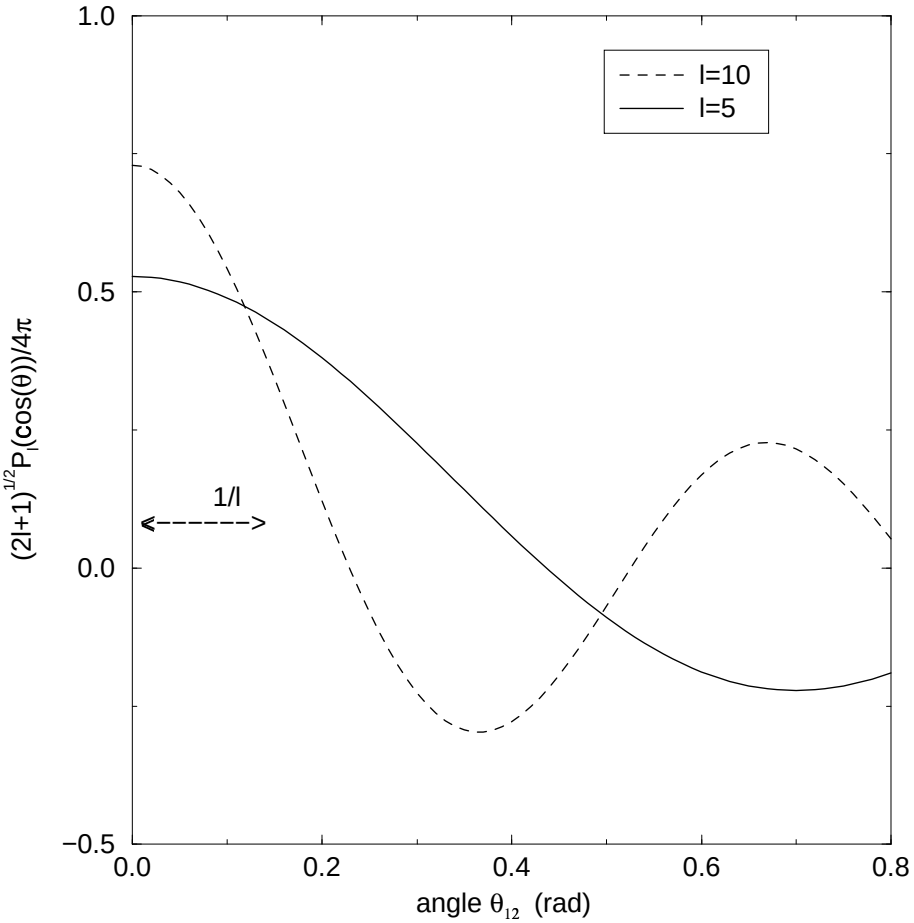

Figure 2.5: Plot of two particle angular correlation function $\frac{\sqrt{2l+1}}{4\pi}P_l(\cos(\theta_{12}))$ versus angle θ_{12}. The dashed line represents the case of $l = 10$ and the solid line corresponds to the $l = 5$ situation. It may be inferred from this that the correlation angle is approximately equal to $1/l$ (in radians).

2.3 Solutions to the pairing problem

2.3.1 Seniority scheme and degenerate model

The dramatic difference of a nuclear case as compared to a usual superconductor is that the number of states for the particles near the Fermi energy is quite limited. The shells in nuclei normally consist of several dozen states, thus despite the relative simplicity of the problem the finite size effects may not be ignored. The discussion presented here follows the works [23] and [26]. Let us denote the single-particle phase space volume as Ω, which for a given j is just $2j+1$. In this space we use an arbitrary basis, denoting by λ and $\tilde{\lambda}$ the two time-conjugate states. With this terminology a two particle paired state could obtained by a creation operator:

$$P^+ = \frac{1}{2}\sum_{\lambda}^{\Omega} a_\lambda^+ a_{\tilde{\lambda}}^+$$

where one should not forget an important property of time conjugated states: $a_{\tilde{\lambda}}^+ = -a_\lambda^+$, and that summation goes over all space Ω. Normalization of these states could be done as follows:

$$\langle 0|PP^+|0\rangle = \frac{1}{4}\sum_{\lambda\lambda'}^{\Omega}\langle 0|a_{\tilde{\lambda}}a_\lambda a_{\lambda'}^+ a_{\tilde{\lambda}'}^+|0\rangle = \frac{1}{4}\sum_{\lambda\lambda'}^{\Omega}(\delta_{\lambda\lambda'}\delta_{\tilde{\lambda}\tilde{\lambda}'} - \delta_{\lambda\tilde{\lambda}'}\delta_{\tilde{\lambda}\lambda'}) = \frac{\Omega}{2} \tag{2.3}$$

Conventionally the notation $|N;s\rangle$ is used for the systems with pairing, where N is the total number of particles and s is the seniority, a quantity that reflects the amount of unpaired particles. In this form one could write:

$$|2;0\rangle = \sqrt{\frac{2}{\Omega}}P^+|0\rangle$$

Operators P^+ and P are to be considered as creation and annihilation of a spin-zero quasiboson. The commutation relation for these bosons is easy to obtain in the form:

$$[P, P^+] = \frac{\Omega}{2} - N \tag{2.4}$$

where N is a number operator. It is seen from here that the right side of Eq.(2.4) almost remains constant, in which case it is just a bosonic commutation relation, with some small N-dependent correction. This correction reflects the fact that quasibosons are almost but not quite bosons, and there exists a residual effect of Pauli blocking due to their fermionic components. In general, normalization of states like $|N,0\rangle$ may be done using Eq.(2.4). As an example $N=2$ gives:

$$\langle 0|P^2(P^+)^2|0\rangle = \langle 0|P([P,P^+]+P^+P)P^+|0\rangle = 2\frac{\Omega}{2}(\frac{\Omega}{2}-1)$$

and for arbitrary N the normalization is:

$$\langle 0|P^N(P^+)^N|0\rangle = \frac{N!(\Omega/2)!}{((\Omega/2)-N)!} \tag{2.5}$$

Finally, since the physical interpretation of a seniority is in existence of several unpaired nucleons, the non zero value of s just reduces the effective phase-space by blocking the creation of possible pairs. For example, the state with $s=1$ would be normalized as:

$$\langle 0|a_\lambda P^N(P^+)^N a_\lambda^+|0\rangle = \frac{N!(\Omega/2-1)!}{((\Omega/2)-1-N)!} \tag{2.6}$$

which follows directly from Eq.(2.5) by substitution $\Omega \to \Omega - 2$ because one pair state is blocked. Caution should be applied here in that two unpaired particles in time conjugated states reduce the available space only by 2 and not by 4. The described above seniority scheme was first introduced by G. Racah and provides a convenient basis for dealing with pairing correlations.

The usual next step of discussion in this direction would be an introduction of BCS and solution of its equations for the approximate ground state. However, the literature often omits that there exists another exactly solvable model of superconductivity which is intriguing enough to be considered at this step. The degenerate model was apparently first studied in 1949 but was not completely understood before the arrival of other microscopic theories of superconductivity. The pairing energy is normally

either smaller or of the same order of magnitude than the separation between single particle levels on the last unfilled shell. In some cases, especially for spherical nuclei, there are large degeneracies and in certain occasions the approximation of the shell as one highly degenerate single-particle level could be adopted. In the case of the harmonic oscillator model with no spin-orbital coupling, the shells are in fact completely degenerate and therefore this model is precise. Thus the degenerate model makes a reasonable assumption that at some distance from the filled core there is one degenerate single particle level at the energy ϵ, filled with N fermions. Secondly, we assume that only particles in time-conjugate orbits interact, and that the energy of this interaction is substituted by some mean value: $-G$ for all pairs. Experimental data give the value of G at about $23/A$ MeV. The Hamiltonian for the degenerate model is :

$$H = \epsilon N - GP^+P$$

The diagonalization of this Hamiltonian could be nicely performed by introducing a quasispin. One may notice that operators P^+, P and N form a ladder structure:

$$[P, N] = 2P, \qquad [P^+, N] = -2P^+$$

so it is possible to define the quasispin $\mathbf{L}$ as:

$$L_- = P, \qquad L_+ = P^+, \qquad L_z = \frac{1}{2}(N - \frac{\Omega}{2}) \tag{2.7}$$

This new vector operator obeys $SU(2)$ symmetry and therefore has all the properties of the angular momentum operator. The integrals of motion are as usual: L_z which obviously is a constant that depends only on the number of particles and the volume of space Eq.(2.7), and the total square of quasispin:

$$\mathbf{L}^2 = L_z^2 - L_z + P^+P \tag{2.8}$$

The eigenvalues of $\mathbf{L}^2$ are $L(L+1)$ where L is an integer or half-integer. For a

particular nucleus the value of L_z is fixed but L could vary in the limits of :

$$\frac{1}{2}|N - \frac{\Omega}{2}| \leq L \leq \frac{\Omega}{4} \tag{2.9}$$

In this picture the state of the system could be determined by the eigenvalues of L_z and $\mathbf{L}^2$ and with the use of (2.8) the eigenstate energy of the Hamiltonian is:

$$E(L, N) = \epsilon N + \frac{G}{4}(N - \frac{\Omega}{2} - 2) - GL(L + 1) \tag{2.10}$$

It would be useful to replace the eigenvalue L with a more physical measure, namely seniority. From Eq.(2.9) it follows that L takes N values up to the maximum $\Omega/4$ that have increments of $1/2$, while at the same time seniority ranges from 0 to N and has steps of 1. At the maximum value L, the ground state of Eq.(2.10), the seniority is zero and one can therefore conclude that:

$$s = 2(\frac{\Omega}{4} - L)$$

and the energy spectrum becomes:

$$E(N, s) = \epsilon N + \frac{G}{4}(N - s)(N + s - \Omega - 2)$$

Examination of this solution shows that the energy gap, i.e. the energy to break one pair which corresponds to $s = 2$, is

$$2\Delta = G\frac{\Omega}{2}$$

and in general the excitation energy of the state with seniority s is:

$$E(N, s) - E(N, 0) = \frac{Gs}{4}(\Omega + 2 - s)$$

If the nucleus has an odd number of nucleons, then the lowest possible seniority is 1 which just reflects the fact that one particle is always unpaired. The energy required for the even system to add one particle is

$$E(N + 1, 1) - E(N, 0) = \epsilon + \frac{GN}{2}$$

This energy could be compared with the energy of two consecutive even systems:

$$E(N+2,0) - E(N,0) = 2\epsilon + GN + \frac{G\Omega}{2}$$

The resulting conclusion is that on average the ground state of the odd system is shifted by one half of the gap above the even system.

$$E(N+1) = \frac{E(N,0) + E(N+2,0)}{2} + \Delta \tag{2.11}$$

2.3.2 BCS theory in the case of nuclei

The general approach of BCS theory as applied to the nuclei is quite standard. The ground state of the system is generated from the Hamiltonian

$$H' = H - \mu N = \sum_{\lambda} \epsilon'_{\lambda}\, a^{+}_{\lambda} a_{\lambda} + \frac{1}{4} \sum_{\lambda\lambda'} G_{\lambda\lambda'} p^{+}_{\lambda} p_{\lambda'}, \quad \epsilon' = \epsilon - \mu \tag{2.12}$$

by minimizing the energy through the probing wave function:

$$|0\rangle = \Pi_{\lambda}(u_{\lambda} - v_{\lambda} p^{+}_{\lambda})|\text{vacuum}\rangle. \tag{2.13}$$

After this is done one arrives at the following solutions:

$$v^2_{\lambda} = n_{\lambda} = \frac{1}{2}(1 - \frac{\epsilon'_{\lambda}}{e_{\lambda}}), \quad u^2_{\lambda} = 1 - n_{\lambda} = \frac{1}{2}(1 + \frac{\epsilon'_{\lambda}}{e_{\lambda}}), \tag{2.14}$$

where $e_{\lambda} = \sqrt{(\epsilon_{\lambda} - \mu)^2 + \Delta^2_{\lambda}}$; Δ_{λ} and μ are the energy gap and chemical potential respectively. Two additional equations are important here:

$$\Delta_{\lambda} = \sum_{\lambda'} G_{\lambda\,\lambda'} \frac{\Delta_{\lambda'}}{4e_{\lambda}}, \quad N = \sum_{\lambda} n_{\lambda}\,. \tag{2.15}$$

The first is a usual gap equation, and the second one preserves the average number of particles in this grand canonical ensemble. As was mentioned before, the number of levels in a nuclear shell is quite small compared to the almost continuum spectrum in solid state physics. For this reason it is not always good to substitute the summation in the gap equation (2.15) by integration over some band around the Fermi surface.

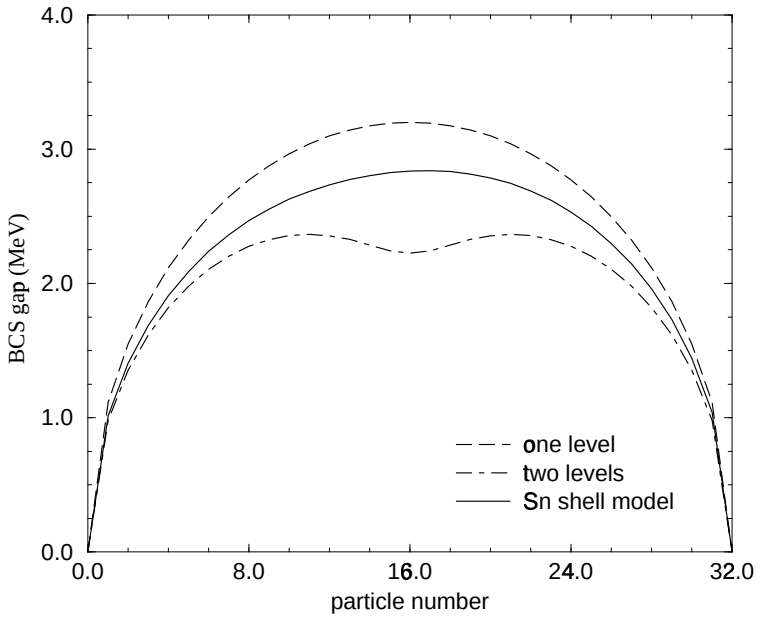

Figure 2.6: Plot of the gap as a function of particle number for three different level spectra. The pairing constant was chosen at $G = 0.4MeV$

A good practical example is the case of nuclei exclusively possessing a filling neutron shell from $N = 50$ to $N = 82$; assuming that the core of 50 neutrons is completely inert. Certainly the gap is zero for any magic nucleus, but for the systems with N between 50 and 82 the gap depends on the single-particle level spectrum. In Figure 2.6 the numerical calculations for the BCS gap are shown as a function of a particle number in the external shell for three different level spectra: of just one level (equivalent to the degenerate model), two equally-degenerate levels, and for the actual distribution of levels within the shell model of tin isotopes.

The BCS is accurate for large systems and becomes exact in the asymptotic limit [27]. The major drawback of the BCS is the violation of particle number conservation, which gives rise to deviations from the exact solutions for small systems. Since this treatment uses a grand canonical ensemble one can study the fluctuation of the particle number arising from particle non-conservation brought by the wave function

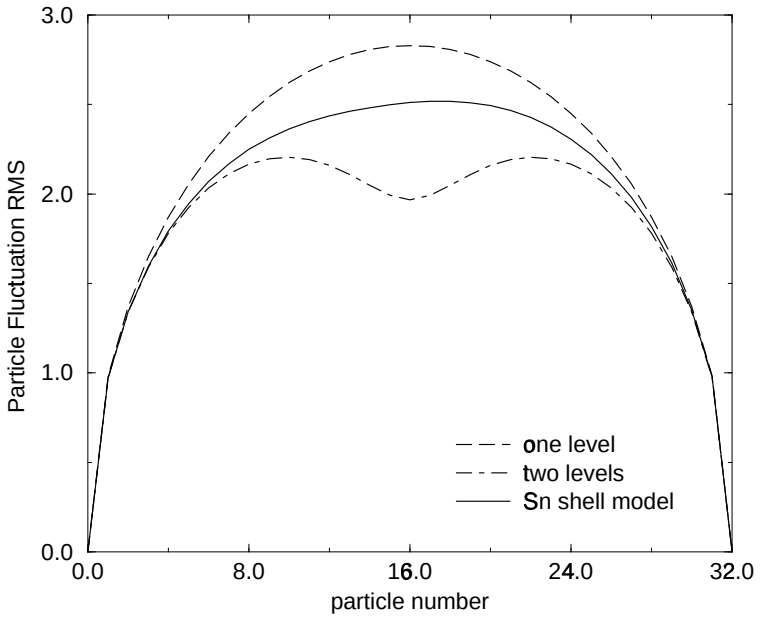

Figure 2.7: Particle number fluctuations for three different level spectra. The pair coupling constant is $G = 0.4 \quad (MeV)$

(2.13), given by the formula

$$\overline{\Delta N^2} = \sum_{\lambda} n_\lambda (1 - n_\lambda)$$

This result is plotted in the Fig. 2.7.

Various ideas were suggested to correct this deficiency, such as the direct particle-projection technique [28], number-projection mean-field methods [29, 30], statistical description [31], and taking into account the residual parts of the Hamiltonian in the random phase approximation [32]. These methods have found only a limited number of practical applications. For some approaches the obtained results did not manifest the desired accuracy, whereas for other methods the complications turn out to be almost on the same scale as for the exact solution by diagonalization.

2.3.3 Exact solutions

The Richardson method, described in the series of papers [33, 34, 35, 36], provides a formally exact way of solving the pairing Hamiltonian with a constant effective pairing force. This method reduces the large-scale diagonalization of a many-body Hamiltonian in truncated Hilbert space to a set of coupled equations of a dimension equal to the number of valence particles.

Recently, exact solutions have been approached by introducing sophisticated mathematical tools such as infinite-dimensional algebras [37]. Nevertheless the numerical complications currently limit the scope of applicability and the need for a good approximate theory still persists, especially because it can provide us with a convenient basis for calculating the effects of other parts of the residual interaction.

2.4 Particle conserving methods

The goal of our research in this area was to investigate a particle-conserving variational approximate solution that is formulated in the form of a recurrence relation in the number of particles N. For each step it is required to solve equations for only two variables, energy gap and chemical potential, as a function of the exact particle number, and thus even for large N the numerical procedure is quite fast. By making additional approximations this solution can be reduced to the BCS. The idea of the method goes back to older papers [38, 39] and to the work of S.T. Belyaev and V.G. Zelevinsky [40] where the set of exact operator equations of motion was formulated by introducing the gauge angle conjugate to the particle number as a collective variable. In discrete space the corresponding equations are of a recurrent type. This method was applied to the so-called pairing rotations (a systematic change of pair separation energy). Below we construct an algorithm for the solution of recurrence relations

derived from operator equations of motion with exact particle number conservation at each stage. In the well known degenerate model the solution coincides with the exact one. In a model with equidistant single-particle levels, our particle-conserving solution is compared to the exact solution and the BCS solution. A remarkable improvement over the BCS is observed. Finally, tin isotopes are considered as a realistic example.

Again, we consider the pairing Hamiltonian of the general form

$$H = \sum_{\nu} \epsilon_{\nu} a_{\nu}^{\dagger} a_{\nu} \; - \; \frac{1}{4} \sum_{\nu,\, \nu'} G_{\nu\nu'} \, p_{\nu}^{\dagger} p_{\nu'} \tag{2.16}$$

acting in the truncated fermion space ("shell") of $\Omega = \sum_{\nu} 1$ orbitals $|\nu)$. For simplicity we assume the time reversal invariant single-particle spectrum $\epsilon_{\nu} = \epsilon_{\tilde{\nu}}$ and real pair scattering matrix elements $G_{\nu\nu'} = G_{\nu'\nu}$; here and below the tilde denotes time conjugation of the single-particle orbitals $|\nu)$ defined with the phase condition $|\tilde{\tilde{\nu}}) = -|\nu)$ (the fermionic nature of particles is responsible for the negative sign). The pair annihilation and creation operators are introduced as

$$p_{\nu} = p_{\tilde{\nu}} = a_{\nu} a_{\tilde{\nu}} \, , \quad p_{\nu}^{\dagger} = p_{\tilde{\nu}}^{\dagger} = a_{\tilde{\nu}}^{\dagger} a_{\nu}^{\dagger} \, . \tag{2.17}$$

The amplitudes $G_{\nu\nu'}$ are invariant under the tilde operation; the factor $1/4$ in Eq. (2.16) is due to the fact that in complete summation both subscripts ν and ν' run over the entire single-particle space.

A sequence of ground states of systems with even particle number N and corresponding energies $E(N)$ will be denoted by $|N\rangle$. It is assumed that the spectra of adjacent odd nuclei start with energies $E(N \pm 1;\, \nu)$ of the states $|N \pm 1;\, \nu\rangle$ of seniority 1 containing one unpaired nucleon with quantum numbers ν. The single-particle transitions between the even and odd systems are described by the amplitudes

$$v_{\nu}(N) = \langle N-1;\, \tilde{\nu} | a_{\nu} | N \rangle, \quad u_{\nu}(N) = \langle N+1;\, \nu | a_{\nu}^{\dagger} | N \rangle \, , \tag{2.18}$$

where again N is even. We also define the energy gaps $\Delta_\nu(N) = \Delta_{\tilde{\nu}}(N)$ as a function of particle number through the pair-transfer matrix elements between the even ground states,

$$\Delta_\nu(N) = \frac{1}{2}\,\langle N-2|\sum_{\nu'} G_{\nu\nu'}\, p_{\nu'}|N\rangle\,. \tag{2.19}$$

The exact operator equations of motion for the single-particle operators a_ν and $a_\nu^\dagger$ are

$$[a_\nu,\, H] = \epsilon_\nu a_\nu \,+\, \frac{1}{2}\sum_{\nu'} G_{\nu\nu'}\, a_{\tilde{\nu}}^\dagger\, p_{\nu'}\,, \tag{2.20}$$

$$[a_\nu^\dagger,\, H] = -\epsilon_\nu a_\nu^\dagger \,-\, \frac{1}{2}\sum_{\nu'} G_{\nu\nu'}\, p_{\nu'}^\dagger\, a_{\tilde{\nu}} = -(\epsilon_\nu - G_{\nu\nu})\, a_\nu^\dagger \,-\, \frac{1}{2}\sum_{\nu'} G_{\nu\nu'}\, a_{\tilde{\nu}}\, p_{\nu'}^\dagger\,. \tag{2.21}$$

Instead of introducing the condensate of the pairs with an uncertain particle number, we make a physically similar splitting of nonlinear terms in the equations of motion that does not violate the conservation law and keeps the N-dependence intact. Our variational approximation can be formulated as a truncation of the full Hilbert space to that spanned by the seniority 0 even ground states and seniority 1 states in odd-N nuclei. Thus, the step beyond BCS is only in that particle number is treated exactly. The matrix elements in the equations of motion are disentangled by neglecting the seniority 2 admixtures in even nuclei. For example,

$$\langle N-1;\nu|\frac{1}{2}\sum_{\nu'} G_{\nu\nu'}\, a_{\tilde{\nu}}^\dagger\, p_{\nu'}|N\rangle \approx$$

$$\langle N-1;\nu|a_{\tilde{\nu}}^\dagger|N-2\rangle\langle N-2|\frac{1}{2}\sum_{\nu'} G_{\nu\nu'}\; p_{\nu'}|N\rangle = \Delta_\nu(N)\, u_{\tilde{\nu}}(N-2)\,, \tag{2.22}$$

In this approximation the equations of motion (2.20) and (2.21) give

$$[E(N) - E(N-1;\,\nu) - \epsilon_\nu]\, v_\nu(N) \,-\, \Delta_\nu(N)\, u_{\tilde{\nu}}(N-2) = 0\,, \tag{2.23}$$

$$[E(N-2) - E(N-1;\,\nu) + \epsilon_\nu - G_{\nu\nu}]\, u_\nu(N-2) \,-\, \Delta_\nu^*(N)\, v_{\tilde{\nu}}(N) = 0\,. \tag{2.24}$$

It is convenient to introduce, instead of $E(N-2)$ and $E(N-1;\,\nu)$, the chemical potential $\mu(N)$ and quasiparticle energies $e_\nu(N)$ according to

$$E(N-2) = E(N) - 2\mu(N), \quad E(N-1;\,\nu) = E(N) - \mu(N) + e_\nu(N) - \frac{G_{\nu,\,\nu}}{2}\,, \tag{2.25}$$

Then we obtain the following simple set of equations:

$$[e_\nu(N) + \xi_\nu(N)]v_\nu(N) + \Delta_\nu(N)u_{\tilde{\nu}}(N-2) = 0\,, \tag{2.26}$$

$$\Delta^*_\nu(N)v_{\tilde{\nu}}(N) + [e_\nu(N) - \xi_\nu(N)]u_\nu(N-2) = 0\,, \tag{2.27}$$

where N is even, and we use the modified single-particle energies

$$\xi_\nu(N) = \epsilon_\nu - \frac{G_{\nu\nu}}{2} - \mu(N)\,. \tag{2.28}$$

With time reversal invariance, we have $u_{\tilde{\nu}} = u_\nu$ and $v_{\tilde{\nu}} = v_\nu$. The nontrivial solution of the set (2.26, 2.27) determines the BCS-like spectrum of quasiparticle excitations for each particle number N,

$$e_\nu = \sqrt{\xi^2_\nu(N) + |\Delta_\nu(N)|^2}\,. \tag{2.29}$$

On the same level of our variational approximation

$$\langle N|\sum_\nu a^\dagger_\nu a_\nu|N\rangle \equiv N = \sum_\nu |v_\nu(N)|^2\,, \tag{2.30}$$

and the fermionic anticommutation relations $[a_\nu, a^\dagger_\nu]_+ = 1$ result in

$$|v_\nu(N)|^2 + |u_\nu(N)|^2 = 1\,. \tag{2.31}$$

Finally Eqs. (2.27, 2.31) result in the recursion relation connecting adjacent even nuclei,

$$|v_\nu(N-2)|^2 = 1 - \frac{|\Delta_\nu(N)|^2}{[e_\nu(N) - \xi_\nu(N)]^2}\,|v_\nu(N)|^2\,. \tag{2.32}$$

Taking into account Eq. (2.30) and summing over all Ω single-particle states, we obtain

$$\Omega - N + 2 = \sum_\nu \frac{|\Delta_\nu(N)|^2}{[e_\nu(N) - \xi_\nu(N)]^2}\,|v_\nu(N)|^2\,. \tag{2.33}$$

The gap defined in Eq. (2.19) is subject to the self-consistency condition

$$\Delta_\nu(N) = -\frac{1}{2}\sum_{\nu'} G_{\nu\nu'}v_{\tilde{\nu}'}(N)u^*_{\nu'}(N-2) = \frac{1}{2}\sum_{\nu'} G_{\nu\nu'}\frac{\Delta_{\nu'}(N)\;|v_{\nu'}(N)|^2}{e_{\nu'}(N) - \xi_{\nu'}(N)}\,. \tag{2.34}$$

The pairing problem formulated in this manner allows a recursive solution in both directions, starting from an empty shell or from a completely filled shell. For example, going down from the completely filled shell with the occupation numbers $|v_\nu(\Omega)|^2 = 1$ by solving Eqs. (2.33) and (2.15), the values of $\mu(\Omega)$ and $\Delta_\nu(\Omega)$ can be found which in turn determine the next set of $|v_\nu(\Omega-2)|^2$ via Eq. (2.32). Similar equations in terms of the amplitudes $u_\nu(N)$ are suitable for the recursive solution climbing up from an empty shell. The particle-hole symmetry with respect to the interchange of u and v with the additional change of sign of the chemical potential and the appropriate level reordering states the equivalence of both directions in the recursive solution and provides a good check. Below we give a number of examples.

1. *The BCS limit* means that the N-dependence is ignored in Eq. (2.32) assuming that $|v_\nu(N)|^2 = |v_\nu(N-2)|^2 = \left|v_\nu(\bar{N})\right|^2$ and similarly for u_ν. This allows us to solve the equations in a standard way,

$$\left|v_\nu(\bar{N})\right|^2 = \frac{1}{2}\left(1 - \frac{\xi_\nu(N)}{e_\nu(N)}\right), \quad \left|u_\nu(\bar{N})\right|^2 = \frac{1}{2}\left(1 + \frac{\xi_\nu(N)}{e_\nu(N)}\right). \tag{2.35}$$

There is some ambiguity in the choice of the argument $\bar{N}$ in equations (2.35). Usually $\bar{N} = N$ is assumed, which makes a better agreement for the less than half-filled shell, but with the assumptions made there it should be no difference if $\bar{N} = N - 2$. The presence of a difference is related to the particle-number nonconservation in BCS theory. Generally, in the region of good applicability of BCS, $N \gg 1$, the exact choice of the argument $\bar{N}$ has no effect. It turns out that BCS works best with the interpolating choice of $\bar{N} = N - 1$. This will be confirmed below for particular cases. Eqs. (2.15) and (2.35) lead to a conventional form of the BCS gap equation, that agrees with Eq. 2.15 from the previous section

$$\Delta_\nu = \frac{1}{2}\sum_{\nu'} G_{\nu\nu'}\frac{\Delta_{\nu'}}{2e_{\nu'}}. \tag{2.36}$$

2. *The degenerate model* [41] assumes that all single-particle levels have the same energy ϵ, and the coupling strength $G_{\nu\nu'} = G$ is independent of ν, ν'. As it was

discussed before this model is exactly solvable in terms of the pseudospin SU(2) group and thus provides a good testing ground. We assume that $\epsilon = G/2$ and therefore $\xi_\nu(N) = -\mu(N)$ according to (2.28). This makes the summation in Eqs. (2.33) and (2.15) trivial:

$$\Omega - N + 2 = \frac{|\Delta(N)|^2}{(e(N) - \xi(N))^2} N \,, \tag{2.37}$$

$$1 = \frac{G}{2} \frac{N}{e(N) - \xi(N)} \,. \tag{2.38}$$

These equations can be easily solved to give

$$\Delta(N) = \frac{G}{2} \sqrt{N(\Omega - N + 2)} \,, \tag{2.39}$$

$$\mu(N) = \frac{G}{2} \left(N - \frac{\Omega}{2} - 1 \right) \,, \tag{2.40}$$

and the occupancies are independent of ν,

$$|v(N)|^2 = \frac{N}{\Omega} \,, \quad |u(N)|^2 = 1 - \frac{N}{\Omega} \,. \tag{2.41}$$

These results coincide with the exact solution.

In the BCS solution for the degenerate model, the occupation probabilities coincide with the exact values (2.41), whereas the gap and the chemical potential are given by

$$\Delta(N) = \frac{G}{2} \sqrt{\bar{N}(\Omega - \bar{N})} \,, \tag{2.42}$$

$$\mu(N) = \frac{G}{2} \left(\bar{N} - \frac{\Omega}{2} \right) \tag{2.43}$$

respectively. As discussed before, $\bar{N}$ is defined approximately within the values of N and $N-2$. The considerable improvement to BCS with a small number of particles is reached if $\bar{N}$ is chosen as an average value, $\bar{N} = N - 1$. With this choice, the chemical potential becomes exact, and the square of the gap is shifted by a constant from its exact value.

The ground state energy of the system is yet another sensitive test for the validity of any approximation. In the recursive algorithm following the definition in Eq.

(2.25), energy of even-N ground states is given as a discrete integral of the chemical potential,

$$E(N) = \sum_{k=2,4,..,N} 2\mu(k)\,. \tag{2.44}$$

This result has to agree with the standard evaluation of the ground state expectation value of the Hamiltonian with the intermediate states of seniority 0 and 1,

$$E(N) = \sum_{\nu} |v_\nu(N)|^2 - \frac{|\Delta(N)|^2}{G}\,. \tag{2.45}$$

For the degenerate model the particle conserving solution is exact and therefore it is not surprising that Eqs. (2.44) and (2.45) agree exactly providing the exact value of energy

$$E(N) = -\frac{G}{4}\,N(\Omega - N)\,. \tag{2.46}$$

In general for all models we have tested, very good agreement was observed between both methods for calculating $E(N)$ within the particle conserving recursive algorithm. Still, the first way that utilizes Eq. (2.44) is preferable as it guarantees exact values at the boundaries (empty and completely filled shell).

The BCS solution does not ensure agreement between the different methods of calculating $E(N)$ and the exact value. In the degenerate model, the evaluation of energy according Eq. (2.44) gives

$$E(N) = -\frac{G}{4}\,N(\Omega - N) + \frac{G}{2}\,N(1 + N - \bar{N})\,, \tag{2.47}$$

while the second method, Eq. (2.45), leads to

$$E(N) = -\frac{G}{4}\,N(\Omega - N) + \frac{GN}{2} + \frac{G}{4}\,(N - \bar{N})(\Omega - N - \bar{N})\,. \tag{2.48}$$

Finally, these are to be compared to the exact solution in Eq. (2.46). The chemical potential method gives an exact result for BCS corrected by the choice of $\bar{N} = N - 1$, but the results of the second method always differ considerably from the exact answer. The fact that the ground state energy found in BCS could be smaller than the actual

value points to the non-variational nature of BCS (or rather super-variational since the classes of states with different N are mixed in the trial function) that can result in uncontrollable errors. The proposed recursive solution is variational, and the resulting ground state energy is always greater than the exact value.

3. *An equidistant model.* Here we consider a model of six double-fold Kramers-degenerate levels (the total space capacity is $\Omega = 12$) with equidistant energies of $\epsilon = 0, 1, \ldots 5$. The coupling amplitudes $G_{\nu\nu'}$ are chosen to be independent of ν and ν'. The choice of this model was made almost at random, and the results are typical for a sufficiently small system, where exact diagonalization is possible, and the error due to particle non-conservation in BCS might be significant.

For comparison, we first consider ground state energies obtained in the particle-conserving solution, BCS, and by exact numerical diagonalization. In both approximate solutions the ground state energy may be found by two different means, Eqs. (2.44) or (2.45), that may not necessarily agree. This would signal poor quality of the approximation. For the exact numerical solution, the ground state energy is given by the lowest eigenvalue of the Hamiltonian matrix. In the largest case of the half-filled shell, $N = 6$, the matrix has a dimension 924 . The numerical results are given in Fig. 2.8 for strong pairing, $G = 5$, upper panel, and for $G = 1$, lower panel. In both cases, the results exhibit a similar trend. The four curves that correspond to exact solution, two ways of calculating energy with the particle conserving algorithm and the BCS result, corrected by the choice $\bar{N} = N - 1$ with Eq. (2.44), agree to the degree they can hardly be distinguished. A separate dashed line that represents a BCS calculation through the gap equation (2.45) is considerably shifted upwards. For the recursive algorithm the largest errors occur at the edges of the occupation. This is also clear from a direct analysis of Eqs. (2.23) and (2.24).

The quality of approximations can be also seen from Fig. 2.9, where the devia-

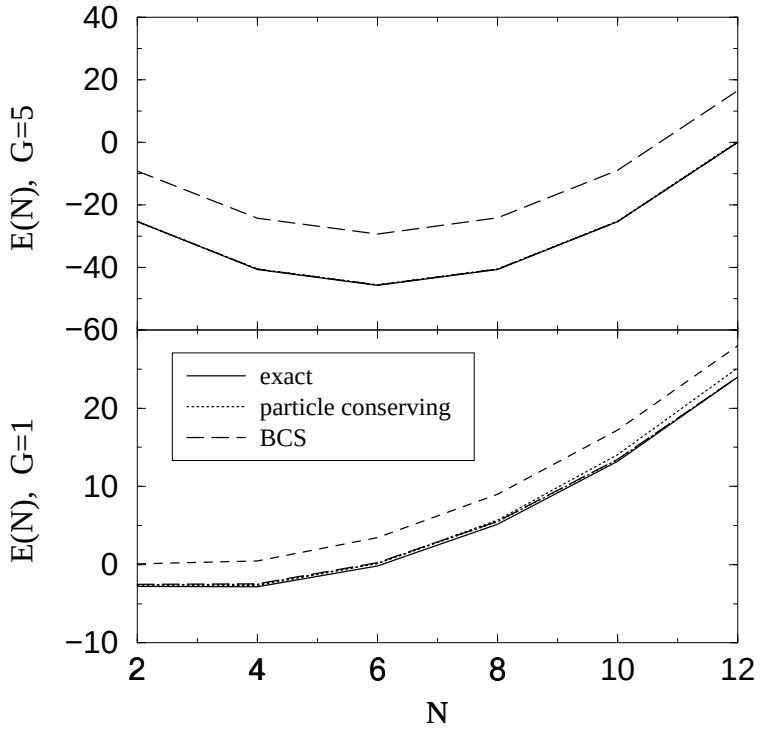

Figure 2.8: Energy of the even-N ground state in the model *3*, the BCS result according to Eq. (2.45), dashed curves, particle conserving solutions, dotted curves, in comparison with the exact results, solid line; the coupling strength is $G = 5$, upper part, and $G = 1$, lower part.

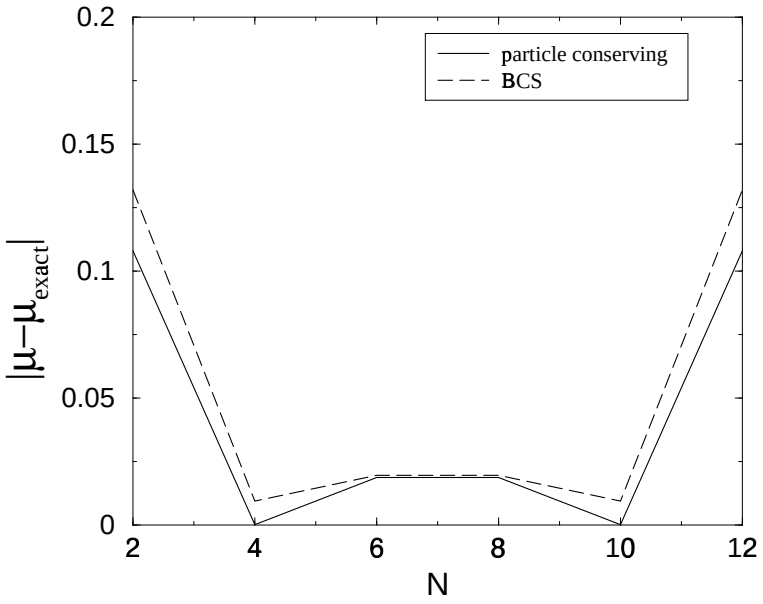

Figure 2.9: Deviation of the chemical potential from the exact solution as a function of the particle number for the particle conserving solution, solid line, and the corrected BCS, dashed line; the coupling constant $G = 1$.

tion of the chemical potential is shown for the particle conserving solution and the corrected BCS.

4. *A realistic example.* The chain of tin isotopes, $^{100-132}$Sn, provides a good place to apply the pairing problem. The outer major neutron shell in these nuclei contains five single-particle j-levels of total capacity $\Omega = 32$. The energies ϵ_ν of these levels, see [42], slightly depend on the number of particles due to the presence of other parts of the residual interaction. For the pairing problem, we assume them to be constant and equal to $\epsilon(d_{5/2}) = -10.371$ MeV, $\epsilon(g_{7/2}) = -9.925$ MeV, $\epsilon(s_{1/2}) = -8.773$ MeV, $\epsilon(d_{3/2}) = -8.122$ MeV, and $\epsilon(h_{11/2}) = -7.612$ MeV. The pairing strength was taken as a constant $G = 0.2$ MeV. In Fig. 2.10 the upper and lower panels display, respectively, the dependence of the gap and ground state energy (relative to the case with no pairing) as a function of the particle number in even-N systems. The BCS

with $\bar{N} = N + 1$ is in a good agreement with the particle conserving solution for the ground state energy ("μ-method" of Eq. (2.44)). A similarly good agreement is observed for the occupancies of single-particle orbitals calculated for the ^{116}Sn isotope. However, the BCS and our results differ considerably for the calculation of the gap, upper part of Fig. 2.10, and for the values of $e_\nu(N)$, Fig. 2.11, that represent the spectrum of broken pairs.

As a conclusion, in this work we discuss and test by a number of models the variational method of solving the pairing problem with the exact conservation of particle number. Being a generalization of the conventional BCS approach, the method reduces to the recursive solution of equations for the energy gap and the chemical potential as functions of the total particle number. The results are in a good agreement with the exact solutions in all considered cases. The BCS value of the ground state energy in even-N systems can be improved by the interpolating the particle number and using for calculation the integration of the chemical potential instead of the expectation value of the Hamiltonian. However, the recursive approach discussed here has an advantage of providing more precise values of the energy gap and quasiparticle energies.

The practical merits of the recursive solution are in its relative computational simplicity and broad applicability. There are no restrictions for the type of single-particle spectrum or pairing matrix elements; extension to other pairing modes and/or the presence of time reversal non-invariant forces is also possible. The method can be incorporated in the self-consistent scheme of the HFB approach taking into account on equal footing non-pairing components of the residual interaction. We expect the importance of exact particle number conservation to increase for the description of soft nuclei where the static mean field is unstable, high order effects play a crucial role, and the nuclear spectra reveal a stronger N-dependence. It would be interesting

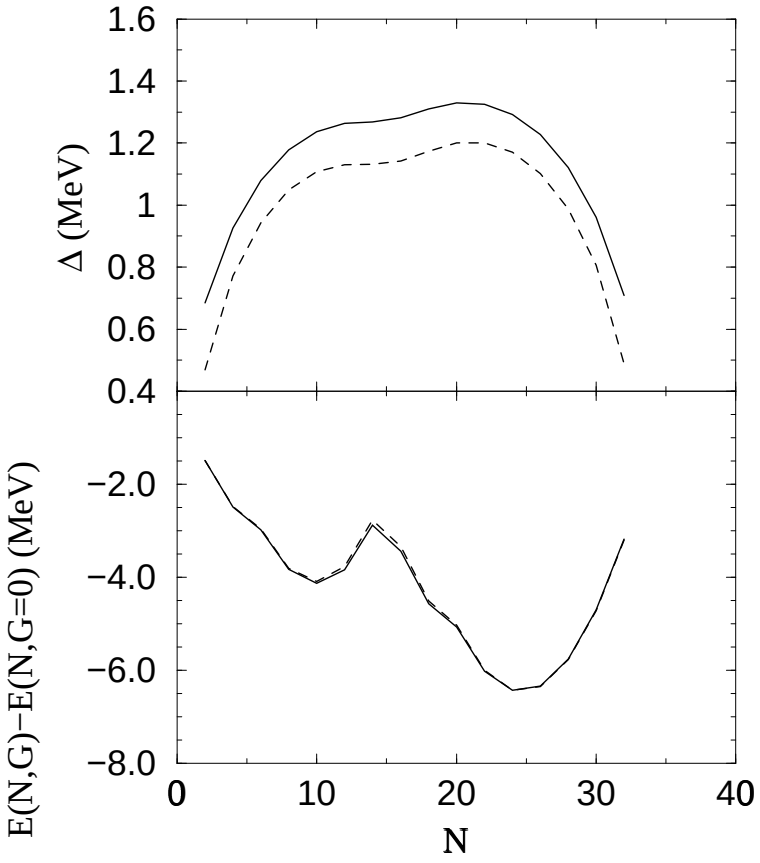

Figure 2.10: Energy gap as a function of the particle number, upper panel; energy of the paired system relative to energy of the system with no pairing, $G = 0$, vs. N; lower panel. On both plots the solid line shows the particle conserving solution, whereas the dashed curve shows the BCS result according to Eq. (2.45).

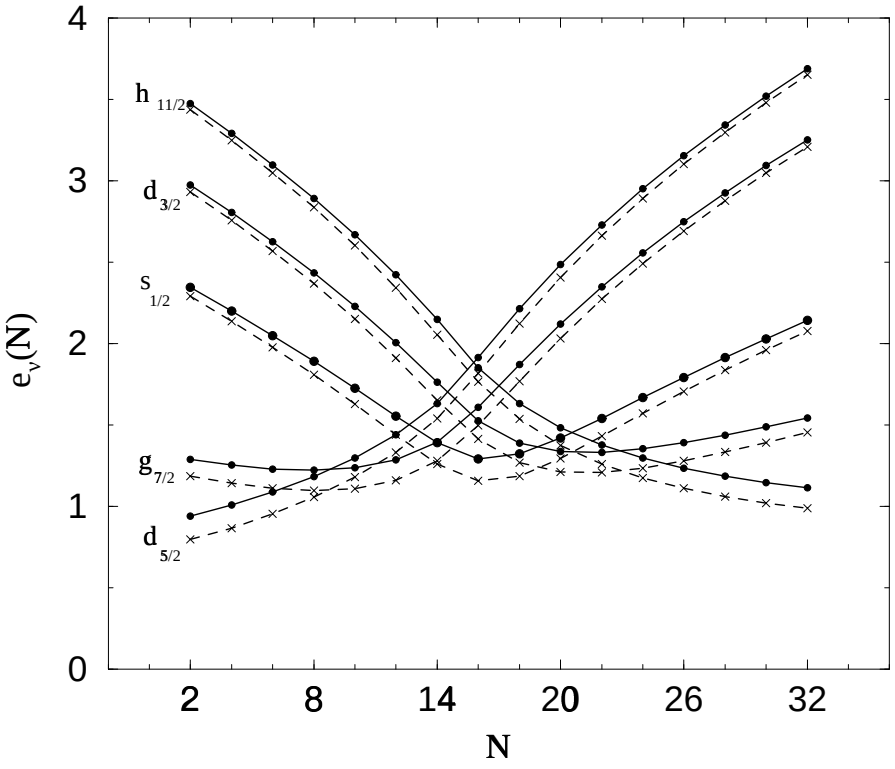

Figure 2.11: Quasiparticle energies e_ν for $^{102-132}$Sn isotopes; the results for the particle conserving algorithm, solid lines with circles marking the valence neutron number, and the BCS result, dashed line with calculated points denoted by crosses.

to proceed beyond the present BCS-like approximation and include explicitly the states of higher seniority and discuss odd particle systems. Other extensions of the particle-conserving method to problems of isovector pairing and pairing in weakly bound systems with the presence of the continuum are plausible and will be the subject of my future work.

Chapter 3

Chaotic wave functions and exponential convergence of low-lying energy eigenvalues

3.1 Introduction

Statistical properties of complex quantum systems have been studied extensively from various viewpoints. The seminal papers by Wigner [43] and Dyson [44] developed the random matrix theory (RMT [45]) where the systems are considered as members of a statistical ensemble, and all Hamiltonians of a given global symmetry appear with certain probabilities. The canonical Gaussian ensembles [46, 47] correspond to systems with complicated dynamics when, in almost all bases connected by the transformations preserving global symmetry, the components of generic eigenfunctions are uniformly distributed on a unit sphere in multidimensional Hilbert space. On a local scale, Gaussian ensembles predict specific correlations and fluctuations of spectral properties which are in agreement with empirical data for atoms, nuclei [48], quantum dots [49] and resonators (microwave [50] and acoustic [51] experiments). These

spectral features are considered usually as signatures of quantum chaos [47, 52, 53].

Recently, the detailed studies of highly excited states in realistic atomic [54] and nuclear [55] calculations demonstrated that such many-body systems are close to the RMT limit although they reveal some deviations, partly due to the presence of the mean field [56], and coherent components [57] of the residual interaction [46, 58]. In complex atoms and nuclei, precise experimental information exists, as a rule, about low-lying states only. Effective residual interactions , such as the Wildenthal-Brown interaction [59] for the *sd*-shell model turned out to be successful well beyond the input used for their original fit. This justifies the use of such interactions for studying generic complicated states in the region of high level density. The shell model approach requires large-scale diagonalization even if one is interested in the low-lying states only. The dimensions of matrices increase dramatically with the number of valence nucleons, which makes the full diagonalization impractical, even after projecting out correct angular momentum and isospin states. This problem is avoided in the Monte Carlo shell model method [60], but, apart from the so-called sign problem [61], which requires the introduction of an extrapolation when working with realistic interactions, this method is better suited for calculating thermal properties or strength functions than spectroscopic characteristics. In order to consider individual levels, one needs to supplement the Monte Carlo sampling with some variational procedure including an additional "stochastic" diagonalization ([62] or the QMCD approach [63]). An important step towards larger dimensions in the standard shell model is made with the development of the DUPSM code [64].

3.2 Examples of exponential convergence

Here we suggest a simple approach which allows one, while calculating energies of low lying states, to reduce large dimensions of matrices under study by orders of

magnitude, maintaining high precision in the results. The approach is based on the statistical properties of complicated many-body states [54, 55]. Because of the strong residual interaction and "geometric chaoticity" [55, 65] of the angular momentum coupling, the eigenstates are extremely complex superpositions of independent particle Slater determinants. However, in contrast to the limiting case of the Gaussian orthogonal ensemble (GOE), the stationary wave functions are not fully delocalized in shell model space. Due to the inherently self-consistent nature of the residual interaction (even if it is extracted in a semiempirical manner), its strength does not exceed the typical spacings between single-particle levels which are determined by the mean field, i.e., by the same original forces. Together with the fact that the two-body forces cannot couple very distinct configurations, this leads to a band-like structure of the Hamiltonian matrices in the shell model basis Fig 3.1.

The theory of banded random matrices did not reach the same degree of completeness as that of canonical Gaussian ensembles. Nevertheless, both mathematical [66] and numerical [67] arguments favor the localization of the eigenstates in Hilbert space, similar to the coordinate localization of electronic states in disordered solids. The generic many-body states in complex atoms or nuclei have a typical localization width [55, 67, 68]. Inversely, the simple shell model configurations are packets of the eigenstates. Their strength function is fragmented over the range of energies characterized by the spreading width Γ which is nearly constant along the spectrum because the coupling matrix elements between the complicated states are small just as it is needed to compensate small level spacings in the region of high level density [69, 70, 71]. The qualitative arguments are confirmed by more general theory [57] as well as by detailed numerical calculations for atoms [54] and nuclei [55, 72]. The nuclear case is close to the strong coupling limit [73, 74, 55] where the typical width, associated with the energy uncertainty, can be estimated [72] as $\Gamma \approx 2\bar{\sigma}$ in terms of

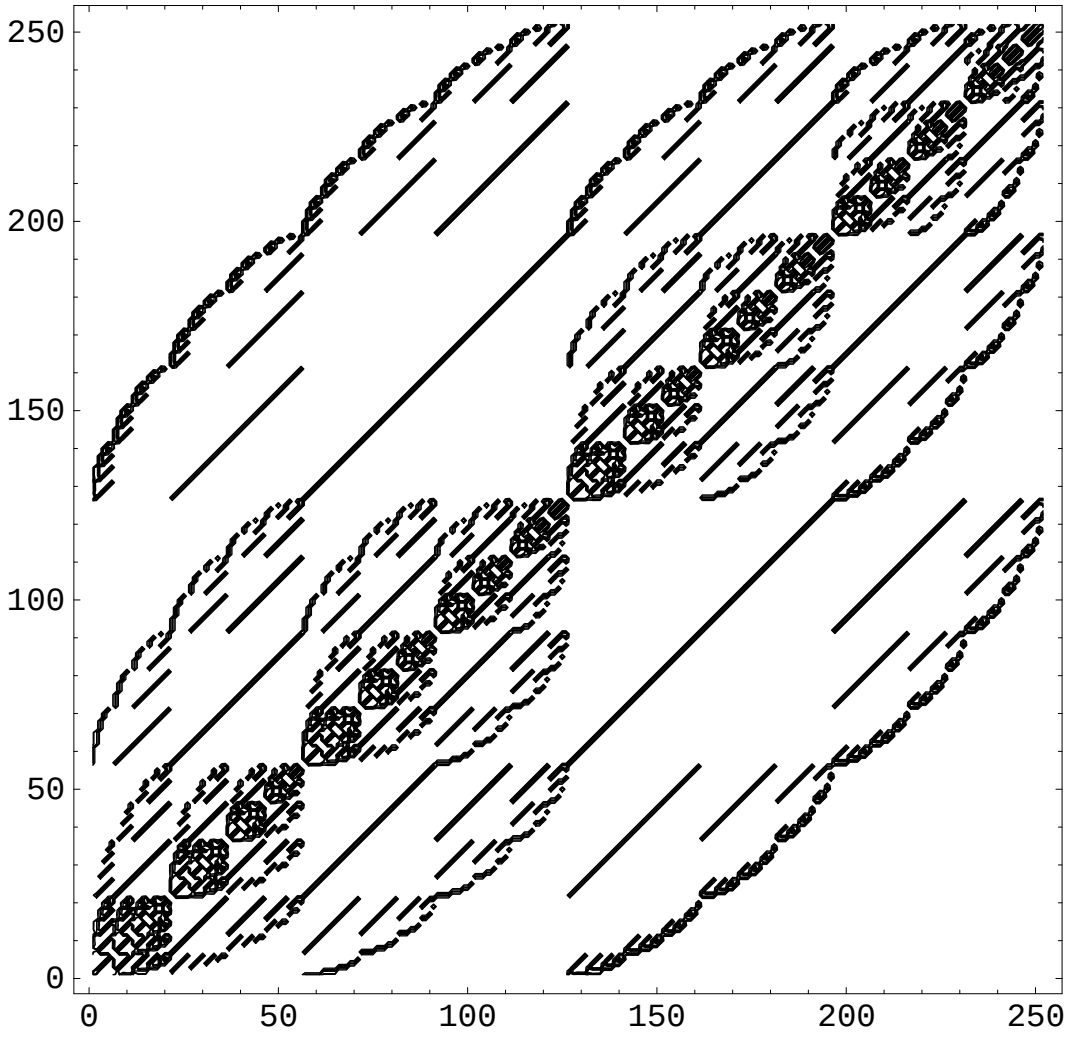

Figure 3.1: The density plot of matrix elements of a typical shell-model Hamiltonian matrix. This particular plot corresponds to the system with a quadrupole-quadrupole residual interaction. The band-like structure is clearly seen along the main diagonal which goes from the lower left to the upper right corners of the plot.

the energy dispersion of a simple configuration $|k\rangle$,

$$\sigma_k^2 = \langle k|H^2|k\rangle - |\langle k|H|k\rangle|^2 = \sum_{l\neq k} |H_{kl}|^2. \tag{3.1}$$

Here H_{kl} are the off-diagonal elements of the residual interaction between the basis states so that the calculation of (3.1) does not require any diagonalization. The dispersions σ_k of different simple states fluctuate weakly [55] and in our estimate of Γ they are substituted by the appropriate mean value $\bar{\sigma}$ which can be found by the methods of statistical spectroscopy [75].

The practical method of truncating large shell model matrices was suggested in [76]. The shell model states are grouped into partitions (sets of states belonging to the same particle configuration). Since the states separated in energy by an interval broader than Γ are not significantly mixed with the studied state, we truncated the matrix retaining only the partitions whose statistical centroids $\bar{E} = \overline{\langle k|H|k\rangle}$ are closer than 3σ. The spin-isospin projection and the elimination of the center-of-mass admixtures can be done within the truncated subspace only. In order to keep the correct shell model structure, the partitions should be included as a whole. As shown in [76], this method allows for the calculation of low-lying energies with sufficient precision in large shell-model spaces. The truncated eigenvectors overlap with the exact ones on the level of better than 90%.

Going beyond the simple truncation, we consider the convergence of level energies to the exact values as a function of the increasing dimension n of the diagonalized matrix. As an example Fig. 3.2 displays the energies of the yrast 2^+ state in ^{48}Cr (the pf-shell model dimension 1922106 in the m-scheme; JT-dimension 27229) and of the lowest $1/2^-$ and $3/2^-$ states in the ^{51}Sc nucleus (JT-dimensions 13016 and 24474, respectively) calculated with the FPD6 interaction [77] for dimensions ranging from $n = 2000$ to the full dimension N. The smallest n lead to a deviation within a few hundred keV for ^{51}Sc and about 1.5 MeV for ^{48}Cr. As n increases, the energies

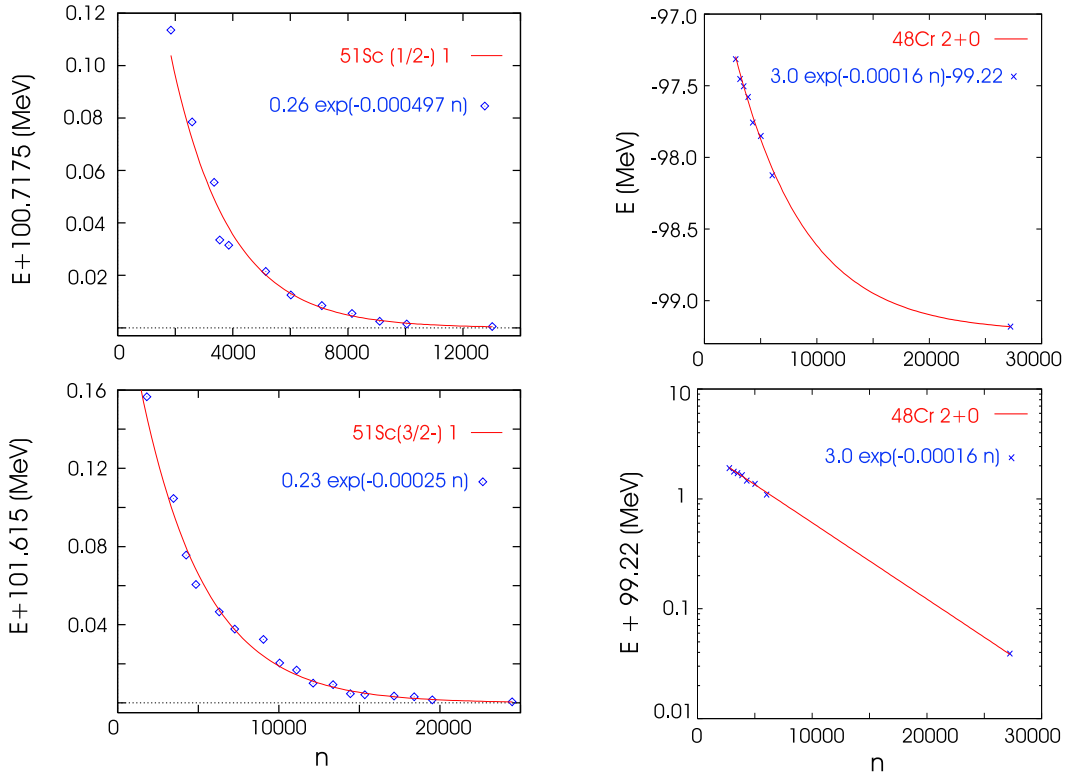

Figure 3.2: Left panel: energies of the lowest states $1/2_1^-$ and $3/2_1^-$ in ^{51}Sc as a function of the matrix truncation n, shell model calculation (points) and fits $A\exp(-\gamma n)$ (solid lines); right panel: energy of the yrast state 2^+ in ^{48}Cr, real scale (top) and logarithmic scale (bottom).

converge very fast and monotonically to the exact values. The convergence is almost purely exponential, $E(n) = E_\infty + A\exp(-\gamma n)$; the rate of convergence $\gamma \approx 6/N$ for Sc and $\gamma \approx 4/N$ for Cr. A similar exponential convergence, with slightly varying parameters (apparently lower γ for strongly collective states as in Cr), is observed in all studied cases for low-lying states. The study of the convergence rate as a function of excitation energy will be delayed for further research. The exponential convergence of eigenvalues would be extremely helpful for shell model practitioners. It would make almost redundant the full large-scale diagonalization if one is interested in the low-lying states only. Instead, the calculations for several increasing dimensions (still

far from the full value and therefore easily tractable) would end in determining the exponential parameters and simply extrapolating to the exact result. At present, the rigorous mathematical theory of convergence is absent, and we limit ourselves by qualitative arguments and plausible conjectures.

The convergence under consecutive truncations is determined by the type of the matrix and by the original unperturbed basis which orders the basis vectors in a certain way. The ordering is done almost uniquely in the spherical shell model where the mean field is fixed and all many-body states are organized into partitions. For the lowest levels, the admixtures of highly excited states outside of the starting truncation correspond to the wings of the strength function

$$F_k(E) = \sum_\alpha |\langle \alpha | k \rangle|^2 \delta(E - E_\alpha) \,, \tag{3.2}$$

which describes the fragmentation of the state $|k\rangle$ over eigenstates $|\alpha\rangle$. As confirmed by atomic [54] and nuclear [55, 72] studies, the strength function has on average a universal shape. This shape evolves from the standard Breit-Wigner function [17] for the "weak damping" case to the Gaussian form at strong damping (semicircle in the RMT limit of uniform spectra [57, 66] which is not reached in practical cases). Correspondingly, the dependence of the spreading width on the strength of the residual interaction changes from quadratic in the standard golden rule [17] to linear [74, 57, 72]. The remote wings of the strength function have their own energy behavior [54, 72]. With high accuracy they can be described [72] by an exponential function of energy Fig. 3.3. This is a clear manifestation of the localization of the eigenfunctions typical for the banded Hamiltonian structures [78, 66]. The strength function is simply a Fourier image of the decay amplitude of the original state $|k\rangle$.

$$F_k(E) = \int \frac{e^{iEt}}{2\pi} dt \, \langle k | e^{-iHt} | k \rangle \,. \tag{3.3}$$

In this limiting regime of distant tails the $t \to 0$ decay region has a Breit-Wigner type

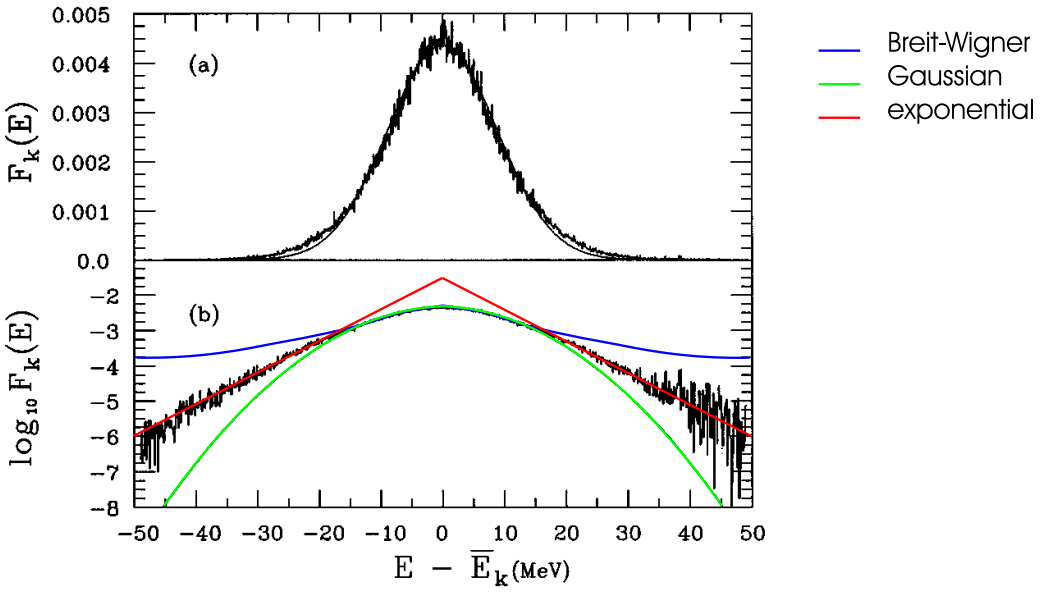

Figure 3.3: Summary of the results obtained in [??], that clearly indicate the exponential nature of the strength function tails.

dependence on time which follows from the Taylor expansion

$$P(t) = \left|\langle k|e^{-iHt}|k\rangle\right|^2 \approx 1 - \sigma_k^2 t^2 \approx 1/(1+\sigma_k^2 t^2)\,, \tag{3.4}$$

where σ_k^2 was defined by the Eq. 3.1. This leads to an exponential form of the strength function tails. The exponentially weak mixing should lead to exponentially small energy shifts and to the corresponding convergence of the eigenvalues.

We can expect the exponential behavior to be generic for large matrices of quasi-banded form with the off-diagonal elements of approximately the same order of magnitude along the spectrum. This conjecture can be checked by generating random matrices with the desired properties and diagonalizing them in a sequence of progressive truncations (the matrices are first ordered according to their diagonal elements). Since there is no "vertical" structure in such random matrices, we do not have here physical arguments concerning the optimal truncation sequence. We show in Fig. 3.4, left, a typical result for the banded GOE matrix with the band width $b = 0.293N$

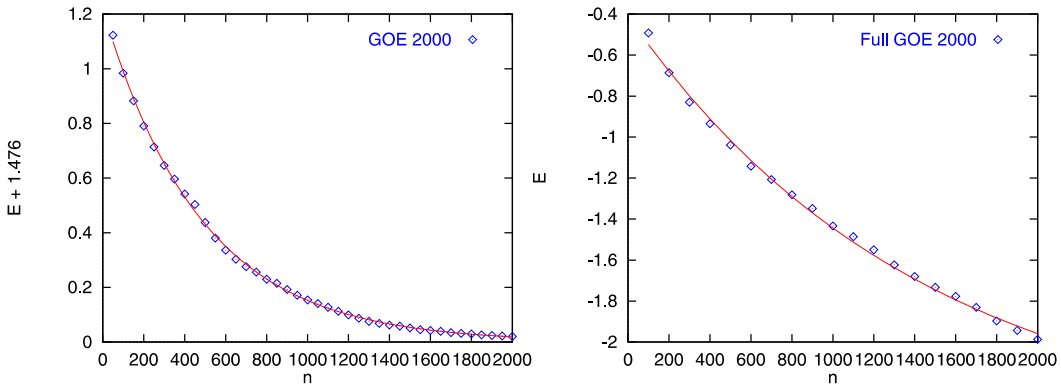

Figure 3.4: Energy deviations for the ground state of random matrices of dimension 2000 as a function of the progressive matrix truncation n (diamonds): the GOE-like banded matrix of width $b = 0.293N$, chosen in such a way that half of the matrix elements vanish, approximately in the same proportion as in typical shell model cases, left panel; the full GOE matrix, right panel. Solid lines show a fit $A\exp(-\gamma n)$ with $A = 1.18$ and $\gamma = 3.8 \times 10^{-3}$, left, and $A = 1.96$, $\gamma = 1.53 \times 10^{-3}$, right. Note the absence of the horizontal asymptotics in the case of the full matrix.

which clearly demonstrates the exponential convergence. The full GOE matrix, Fig. 3.4, right, converges more slowly in the absolute sense and does not saturate. This is a simple consequence of the fact that the ground state of a GOE matrix is repelled by the higher states to the edge of the semicircle (-2 with the GOE definition accepted here and in [55]). This process is driven by the off-diagonal elements; all of them on average have the same magnitude. Their number and, thence, the dispersion σ, Eq. (3.1), are greater in the full GOE. Therefore, the distance from the unperturbed position is also greater in this case (the diagonal and off-diagonal contributions add in quadrature). In all studied cases with the width b changing from $0.1N$ to the full GOE, the convergence is exponential and the exponent γ is approximately scaled inversely proportional to b.

In realistic cases there is also a leading sequence of regular diagonal elements. A

similar banded matrix example, considered in [54], goes back to Wigner [43]. The matrix consists of the equidistant diagonal with the spacing D and random off-diagonal matrix elements V_{kl} within the band $|k-l| \leq b$. At the relatively weak interaction, $g \equiv \langle V^2 \rangle / D^2 < 1$, the main contribution in the perturbation series for the admixture $w_n = C_n^2$ of a very remote state $|n\rangle$, $n \gg 1$, to the wave function of a low-lying state $|0\rangle$ is given by the summation of long "straight" paths in Hilbert space connecting the initial state with the final one through various intermediate stops. Because of the random character of the off-diagonal interaction, the mean value of w_n is determined by the squares of the contributions of these paths (no interference). In the approximation of a weakly changing level density, this can be approximately written as an integral equation of the random-walk type,

$$w_n = \frac{g}{n^2} f_n + \frac{g}{n^2} \sum_k f_{n-k} w_k \tag{3.5}$$

where the factor $1/n^2$ comes from the energy denominators, and f_n shows the behavior of typical squared off-diagonal matrix elements V_{n0}^2 as a function of the distance n from the diagonal. With the sharp band boundary [54], the weights w_n decrease quickly, essentially as $\exp(-n \ln n) \sim (n!)^{-1}$. With the smooth cut-off, the convergence is nearly exponential. Thus, for the exponential cut-off of matrix elements, $V_{kl} \sim \exp(-|k-l|/b)$, we have $f_n = \exp(-2n/b)$, and Eq. (3.5) allows a simple solution $w_n = A \exp(-2n/b)/n^2$. Therefore, the contributions to energy of the state $|0\rangle$ should converge $\sim nDw_n = DA \exp(-2n/b)/n$. Fig. 3.5 illustrates this consideration by an example of the numerical diagonalization of a random matrix with the equidistant diagonal and the exponential cut-off. One may note that the rate of convergence is similar to that in a shell-model calculation, see above, where the effective width of the band is close to $b \approx N/4$ [55]. However, the method of Eq. (3.5) becomes invalid in the case of strong interaction when the contributions to the perturbation series of additional loops in Hilbert space cannot be neglected. The range

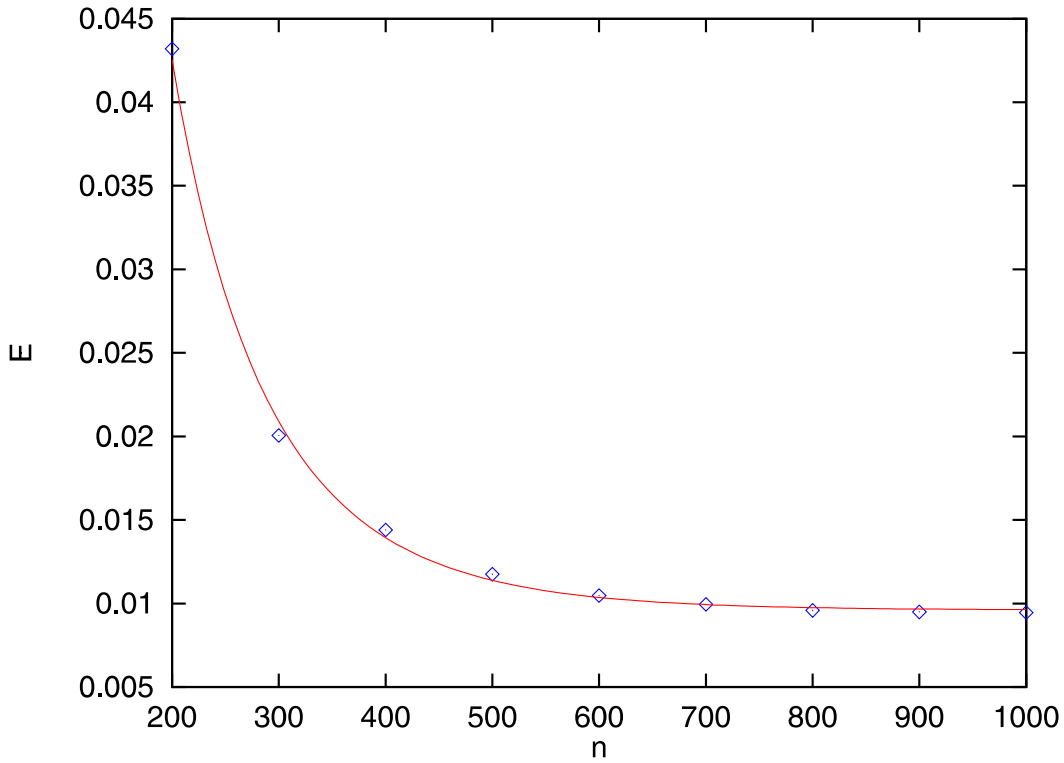

Figure 3.5: Convergence of the ground state energy for a banded random matrix with the exponential cut-off of matrix elements $V_{kl} \sim \exp(-|k-l|/b),\ b = 0.293N$, shown by diamonds; the solid line shows the fit const$\cdot \exp(-2n/b)/n$.

of convergence is seen from the expression for the constant in the above solution, $A = g/[1 - g\sum_{k=1} k^{-2}]$, which determines the critical value $g_c = 6/\pi^2$.

3.3 Solvable models

It is interesting to test the character of the convergence in simple solvable models. A harmonic oscillator, shifted from the equilibrium position by a constant force, $H = a^\dagger a + \lambda(a + a^\dagger)$, lowers its energy by λ^2. The exact ground state is a coherent combination of unperturbed states $|n\rangle$. In accordance with the composition of the coherent state, the convergence of the energies in the unperturbed basis of the original

oscillator is $\sim \lambda^{2n}/n!$. This is clearly seen in the left panel of Fig. 3.6. The fast convergence is due to the constant level density along the main diagonal while the perturbation has matrix elements growing only proportional to $n^{1/2}$. In the case of a quartic anharmonic oscillator, the exponential convergence is modulated with oscillations.

Another example displays the case of slow convergence. The tight-binding model of a finite one-dimensional lattice has degenerate levels in each of N identical wells. The amplitude of hopping between adjacent wells is labeled as v. The eigenstates of the model are delocalized standing Bloch waves with energies within the band, $E_q = 2v\cos\varphi_q,\ \varphi_q = \pi q/(N+1),\ q = 1, 2, \ldots, N$. It is straightforward to to see that the truncation in the site basis corresponds to the convergence $\sim 1/n^2$, see Fig. 3.6, right.

Tridiagonal matrices with the entries $H_{nn} \equiv \epsilon_n$ and $H_{n-1,n} = H_{n,n-1} \equiv V_n$ smoothly depending on n can be analyzed in a general way using the recurrence relation for the secular determinants $D_n(E)$ of the matrix $(H - E)$ truncated at the nth step,

$$D_n(E) = (\epsilon_n - E)D_{n-1}(E) - V_n^2 D_{n-2}(E). \tag{3.6}$$

The consecutive approximations for $E^{(n-1)}$ and $E^{(n)},\ n \gg 1$, to a low-lying eigenvalue E are the roots of $D_{n-1}(E^{(n-1)}) = 0$ and $D_n(E^{(n)}) = 0$, respectively. For $\epsilon_n \gg E^{(n)}$ (with a slight modification, the method works also for initially degenerate matrices with ϵ_n =const), the asymptotic behavior of the energy increments $\Delta_n = E^{(n)} - E^{(n-1)}$ follows from (3.6) as

$$\frac{\Delta_n \Delta_{n-2}}{(\Delta_n + \Delta_{n-1})(\Delta_{n-1} + \Delta_{n-2})} = \frac{V_n^2}{\epsilon_n \epsilon_{n-1}} \equiv \lambda_n. \tag{3.7}$$

The exponential convergence corresponds to $\lambda_n \to \lambda \neq 0$ at large n (proportional increase of diagonal and off-diagonal elements). Then the increment ratio $\xi_n = \Delta_n/\Delta_{n-1}$ also goes to a constant limit $\xi = (1/2\lambda)[1 - (1 - 4\lambda^2)^{1/2}]$ which restricts the

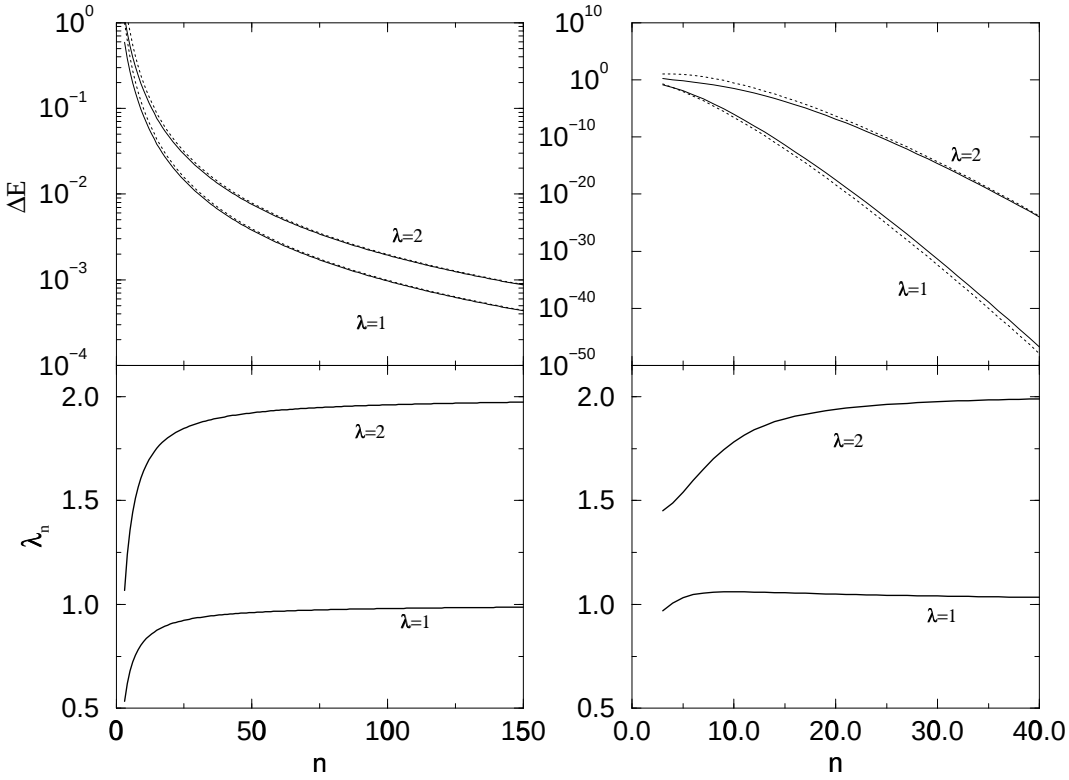

Figure 3.6: Convergence of the ground state energy in the tight-binding model of a finite one-dimensional lattice with λ as a hopping parameter, left panels, and for a shifted harmonic oscillator with the Hamiltonian $H = a^\dagger a + \lambda(a + a^\dagger)$, right panels. The upper parts show the energy deviation $\Delta E_n = E_0(n) - E_0(\infty)$ as a function of the truncated dimension n (solid lines for $\lambda = 1$ and $\lambda = 2$); dotted lines show the predicted analytical convergence of the models, $\lambda\pi^2/n^2$ (left) and $\lambda^{2n}/n!$ (right). The lower parts characterize the convergence rate $\lambda_n \to \lambda$ by plotting $\lambda_n \equiv \Delta E_n n^2/\pi^2$, left, and $\lambda_n = (\Delta E_n n!)^{1/2n}$, right.

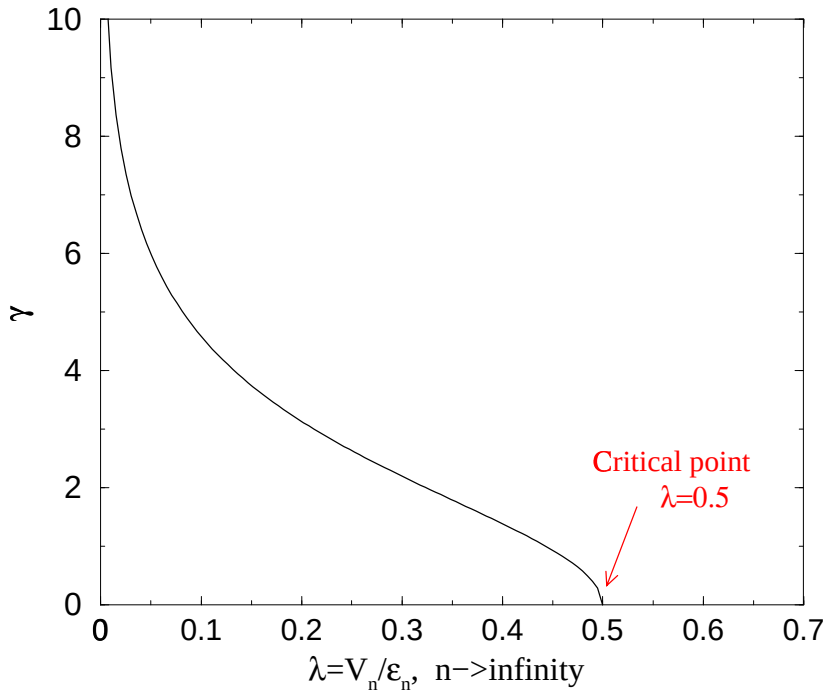

Figure 3.7: The exponential convergence rate γ is shown as a function of the limiting perturbation λ in the case of a tri-diagonal matrix. The critical point at $\lambda = 0.5$ is indicated.

exponential convergence region to $\lambda^2 < 1/4$. The existence of the constant limit is still compatible with an additional pre-exponential factor weakly dependent on n; at large n corresponding fits are usually indistinguishable. An explicitly solvable (by the Bogoliubov transformation) model of the harmonic oscillator with the perturbation $\lambda(a^2 + a^{\dagger 2})$ agrees completely with this estimate. The case $\lambda^2 = 1/4$ corresponds here to the degeneracy of the oscillator with zero frequency, and at $\lambda^2 > 1/4$ the spectrum is inverted. In general, $\lambda = 1/2$ corresponds to a critical point as shown in Fig. 3.7; the convergence here is described by a power law being exponential outside of this region.

The main difference of the tight-binding case from the oscillator model is the degeneracy of the unperturbed levels (absence of the leading diagonal) which results

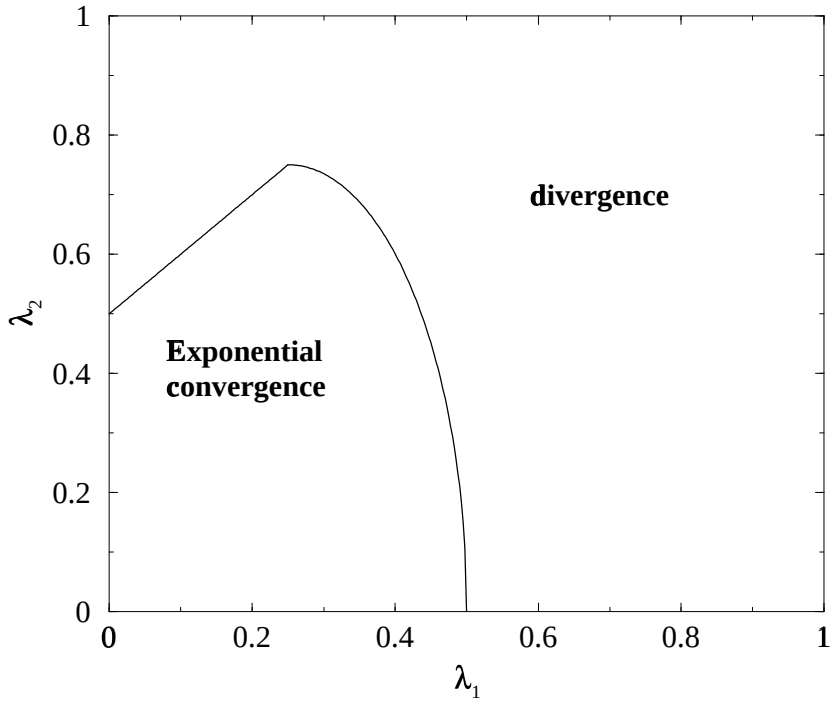

Figure 3.8: Convergence region of five-diagonal matrices shown in the two-parameter space of the off-diagonal matrix strengths λ_1 and λ_2 .

in delocalized wave functions for eigenstates. Because of the degeneracy, the analog of Eq. (3.7) contains, instead of λ_n^2, the ratio $v^2/E^{(n)}E^{(n-1)}$ which is just equal to the critical value $1/4$ in the limit of large n. The situation is similar for the spin chains with the nearest neighbor interaction where finite size effects on the ground state energy were repeatedly studied [79] and corrections also go as n^{-2}. We expect the presence of disorder (random positions of the original site levels), which leads to the localization of the eigenfunctions, to be accompanied by the transition to exponential convergence of the eigenvalues. Numerical studies of five-diagonal matrices show a similar trend in Fig. 3.8. Depending on the limiting, relative to diagonal, strength of the off-diagonal elements λ_1 (nearest to diagonal) and λ_2, there is a region of exponential convergence separated by the phase boundary from the divergent region, where the lowest eigenvalue is unbound.

3.4 Conclusion

In conclusion, we discussed the convergence of the low-lying eigenvalues of large matrices describing realistic many-body Hamiltonians of the shell-model type. We gave arguments in favor of the conjecture that the exact diagonalization of relatively small matrices, truncated on the grounds of physical partitions and generic spreading widths of simple configurations, provides a starting approximation which can be extrapolated to the exact result with the aid of a simple exponential continuation. The arguments are based on the generic features of quantum chaotic many-body dynamics, simple models and the results of numerical analysis.

Chapter 4

Modeling pionic fusion

4.1 Introduction

Nuclear fusion reactions which produce a pion are often referred to as pionic fusion. Pion production has been observed [80, 81, 82] at energies approaching absolute threshold, where the entire available energy is converted into the pion, demonstrating an amazing collective behavior of nucleon systems. However, it remains quite difficult to incorporate the observed collectivity into existing theoretical models. A variety of studies [83, 84, 85, 86] have dealt with subthreshold pion production in heavy ion collisions, where the energy per nucleon is below the energy threshold of the elementary single-particle reaction $NN \rightarrow NN + \pi$. Most models, such as those featuring pion bremsstrahlung mechanisms [87, 88], quantum molecular dynamics approaches[89], perturbative calculations using Boltzmann-Nordheim-Vlasov equations [90] or nuclear structure functions [91], provide a good picture at energies starting from $E/A \approx 30$ MeV up to the single-particle threshold $E/A = 280$ MeV in the laboratory frame. In the present work motivated by the experimental results of [80, 81, 82] our aim is to consider even lower energies and study the behavior of the cross section of fusion reaction in the region down to $\approx$10 MeV above the absolute threshold. This neces-

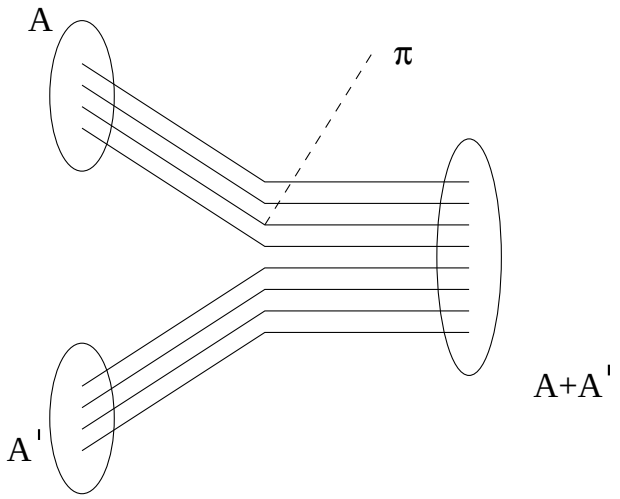

Figure 4.1: The pionic fusion of two nuclei in the sudden approximation is illustrated.

sitates a careful consideration of limitations on the reaction given by conservation laws and the Pauli exclusion principle which govern the behavior of the cross section in this extreme situation. The statistical approach used in most existing models at higher energy has to be substituted by low energy many-body structure physics.

Our model, that is described in Sect. 4.2, considers the cross section in the Born approximation, assuming that pion production occurs through coupling to a single nucleon. All possible further rescatterings of the pion are expected to significantly reduce the probability of the reaction and are ignored as higher-order processes. A schematic picture of the reaction is shown in Fig. 4.1 demonstrating the pionic fusion of two nuclei A and A'. Many-body nuclear mean-field parameters are assumed to be constant and to suddenly change from the initial to the final values. This will be referred to as the sudden approximation. The three-dimensional harmonic oscillator shell model is used to describe the structure of the incoming and outgoing nuclei. This allows analytical calculation of all necessary overlap amplitudes. The stationary wave functions are constructed as Slater determinants projected onto good angular

momentum. Taking into account the center-of-mass motion we preserve linear momentum. Sect. 4.3 shows the implementation of the model for the case of pionic fusion of two identical nuclei. In Sect. 4.4 we present a low pion momentum approximation, for which more general results could be derived. The parallel discussion of mathematical details is given in the appendices. The application of this model to experimentally observed pionic fusion reactions shows surprisingly good agreement with data. The comparison is presented in Sect. 4.5 along with some predictions for heavy nuclei.

4.2 Description of the model

4.2.1 The transition amplitude

We approach the problem of pionic fusion as a stationary scattering problem. We consider the reaction cross section to be given by the Fermi golden rule in terms of the transition amplitude $\langle F|H|I\rangle$, where I and F refer to the initial and final states, respectively, of the whole system including the emitted pion. The density of final pion states is given by $Vk^2dk\,d\Omega/(2\pi)^3$ with k as a momentum of the pion produced; Ω is a solid angle in the center of mass (CM) frame, and V stands for the quantization volume. In all further calculations the pion is assumed to be fully relativistic whereas nucleons obey non-relativistic quantum mechanics. We use a set of natural units with $\hbar = c = 1$. In this framework the differential cross section can be written as

$$d\sigma = \frac{\omega k m}{2p_n(2\pi)^2}|\langle F|H|I\rangle|^2 V^2 d\Omega \quad , \tag{4.1}$$

where m is a nucleon mass, p_n is the CM momentum per nucleon in the initial state and $\omega = \sqrt{k^2 + m_\pi^2}$ is pion energy.

On the single-nucleon level one can use a phenomenological Hamiltonian density

for the pion-nucleon interaction [92],

$$\mathcal{H} = g\overline{\psi}\gamma_5\vec{\tau}\psi\vec{\pi} + 4\pi\frac{\lambda_1}{m_\pi}\bar{\psi}\vec{\pi}\cdot\vec{\pi}\psi + 4\pi\frac{\lambda_2}{m_\pi^2}\bar{\psi}\mathbf{r}\cdot\vec{\pi}\times\dot{\vec{\pi}}\psi \quad . \tag{4.2}$$

A number of studies have been performed analyzing this form of the interaction within the context of chiral perturbation theory [93]. The first term, often called in the literature the impulse or Born term, is responsible for single-pion production in a p-wave. We neglect the second and the third s-wave terms which require an additional interaction to absorb the extra pion created in the four-point vertex. We believe that due to the difficulty of recombining the nucleons into an appropriate final state the second and third terms become increasingly unimportant for larger nuclei. It has also been experimentally observed that in pionic fusion reactions the pion is predominantly produced in a p-wave [80, 81]. Reduction of the first term in the Hamiltonian to a non-relativistic case gives an interaction of the form

$$\Gamma = g\frac{\vec{\sigma}\cdot\mathbf{k}}{2m} \quad , \tag{4.3}$$

with the coupling g appropriately defined according to isospin. Separation of the quantized pion field,

$$\pi(x) = \sum_k \frac{1}{\sqrt{2\omega V}}(a_k^+ e^{-i\mathbf{k}\cdot\mathbf{x}} + a_k e^{+i\mathbf{k}\cdot\mathbf{x}}), \tag{4.4}$$

in the matrix element of Eq. (4.1) reduces the transition amplitude to the following form

$$\langle F|H|I\rangle = \frac{1}{\sqrt{2\omega V}}\frac{1}{2m}\langle f|\sum_{\text{nucleons}} g\,\mathbf{k}\cdot\vec{\sigma}e^{-i\mathbf{k}\cdot\mathbf{x}}|i\rangle \quad , \tag{4.5}$$

where $|f\rangle$ and $|i\rangle$ are final and initial states of the nucleon system.

4.2.2 Nuclear wave functions

We will approximate a state of a nuclear system with an antisymmetric combination built upon single-particle (s.p.) states. We take these states from the harmonic

oscillator shell model, which allows for the analytic calculation of corresponding overlaps. The approach however can be extended to any single-particle basis. Each of the single-particle states can be characterized by the number of excitation quanta in three Cartesian directions, the nucleon spin and isospin projections. The locations of the centers of the harmonic oscillator potentials for all separate nuclei have to be introduced as additional parameters to the wave function. The importance of these parameters in projecting a nucleon wave function onto a state with correct total momentum for every nucleus participating in the process is discussed below. Following these assumptions we will write the wave function of a nucleon system as follows

$$|\underbrace{(\vec{\alpha}_1, s_1, t_1; \vec{\alpha}_2, s_2, t_2; \ldots; \mathbf{r})}_{\text{nucleus } A}, \underbrace{(\overbrace{\vec{\alpha}_{A+1}, s_{A+1}, t_{A+1}}^{(A+1)\text{th s.p. state}}; \vec{\alpha}_{A+2}, s_{A+2}, t_{A+2}; \ldots; \mathbf{r}')}_{\text{nucleus } A'}\rangle \quad . \tag{4.6}$$

In this example we assume that the system consists of two nuclei A and A' with the centers of their respective harmonic oscillator potentials at $\mathbf{r}$ and $\mathbf{r}'$. The single-particle orbitals are numbered from 1 to A for the first nucleus and from $A+1$ up to the total number of nucleons $A_f = A + A'$ for the second one. Labels $\vec{\alpha} = (\alpha_x, \alpha_y, \alpha_z)$ are Cartesian quantum numbers of single-particle states, while s and t are the spin and isospin projections. Protons and neutrons can be considered separately as well as different spin projections of the nucleons, reducing the wave function of the state to a product of four components. If the described separation is performed and the resulting part of the wave function contains only single-particle states with the same values of either s or t, then the corresponding index is omitted in writing. We use a standard form for the one-dimensional harmonic oscillator wave functions centered at r in the coordinate representation:

$$\langle x|(\alpha; r)_v\rangle = \sqrt{\frac{v}{\sqrt{\pi} 2^\alpha \alpha!}}\, H_\alpha(v(x-r)) e^{-v^2(x-r)^2/2} \quad . \tag{4.7}$$

The parameter v is defined for a single oscillator as $v = \sqrt{m\omega}$. These parameters characterize the mean field potentials for every incoming or outgoing nucleus. The

function $H_n(x)$ is the nth order Hermite polynomial of the variable x. The discussion of the overlap integrals such as $\langle(\alpha', r')_{v'}|(\alpha, r)_v\rangle$, and the general form of the results are presented in Appendix 4.7.1.

A simple projecting technique was used to construct wave functions as eigenstates of the momentum operators that correspond to the total momenta of each individual nucleus,

$$|(\vec{\alpha}_1, s_1, t_1; \ldots; \mathbf{p}), (\vec{\alpha}_{A+1}, s_{A+1}, t_{A+1}; \ldots; \mathbf{p}')\rangle =$$
$$\mathcal{N}^{-1} \int\int_{-\infty}^{+\infty} d^3r\, d^3r'\, |(\vec{\alpha}_1, s_1, t_1; \ldots; \mathbf{r}), (\vec{\alpha}_{A+1}, s_{A+1}, t_{A+1}; \ldots; \mathbf{r}')\rangle e^{i(\mathbf{p}\cdot\mathbf{r}+\mathbf{p}'\cdot\mathbf{r}')} \quad . \tag{4.8}$$

It is easy to check that

$$-i\sum_{j=1}^{A} \nabla_j |(\vec{\alpha}_1, \ldots; \mathbf{p}), (\vec{\alpha}_{A+1}, \ldots; \mathbf{p}')\rangle = \mathbf{p}\, |(\vec{\alpha}_1, \ldots; \mathbf{p}), (\vec{\alpha}_{A+1}, \ldots; \mathbf{p}')\rangle \tag{4.9}$$

and

$$-i\sum_{j=A+1}^{A+A'} \nabla_j |(\vec{\alpha}_1, \ldots; \mathbf{p}), (\vec{\alpha}_{A+1}, \ldots; \mathbf{p}')\rangle = \mathbf{p}'\, |(\vec{\alpha}_1, \ldots; \mathbf{p}), (\vec{\alpha}_{A+1}, \ldots; \mathbf{p}')\rangle \quad . \tag{4.10}$$

In the above example the situation with two-nuclei state is shown, which is appropriate for describing the initial state in pionic fusion. The final state containing just one fused nucleus is constructed analogously.

Due to the finite range of the interaction, the overall normalization $\mathcal{N}$ of the state (4.8) that contains several moving nuclei, is just a product of normalizations for each of the constituent nuclei individually. It is useful to write the CM coordinates separately from the relative coordinates of the nucleons

$$|(\vec{\alpha}_1; \vec{\alpha}_2; \ldots \vec{\alpha}_A; \mathbf{r})_v\rangle = |(\vec{\alpha}_{\rm CM} = (0,0,0); \mathbf{r})_{v\sqrt{A}}\rangle\, |\psi_{\rm rel}\rangle \quad . \tag{4.11}$$

The relative coordinate wave function $|\psi_{\rm rel}\rangle$ can be complicated but the CM part for the ground state nucleus is simply represented by the unphysical ground state oscillation of the center of mass in the effective harmonic potential with the parameter

$v\sqrt{A}$. This is removed by a projection (4.8) onto the correct momentum state. The normalization integral can be expressed as

$$\mathcal{N}^2 = \int\int d^3r\, d^3r' \langle(\vec{\alpha}_{\rm CM};\mathbf{r}')_{v\sqrt{A}}|(\vec{\alpha}_{\rm CM};\mathbf{r})_{v\sqrt{A}}\rangle\, \langle\psi_{\rm rel}|\psi_{\rm rel}\rangle e^{i\mathbf{p}(\mathbf{r}-\mathbf{r}')}$$
$$= \int d^3r \int d^3r' e^{-A(\mathbf{r}-\mathbf{r}')^2v^2/4} e^{i\mathbf{p}(\mathbf{r}-\mathbf{r}')} = \left(\frac{4\pi}{v^2A}\right)^{3/2} V e^{-p^2/Av^2} \quad . \tag{4.12}$$

A different method of calculating the normalization along with further justification of this form for the CM part of the wave function is discussed in Appendix 4.7.2. We also note here that with a slight modification of Eq. (4.12) the orthogonality of the nucleon wave functions can be shown

$$\langle(\vec{\alpha}_1;\vec{\alpha}_2;\ldots\vec{\alpha}_A;\mathbf{p}')_v|(\vec{\alpha}_1;\vec{\alpha}_2;\ldots\vec{\alpha}_A;\mathbf{p})_v\rangle = \mathcal{N}^2\delta_{\mathbf{p},\,\mathbf{p}'}\,.$$

4.3 Fusion reactions $A + A \to 2A + \pi$

For the remainder of the paper we will assume A to be the mass number of each of the initial nuclei with proton-neutron composition (Z,N) and w the oscillator parameter. The entire initial state is characterized by a set of the single-particle quantum numbers $\{\vec{\alpha}_i\}$. The fusion product has $2A = A_f$ nucleons, the oscillator parameter v, and the final state quantum numbers $\{\vec{\beta}_i\}$. The collision is considered in the CM reference frame; therefore we use $\mathbf{p}$ and $-\mathbf{p}$ to denote the momenta of the incoming nuclei and $\mathbf{k}$ for a final pion momentum with corresponding $\mathbf{p}_f = -\mathbf{k}$ as the total momentum of the recoil nucleus. The integration of the wave functions leading to correct momenta, Eq. (4.8), is performed at a final stage so initially overlaps are calculated as functions of $\mathbf{r}$, $\mathbf{r}'$ and $\mathbf{R}$, the locations of the centers of the two initial nuclei and the final nucleus, respectively.

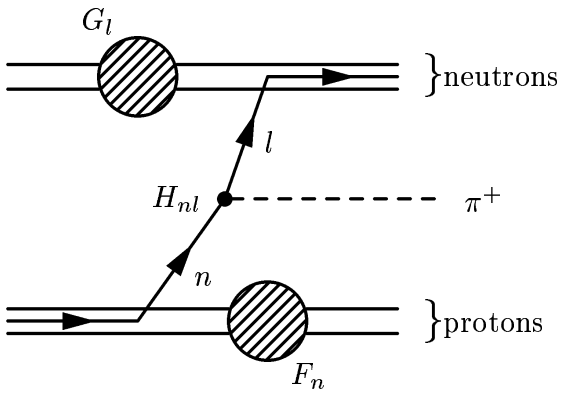

Figure 4.2: One of the amplitudes of the total fusion process: an initial proton from the nth orbit produces a π^+ and ends at the lth final neutron single-particle orbit. F_n is the remaining overlap of a proton system with the nth initial single-particle state missing. G_l is the neutron overlap with no lth state in the final system.

4.3.1 Charged pion production

We begin with the case of π^+ production where one of the initial protons interacts with the pion field producing a neutron and a real on-shell pion. With the assumption that the pion was produced in a single-particle interaction, the total amplitude of the process becomes a sum over all possible amplitudes shown in Fig. 4.2, with the pion vertex connecting any of the initial protons to any of the final state neutrons with the correct relative sign to preserve antisymmetry. Suppose the interacting proton in the single-particle state n produced a neutron in the state l of the final nucleus. In the initial state we sum over the occupied orbitals of the first and the second colliding nucleus, for $n \leq Z$ and for $Z < n \leq 2Z$, respectively. We use the notations $G_l(r, r', R)$ for the neutron overlap

$$G_l = \langle \underbrace{(\vec{\beta}_1, \tilde{s}_1; \ldots \vec{\beta}_{l-1}, \tilde{s}_{l-1}; \vec{\beta}_{l+1}, \tilde{s}_{l+1}; \ldots; \mathbf{R})}_{\text{no } l\text{th s.p. state}} | (\vec{\alpha}_1, s_1; \ldots; \mathbf{r})(\vec{\alpha}_{A+1}, s_{A+1}; \ldots; \mathbf{r}') \rangle \,, \tag{4.13}$$

$F_n(r, r', R)$ for the proton overlap

$$F_n = \langle(\vec{\beta}_1, \tilde{s}_1; \ldots; \mathbf{R})| \underbrace{(\vec{\alpha}_1, s_1; \ldots; \vec{\alpha}_{n-1}, s_{n-1}; \vec{\alpha}_{n+1}, s_{n+1}; \ldots)}_{\text{no } n\text{th s.p. state}}\rangle \,, \tag{4.14}$$

and $H_{n\,l}$ for a single-particle matrix element

$$H_{n\,l} = \begin{cases} \langle(\vec{\beta}_l, \tilde{s}_l; \mathbf{R})|g\,\vec{\sigma}\cdot\mathbf{k}\,e^{-i\mathbf{k}\cdot\mathbf{x}}|(\vec{\alpha}_n, s_n; \mathbf{r})\rangle & n \le Z \\ \langle(\vec{\beta}_l, \tilde{s}_l; \mathbf{R})|g\,\vec{\sigma}\cdot\mathbf{k}\,e^{-i\mathbf{k}\cdot\mathbf{x}}|(\vec{\alpha}_n, s_n; \mathbf{r}')\rangle & n > Z \end{cases} . \tag{4.15}$$

Finally, following Eq.(4.5), the total amplitude can be expressed in terms of the following sum:

$$\langle F|H|I\rangle = \frac{1}{\mathcal{N}_i\mathcal{N}_f}\frac{1}{\sqrt{2\omega V}}\frac{1}{2m}\int\int d^3r\, d^3r'\, d^3R \sum_{nl}(-1)^{n+l}F_nG_lH_{nl}e^{i\mathbf{p}(\mathbf{r}-\mathbf{r}')-i\mathbf{p}_f\cdot\mathbf{R}} \tag{4.16}$$

The determinants of the matrices are constructed from a product of the single-particle overlaps of size $(2N)\times(2N)$ for the neutrons (G_l) and $(2Z-1)\times(2Z-1)$ for the protons (F_n). The Gaussian nature of the single-particle overlaps allows one to separate all exponential factors that govern the general trend of the cross section leaving only some polynomials of a general form that carry spin, isospin and Pauli blocking information. These mathematical manipulations are discussed in some detail in Appendix 4.7.2. Here we present a final expression for the square of the transition amplitude

$$|\langle F|H|I\rangle|^2 = \frac{2g^2}{V^2}\left(\frac{2\pi}{v^2A}\right)^{3/2}\frac{|\mathbf{k}|^2\,\xi}{\omega m^2}\,\eta^{6(A-1)}\,|M_+|^2 \,, \tag{4.17}$$

in which the exponential factor ξ, effective oscillator parameter η and reduced amplitude M_+ are introduced as follows

$$\xi \equiv \exp\left(-\frac{2p^2}{Av^2} - \frac{k^2}{v^2+w^2} - \frac{k^2(w^2-v^2)}{2Av^2(v^2+w^2)}\right) \quad , \tag{4.18}$$

$$\eta \equiv \frac{2vw}{v^2+w^2} \quad , \tag{4.19}$$

and

$$M_+ \equiv P(k,p)e^{\mathbf{p}\cdot\mathbf{k}/Av^2} + Q(k,p)e^{-\mathbf{p}\cdot\mathbf{k}/Av^2} \,. \tag{4.20}$$

Here, P and Q are dimensionless polynomials of p and k, the total CM momentum of the initial nuclei and the final pion momentum. The polynomials are to be determined using particular configurations of the initial and final nuclei. They are also functions of v and w which determine the appropriate momentum scale. If the two colliding nuclei have the same initial shell model state then $P(k,p) = \pm Q(k,-p)$ (the phase difference given by $\pm$ sign for even or odd Z, respectively, is due to imposed Pauli antisymmetry, see Appendix 4.7.2). The procedure of analytically calculating P and Q involves finding the determinants of the matrices constructed from polynomials that result from integrating a product of Hermite polynomials of the form $\langle(\beta,R)|(\alpha,r)\rangle$; and performing the integrational Fourier-type conversion, Eqs. (4.8). This process is discussed in Appendix 4.7.3. The size of the matrices is determined by the number of nucleons of the same spin-isospin type.

4.3.2 Neutral pion production

The case of π^0 production can be considered in a similar fashion. A neutral pion can be produced either by one of the protons or by one of the neutrons, which couple with a negative relative sign. Compared to charged pions the coupling is larger by a factor $\sqrt{2}$. The final amplitude can then be expressed, similarly to Eq. (4.17), as

$$|\langle F|H|I\rangle|^2 = \frac{g^2}{V^2}\left(\frac{2\pi}{A\,v^2}\right)^{3/2}\frac{|\mathbf{k}|^2\,\xi}{\omega m^2}\,\eta^{6(A-1)}\,|M_0|^2\ . \tag{4.21}$$

Here the reduced amplitude can be split into a proton and a neutron part:

$$M_0 = P_p(k,p)e^{\mathbf{p}\cdot\mathbf{k}/Av^2}+Q_p(k,p)e^{-\mathbf{p}\cdot\mathbf{k}/Av^2}-P_n(k,p)e^{\mathbf{p}\cdot\mathbf{k}/Av^2}-Q_n(k,p)e^{-\mathbf{p}\cdot\mathbf{k}/Av^2}\ . \tag{4.22}$$

4.4 Low pion momentum approximation

Due to the specific form of the polynomials discussed above, further simplifications can be made for the case of π^0 production. Near the absolute threshold, the pion

momentum $|\mathbf{k}|$ is small compared to all other momentum parameters $|\mathbf{p}|$, v and w, and can be ignored in polynomials. Then

$$H_{n\,l} = \langle (\vec{\beta}_l, s_l; \mathbf{R})_v | \vec{\sigma} \cdot \mathbf{k}\, e^{-i\mathbf{k}\cdot\mathbf{x}} | (\vec{\alpha}_n, s_n; \mathbf{r})_w \rangle$$
$$\approx \langle s_l | \vec{\sigma} \cdot \mathbf{k} | s_n \rangle \, \langle (\vec{\beta}_l; \mathbf{R})_v | (\vec{\alpha}_n; \mathbf{r})_w \rangle \exp\left(\frac{-k^2}{2(v^2+w^2)} - \frac{i\mathbf{k}\cdot(\mathbf{R}v^2 + \mathbf{r}w^2)}{(v^2+w^2)} \right) . \quad (4.23)$$

With this approximation, the interaction part is factorized into exponents as shown in the expression above. Therefore the total pionic fusion amplitude is a product of a pure fusion amplitude and the expression that arises from the operator $\vec{\sigma} \cdot \mathbf{k}$ acting on the nucleons. For a given type of the initial and final nucleon, the sum of a single-particle matrix element multiplied by the corresponding overlap of the remaining particles reduces to a sum of matrix elements multiplied by the corresponding minor which is related to a determinant of a full matrix. It is shown in Appendix 4.7.3 that the polynomials can be expressed in an analytical form if all inner harmonic oscillator shells are completely filled without any gaps in all participating nuclei. This restriction allows any type of particle-hole excitations within the outer unfilled shell.

The total differential cross section for neutral pion production close to absolute threshold is given by the form:

$$\frac{d\sigma}{d\Omega} = \frac{g^2 A k^3}{(2\pi)^2 2pm} \left(\frac{2\pi}{A\,v^2} \right)^{3/2} \eta^{6(A-1)+\mathcal{Q}_f+\mathcal{Q}_i} \left(\frac{4w}{Av} \right)^{\mathcal{Q}_f-\mathcal{Q}_i} e^{-2p^2/Av^2} \times$$
$$\left| 2^{q_z/2} T_{q_z} \left(ip\sqrt{\frac{2}{A\eta v w}} \right) (q_x-1)!!\,(q_y-1)!! \right|^2 \frac{1}{\gamma^2} \left| \tilde{M} \right|^2 . \quad (4.24)$$

Here the integers q_j, $j = x, y, z$ are introduced as differences between numbers of quanta in final and initial systems for three Cartesian directions; $\mathcal{Q}_i$ and $\mathcal{Q}_f$ are total numbers of quanta in initial and final systems. These values are defined as

$$q_j = \sum_{\text{nucleons}} \beta_j - \sum_{\text{nucleons}} \alpha_j\,, \quad \mathcal{Q}_i = \sum_{\text{nucleons}} (\alpha_x + \alpha_y + \alpha_z)\,, \quad \mathcal{Q}_f = \sum_{\text{nucleons}} (\beta_x + \beta_y + \beta_z)\,. \quad (4.25)$$

The spin and radial parts of the wave function are completely decoupled in our non-relativistic description of the nucleon system. This allows one to introduce the matrix element used in Eq. (4.24)

$$\tilde{M} = \frac{1}{|\mathbf{k}|} \langle \tilde{f} | \sum_{\text{nucleons}} \tau_z \, \vec{\sigma} \cdot \mathbf{k} | \tilde{i} \rangle \,, \tag{4.26}$$

where $\tilde{i}$ and $\tilde{f}$ are the spin-isospin parts of nucleon wave function of the initial and final systems, respectively. This matrix element could be directly computed for every particular nuclear configuration, but for a large number of states, degenerate within the harmonic oscillator model, it is useful to use an approximation for the average

$$\overline{\tilde{M}} \; = \; \overline{(Z_\uparrow - Z_\downarrow - N_\uparrow + N_\downarrow)} \,. \tag{4.27}$$

The Cartesian directions of the harmonic oscillator quantization axes are chosen in such a way that the z axis coincides with the beam direction, though the spin is quantized along the $\mathbf{k}$ axis, simplifying the action of $\vec{\sigma} \cdot \mathbf{k}$ which is used to obtain Eq. (4.27). Integers $Z_\uparrow$, $Z_\downarrow$, $N_\uparrow$ and $N_\downarrow$ are mean numbers of particles for each spin-isospin combination with respect to our axis of spin quantization. The polynomials $T_n(x)$, defined in Eq. (4.36) of Appendix 4.7.1, can be approximated as

$$2^{q_z/2} T_{q_z} \left(ip \sqrt{\frac{2}{A\eta v w}} \right) \; \approx \; \left(ip \sqrt{\frac{2}{A\eta v w}} \right)^{q_z} \quad . \tag{4.28}$$

This approximation is valid in the limit that the arguments become large and allows for a better quantitative understanding of the behavior of the cross section. The value of the argument is almost independent of the mass number A at threshold energy:

$$p \sqrt{\frac{2}{A\eta v w}} \; \approx \; 6 \,.$$

In Eq. (4.24) only the lowest order term in the pion momentum is retained resulting in a p-wave cross section (exponents with k are also ignored). The equation has only one numerical parameter γ, the origin of which is discussed in Appendix

4.7.3. This parameter is a product of four factors, one for every spin/isospin nucleon species. Each factor depends on the number of particles of corresponding type and on their distribution within the highest harmonic oscillator shell for both initial and final nuclei. Numerically, γ ranges from 1 to 10 for light nuclei. The cross section can be zero if some symmetries are not preserved (spin, isospin, oscillator symmetry) as well as by virtue of Eq. (4.39) in Appendix 4.7.1 if creation of the final system requires an odd number of quanta relative to the initial system in any of the transverse directions.

4.5 Application of the model and results

4.5.1 The reaction $p + p \to d + \pi^+$

The first and the simplest example to calculate is the two-nucleon fusion reaction $p + p \to d + \pi^+$. This example serves here only for illustrative purpose as we do not include pion rescattering due to the full interaction given by Hamiltonian density of Eq. (4.2) which is important for this elementary process. Moreover, the deuteron can hardly be approximated with the harmonic oscillator shell model. The polynomials P and Q, Eq. (4.20), in this case do not depend on p being equal to the matrix element of $\vec{\sigma} \cdot \mathbf{k}/|\mathbf{k}|$ evaluated between the spinors of initial interacting proton and final neutron. Here, P and Q correspond to the choice of the first or second initial proton to produce a pion, respectively.

Dominant partial wave channels are summarized in the following table along with our results for their reduced amplitudes. The table was constructed by separation of initial singlet and triplet states of the NN system. The table shows partial waves of the $\pi - d$ system printed in the left column that yield the dominant contributions to

the amplitudes which are shown in the right column.

pion	NN state	amplitude
$s-$wave	${}^3P_1$	$2\sqrt{2}\,\sinh(\frac{k\,p\,\cos\theta}{A\,v^2})$
$p-$wave	${}^1S_0$	$2\,\cosh(\frac{k\,p\,\cos\theta}{A\,v^2})$
$p-$wave	${}^1D_2$	

(4.29)

As can be seen from the table above, this cross section is predominantly p-wave in nature at low pion energies. The s-wave contribution that comes [92] from rescattering of the pion due to the interaction (4.2) was not included. The total cross section averaged over spin projections in the initial state and summed over final states is

$$\frac{d\sigma}{d\Omega} = \frac{g^2\,k^3}{2\,m\,p\,\sqrt{2\,\pi}\,v^3}\exp\left(-\frac{4\,p^2+k^2}{2\,v^2}\right)\left[3\,\cosh\left(\frac{2\,k\,p\,\cos\theta}{v^2}\right)-1\right] \quad . \tag{4.30}$$

The obtained p-wave cross section behaves at low energies as

$$\sigma(pp\to d\pi^+) = \tilde{\sigma}\,(k/m_\pi)^3\ , \tag{4.31}$$

where

$$\tilde{\sigma} = \frac{2\sqrt{2\pi}g^2 m_\pi^{5/2}}{m^{3/2}v^3}e^{-2mm_\pi/v^2}\ . \tag{4.32}$$

Choosing the oscillator parameter $v = 216$ MeV/c reproduces the experimental value[94], $4\tilde{\sigma} \approx 0.42$ fm^2. For this case the fusion is sensitive to the tail of the wave function in momentum space. Since the wave function of a deuteron is extremely non-Gaussian with a long tail in coordinate space, choosing v to reproduce the deuteron's r.m.s. charge radius would result in a grossly underpredicted cross section. For the fusion of heavier ions, the incoming nuclei are moving at a slower velocity and their momenta per nucleon are similar to characteristic momentum scales of the wave functions.

The oscillator parameter v can be best obtained by matching the harmonic oscillator type deuteron wave function used here to its experimentally known behavior [94]. The choice of this parameter between 180 and 220 fm would lead to the values of $4\tilde{\sigma}$ in the range of 0.06 to 0.48 fm^2.

4.5.2 The reaction ^{3}He + ^{3}He $\rightarrow$ ^{6}Li + π^+

As a next step, we apply the model to the experimentally studied pionic fusion reaction ^{3}He + ^{3}He $\rightarrow$ ^{6}Li + π^+, where even first excited states of the ^{6}Li nucleus have been resolved [81]. This reaction involves heavier nuclei so that the process of pion rescattering becomes less important as discussed above. The polynomials P and Q for Eq. (4.20) can be constructed in a direct way considering the shell model structure of all nuclei involved in the reaction. The ground 1^+ and first excited 3^+ states of ^{6}Li were constructed within the $p_{3/2}$ j-subshell. In Fig. 4.3, the total cross section for this reaction is calculated for fusion into the ground state (left panel) and the first excited state (right panel). The contributions of the s-wave and p-wave to the cross section are plotted together. We choose a value $v = 118.91$ MeV/c for ^{6}Li as it corresponds to the oscillator frequency of 15.06 MeV, the parameter of the MK3W model [95]. The initial parameter $w = 112.7$ MeV/c was chosen by assuming the r.m.s. size 2.14 fm of ^{3}He. In Fig. 4.4 we show the differential cross section for this fusion reaction going into the ground state of ^{6}Li (solid line) and the first excited state (dashed line). The beam energy is assumed to be fixed so that the corresponding absolute values of the pion momentum are 96 and 90 MeV/c, respectively.

Comparison with the experiment [81] in which pionic fusion resolves the few lowest levels of ^{6}Li shows that we obtain a reasonable ratio of the cross sections. However, we underpredict the magnitude by approximately 40%, compared to the estimated experimental value of 111 ± 11 nb for the ground state transition. We note that the result is extremely sensitive to parameters of the shell model, and their choice in the harmonic oscillator approximation is quite uncertain for light nuclei. For example, a variation of the final oscillator frequency within 10% range of the used value would lead to values of the cross section between about 20 and 140 nb. Using more realistic non-Gaussian wave functions might significantly improve the model. We might also

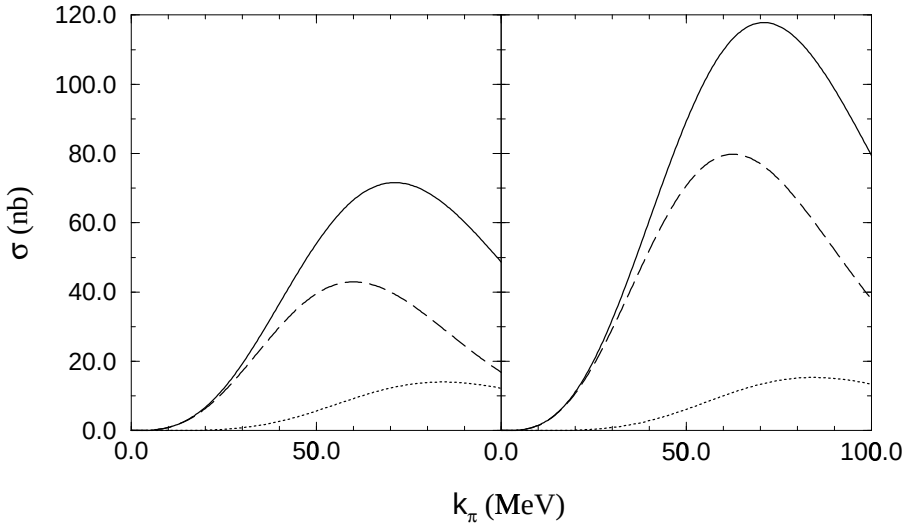

Figure 4.3: Reaction cross sections for ^{3}He + ^{3}He $\rightarrow$ ^{6}Li + π^+. The left panel shows the transition to the ground state and the right panel to the first excited state of ^{6}Li at 2.18 MeV. The solid lines represent the total cross section, dashed and dotted lines are p and s-waves, respectively.

be underestimating the cross section due to inherent limitations of the approach. For instance, we do not consider a gradual change of the nuclear mean field in the process of fusion substituting it with the sudden approximation.

4.5.3 The reaction ^{12}C + ^{12}C $\rightarrow$ ^{24}Mg + π^0

Here we apply our approach to the cross section of the ^{12}C + ^{12}C $\rightarrow$ ^{24}Mg + π^0 reaction. This process, along with its isospin analog ^{12}C + ^{12}C $\rightarrow$ ^{24}Na + π^+, represents those few heavy ion pionic fusion reactions for which experimental data exist [80]. The application of the developed theory does not present a great difficulty except for the fact that the cross section is quite dependent on the structure of the initial and final states of the interacting nuclei. Within the harmonic oscillator picture we have approximately 3×10^8 different combinations of interacting states that correspond

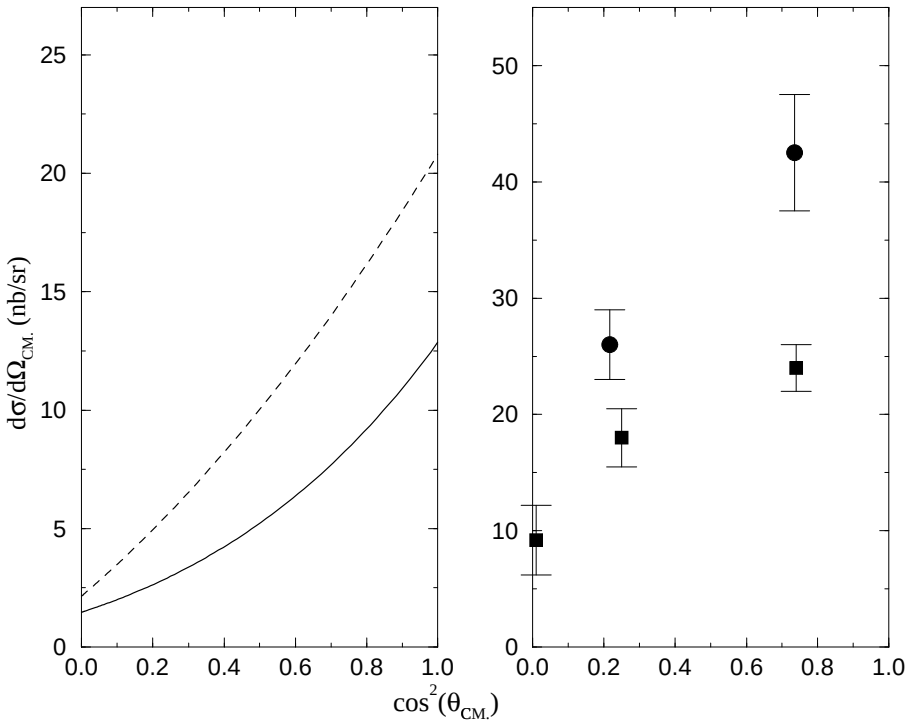

Figure 4.4: Differential cross section of the reaction ^{3}He + ^{3}He $\rightarrow$ ^{6}Li + π^+. On the left panel the solid line represents the transition to the ground state of ^{6}Li and the dashed line to the first excited state; the corresponding absolute values of pion momentum are 96 and 90 MeV/c, respectively. The right panel displays the experimentally observed values [2] of the differential cross section of the transition to the ground state (squares) and to the first excited state (circles) of ^{6}Li.

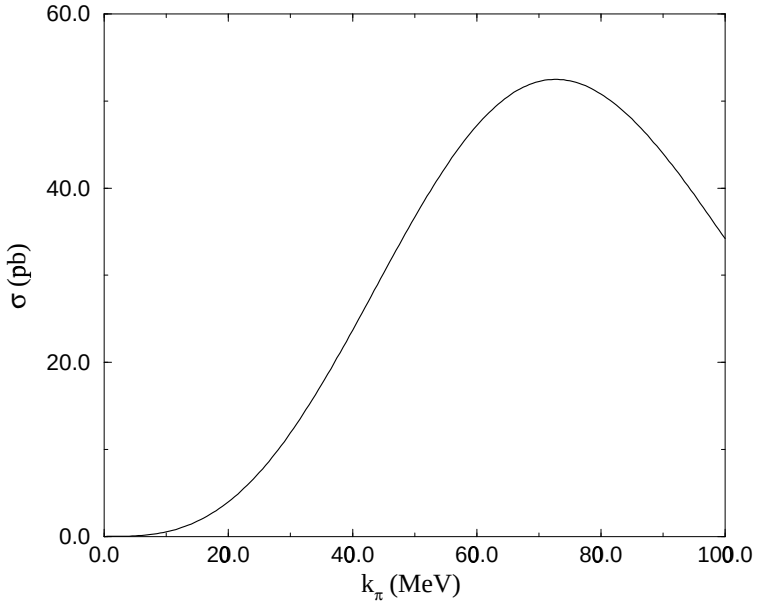

Figure 4.5: The reaction cross section for $^{12}C + {}^{12}C \rightarrow {}^{24}Mg + \pi^0$ with oscillator parameters $v = 104$ MeV/c and $w = 119$ MeV/c as a function of pion momentum.

to the same energy. Angular momentum and isospin conservation constraints reduce this number by several orders of magnitude. Additional shell model interactions have to be introduced to build up a realistic nuclear state for each of the nuclei and reduce this large number of states, that are degenerate in our model, to the ones of interest. Based on this argument we will present here the Monte-Carlo averaged cross section, where we average over random Cartesian states. In the following Fig. 4.5 we display the total reaction cross section as a function of pion momentum. We use here the oscillator parameters $v = 104$ MeV/c and $w = 119$ MeV/c which are estimated by various theoretical models [96, 97]. The experimentally estimated cross section for this reaction is 208 ± 38 pb which was observed for pion momentum of 41 MeV/c [80]. In this example we again underestimate the cross section. To see the sensitivity of our results we present in Fig. 4.6 the dependence of the cross section on oscillator parameters for pion energy at about 6 MeV (momentum 41 MeV/c). This

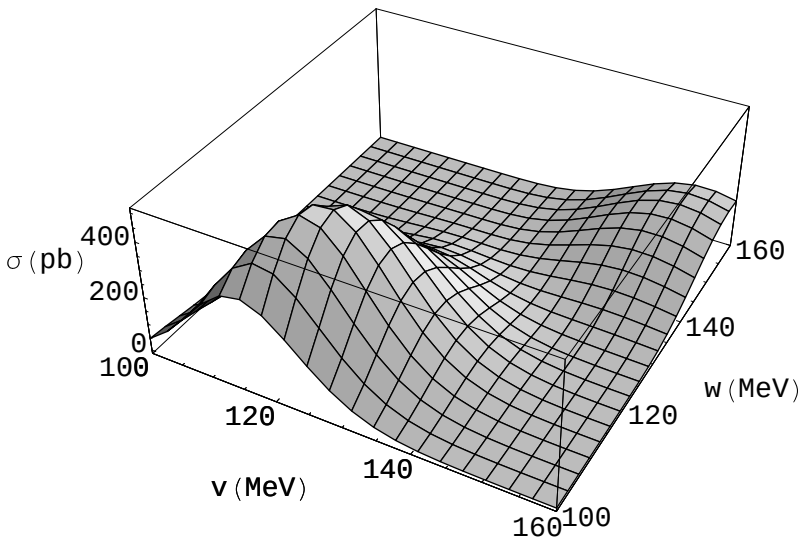

Figure 4.6: The total cross section of $^{12}\mathrm{C} + {}^{12}\mathrm{C} \to {}^{24}\mathrm{Mg} + \pi^0$ as a function of the model parameters v and w. The calculation is done for a pion momentum 41 MeV/c which corresponds to the total energy of about 6 MeV above threshold.

figure indicates that a reasonable variation of parameters could cause a change in the answer by an order of magnitude. We emphasize again that in our calculations we did not project the participating nuclei onto appropriate shell-model states. Such a projection would require additional nuclear structure input. Given that the existing experimental data do not clearly resolve the structure of the final state this seems sufficient. As a conclusion, within all the limitations discussed above, the agreement between the introduced theory and the experimental results of this rare process seems to be remarkable.

4.5.4 Calculations for heavy nuclei

In this section we apply the low-momentum approximation for the cross section described by Eq. (4.24) to several reactions, with the goal of understanding the general dependence with respect to the mass of the incoming nuclei. In order to calculate the

cross section, one needs the harmonic oscillator parameter v which can be estimated from the experimentally determined r.m.s. radii of the nuclei[99],

$$r^2_{\text{r.m.s.}} = \frac{1}{A}\sum_i \left\langle r_i^2 \right\rangle = \frac{1}{A}\sum_i \frac{1}{v^2}\left(\alpha_i + \frac{3}{2}\right). \tag{4.33}$$

In order to calculate the cross section, one needs to know the incoming energy of the nuclei as well as the energy of the outgoing pion. Calculations of the cross sections were performed for incoming nuclei ^{9}Be, ^{12}C, ^{16}O and ^{20}Ne with corresponding fusion products ^{18}O, ^{24}Mg, ^{32}S and ^{40}Ca in the limit of low pion momentum. In this limit the cross section is proportional to the cube of the pion momentum,

$$\sigma = \tilde{\sigma}(k^3/m_\pi^3). \tag{4.34}$$

Values of $\tilde{\sigma}$ are displayed as a function of the mass number of the incoming nuclei in Figure 4.7. The shell model configurations are again randomly chosen from the available set of Cartesian states that conserve isospin and parity. Average values are represented by filled diamonds while the states with the highest and lowest cross sections are represented by the boundaries of the error bars. The large error bars demonstrate the wide fluctuation in strengths for individual states. However, despite the fluctuations, it is clear that the overall trend is of a decreasing cross section with increasing mass.

Also shown in Figure 4.7 are experimental measurements represented by open circles for the pp, ^{3}He^{3}He and ^{12}C^{12}C cases discussed previously. The corresponding calculations, which were performed for the experimentally measured pion momenta rather than in the low-momentum limit are also displayed with closed circles. One sees that the cross sections fall by several orders of magnitude, but the measurements are still feasible throughout the wide range of masses. Calculations could be performed for heavier nuclei, but for larger masses the Coulomb barrier becomes important, and shuts off the possibility of fusion for masses larger than 20.

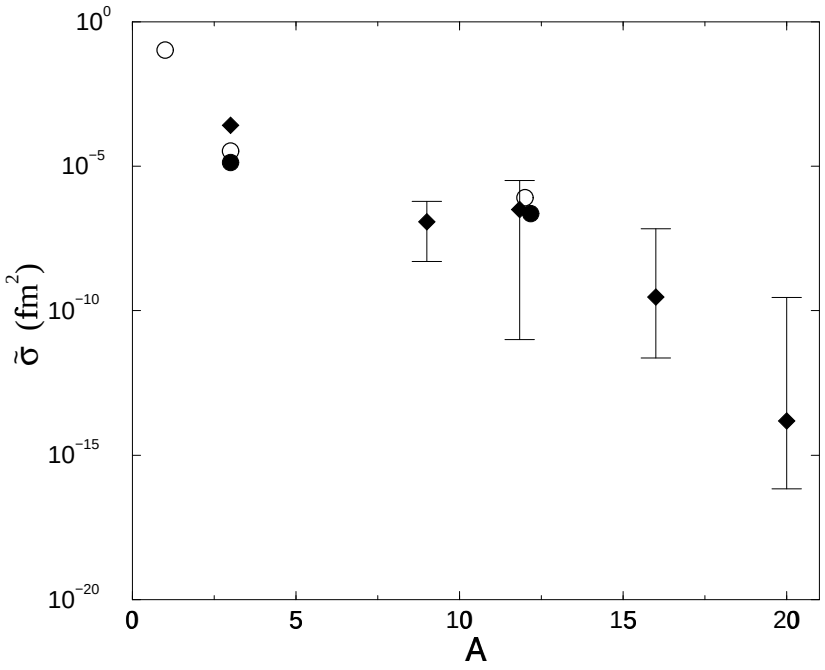

Figure 4.7: The general behavior of the pionic fusion cross section $A + A \rightarrow 2A + \pi$ versus the mass number of initial nucleus A. The plotted value $\tilde{\sigma}$ is related to a total cross section as $\sigma = \tilde{\sigma}\,(k/m_\pi)^3$. Calculations in the low-momentum limit (filled diamonds) show that cross sections fall by several orders of magnitude in this mass range, but remain in the picobarn region for nuclei as large as oxygen. The highest and the lowest cross section found within the shell model configurations are represented by error bars. Experimental measurements are displayed (open circles) and compared to calculations (filled circles) which were performed for the finite pion momenta corresponding to the experiments.

4.6 Conclusions

Near threshold meson production represents a unique area of heavy ion reactions. In this area the reactions underline the pronounced features of quantum many-body physics. Most theoretical approaches to understanding and predicting these phenomena lose their validity in such an extreme regime. In this paper we have proposed a simple model to study the processes of deep subthreshold pion production. The pionic fusion cross section was obtained in a Born approximation with respect to pion production and in the sudden approximation for the nuclear rearrangement. The participating nuclei were described by the harmonic oscillator shell model in moving oscillator potentials. The advantage of the method is that it allows one to incorporate energy, momentum, spin and isospin conservation laws precisely and respect the Pauli principle at all steps of the calculation. Further aspects of nuclear structure could be additionally taken into account. At threshold energies these constraints pose the most powerful restriction on the reaction and cannot be ignored as is done in statistical and kinetic models which are reasonable at higher energy. The obvious disadvantage of the model is that the sudden approximation does not consider the slow changes of the nuclear mean field in the process of interaction. For the future developments it seems feasible to incorporate the time dependence and solve the equations for the evolution of the nuclear mean field.

The nearly analytical form of overlaps greatly simplified the calculations for this study. We used a spherically symmetric nuclear mean field but in some cases this symmetry prohibits the transition and this would require a consideration of deformations, i.e., different oscillator parameters for different directions. The above mentioned limitations are reflected by the difficulty in determining the parameters of the model, and lead to about an order of magnitude ambiguity in the results for *s-d* shell nuclei. More realistic single-particle wave functions could be incorporated into the model. Some of

the exponential factors in Eq. (4.18) arise directly from the Fourier transformation of the Gaussian tails in harmonic oscillator wave functions and could be substituted with modified factors that would reflect a more realistic behavior.

We would like to stress here again that pionic fusion is a very rare process presenting a tiny fraction of the total cross section. The agreement that was observed between calculations and experimental data for the cross sections ranging from 10^{-4} to 10^{-9} barns is remarkable. Within the limits of the low pion momentum approximation in the class of the reactions $A+A \to 2A+\pi$, we were able to obtain a general formula, Eq. (4.24), for the cross sections. The proposed techniques can certainly be applied in the same manner to other pion production reactions. The processes of electrofission [100] present another interesting avenue to exercise this technique.

4.7 Appendix

4.7.1 Harmonic oscillator wave functions and overlaps

Work with harmonic oscillator wave functions often involves integrations of the expressions constructed of polynomials and Gaussian weights. Thus, the following integral is useful ($a > 0$),

$$\int_{\infty}^{+\infty} x^n e^{-ax^2+ibx}\, dx = \sqrt{\frac{\pi}{a}} e^{-b^2/4a} \quad a^{-n/2}\, T_n\left(\frac{ib}{2\sqrt{a}}\right) \quad , \tag{4.35}$$

where $T_n(x)$ is a sum arising from the binomial expansion,

$$T_n(x) = \sum_{j=0,2,4\ldots}^{n} \frac{n!(j-1)!!}{j!(n-j)!2^{j/2}} x^{n-j} \quad . \tag{4.36}$$

This expression can be used for the evaluation of any integral encountered in this work. There are two important limiting cases for the sum $T_n(x)$, $x \to 0$ and $x \gg 1$:

$$\lim_{x\to 0} T_n(x) = \begin{cases} \frac{(n-1)!!}{2^{n/2}} & \text{if } n \text{ is even} \\ 0 & \text{if } n \text{ is odd} \end{cases} \quad , \quad \lim_{x\to\infty} T_n(x) = 2^{-n/2}\, x^n \quad . \tag{4.37}$$

The Gaussian-Fourier integration of Eq. (4.35) is a transformation on the space of polynomials defined on the basis

$$x^n \to [x^n](p) = T_n(p) \tag{4.38}$$

The following two-dimensional integrals often appear in our calculations,

$$\int\int (x-y)^n e^{-a(x^2+y^2)} dx\, dy = \begin{cases} \pi a^{-1-n/2}(n-1)!! & \text{if } n \text{ is even} \\ 0 & \text{if } n \text{ is odd} \end{cases} , \tag{4.39}$$

$$\int\int (x-y)^n e^{-a(x^2+y^2)} e^{ip(x-y)} dx\, dy = \frac{\pi}{a}\left(\frac{2}{a}\right)^{n/2} e^{-p^2/2a} T_n\left(\frac{ip}{\sqrt{2a}}\right) . \tag{4.40}$$

The basic block of the calculations is the overlap of two one-dimensional harmonic oscillator wave functions with different oscillator parameters, shifted locations of the centers and a possible additional factor e^{-ikx} that enters the single-particle interaction integral from Eq.(4.5). This type of integral, the generalized Debye-Waller factor, can be written in a factorized form:

$$\langle(\beta;r)_v|e^{-ikx}|(\alpha;r')_w\rangle = \eta^{1/2} \times$$
$$\exp\left(\frac{-k^2}{2(v^2+w^2)} - \frac{(r-r')^2 v^2 w^2}{2(v^2+w^2)} - \frac{ik(rv^2+r'w^2)}{(v^2+w^2)}\right) P_{\beta\,\alpha}((r'-r),k;v,w)\,, \tag{4.41}$$

where η is given by Eq. (4.19) and $P_{n\,m}(r,k;v,w)$ is a dimensionless polynomial of r and k of the highest power $n+m$ with coefficients dependent on w and v. The following are examples of these polynomials for the smallest values of n and m:

$$P_{0\,0}(r,k;v,w) = 1\,,$$
$$P_{0\,1}(r,k;v,w) = P_{1\,0}(-r,k;w,v) = -\frac{\sqrt{2}\;(i\,k + r\,v^2)\;w}{v^2+w^2}\,,$$
$$P_{1\,1}(r,k;v,w) = \frac{2\,v\,w\;\left(v^2+w^2-(k-i\,r\,v^2)\;(k+i\,r\,w^2)\right)}{\left(v^2+w^2\right)^2}\,.$$

The technique of obtaining these expressions is simple though tedious. An important situation $k=0$ would correspond to the overlap of two wave functions without pion production, in this case we will not write k as an argument. It can be shown that [98]

$$P_{i\,j}(r;v,w) = \sum_{k+l=0,2,4\ldots}^{k=i,l=j} \sqrt{\frac{i!\,j!}{k!\,l!}}\,\frac{(-1)^{j-l}\,v^{j-l}\,w^{i-k}}{(i-k)!\;(j-l)!}\left(\frac{r\,\eta}{\sqrt{2}}\right)^{i+j-k-l} P_{k\,l}(0;v,w) \tag{4.42}$$

and

$$P_{kl}(0;v,w)=\sqrt{\frac{k!}{l!}}\mathcal{P}^{(l-k)/2}_{(k+l)/2}(\eta) \quad , \tag{4.43}$$

with $\mathcal{P}^{\beta}_{\alpha}$ being the associated Legendre polynomials. A bit simpler case is

$$P_{i\,j}(r;v=w=1)=\sqrt{\frac{i!j!}{2^{i+j}}}(-1)^j\sum_{k=0}^{min(i,j)}(-1)^k r^{i+j-2k}\frac{2^k}{k!(i-k)!(j-k)!} \quad . \tag{4.44}$$

Any three-dimensional overlap is reduced to the one-dimensional form of Eq. (4.41) in a direct way

$$\langle(\vec{\beta};\mathbf{R})|(\vec{\alpha};\mathbf{r})\rangle=\prod_{x=1,2,3}\langle(\beta_x;R_x)|(\alpha_x;r_x)\rangle \quad . \tag{4.45}$$

Similarly we introduce

$$\langle(\vec{\beta},\mathbf{r})|e^{-i\mathbf{k}\cdot\mathbf{x}}|(\vec{\alpha},\mathbf{r}\,')\rangle=\eta^{3/2}\times$$
$$\exp\left(\frac{-k^2}{2(v^2+w^2)}-\frac{(\mathbf{r}-\mathbf{r}\,')^2v^2w^2}{2(v^2+w^2)}-\frac{-i\mathbf{k}(\mathbf{r}v^2+\mathbf{r}\,'w^2)}{(v^2+w^2)}\right)P_{\vec{\beta}\,\vec{\alpha}}((\mathbf{r}\,'-\mathbf{r}),\mathbf{k};v,w) \tag{4.46}$$

where

$$P_{\vec{\beta}\,\vec{\alpha}}((\mathbf{r}\,'-\mathbf{r}),\mathbf{k};v,w)=\prod_{x=1,2,3}P_{\beta_x\,\alpha_x}(r'_x-r_x,k_x;v,w) \quad . \tag{4.47}$$

4.7.2 Calculational details of the $A+A\to 2A+\pi^+$ reaction

Overlaps of many-body nucleon wave functions can be expressed in our approximation by a determinant of single-particle overlaps:

$$\langle(\vec{\beta}_1,\ldots,\vec{\beta}_n;\mathbf{R})|(\vec{\alpha}_1,\ldots;\mathbf{r})(\ldots;\mathbf{r}\,')\rangle=\begin{vmatrix}\langle(\vec{\beta}_1;\mathbf{R})|(\vec{\alpha}_1;\mathbf{r})\rangle & \cdots & \langle(\vec{\beta}_1;\mathbf{R})|(\vec{\alpha}_n;\mathbf{r}\,')\rangle\\ \vdots & \ddots & \vdots\\ \langle(\vec{\beta}_n;\mathbf{R})|(\vec{\alpha}_1;\mathbf{r})\rangle & \cdots & \langle(\vec{\beta}_n;\mathbf{R})|(\vec{\alpha}_n;\mathbf{r}\,')\rangle\end{vmatrix} . \tag{4.48}$$

Eq. (4.46) allows one to take identical exponential multipliers in each row outside the determinant as a common factor in all calculations leaving only the matrix of polynomials $P_{\vec{\beta}\,\vec{\alpha}}$ to be evaluated. A simple example of this is the calculation of the normalization:

$$\langle(\vec{\alpha}_1,\vec{\alpha}_2\ldots\vec{\alpha}_A;\mathbf{r})_v|(\vec{\alpha}_1,\vec{\alpha}_2\ldots\vec{\alpha}_A;\mathbf{r}\,')_v\rangle=||P(\mathbf{r}-\mathbf{r}\,';v,v)||e^{-A(\mathbf{r}-\mathbf{r}\,')^2v^2/4}\,e^{i\mathbf{p}(\mathbf{r}-\mathbf{r}\,')}\,. \tag{4.49}$$

In this expression $||P(\mathbf{r}-\mathbf{r}';v,v)||$ is a determinant of a matrix with the entries $P_{\vec{\alpha}_i\,\vec{\alpha}_j}$. As discussed in Sect 4.2, this overlap is equal to that of the CM wave functions of two harmonic oscillators located at $\mathbf{r}$ and $\mathbf{r}'$. For a nucleon system in the lowest state (in terms of harmonic oscillator shell excitations), the CM wave function is the harmonic oscillator wave function of the ground state $|(0,\mathbf{r})_\varsigma\rangle$. We obtain an interesting mathematical fact

$$||P(\mathbf{r}-\mathbf{r}';v,v)|| = P_{0\,0}(\mathbf{r}-\mathbf{r}';\varsigma,\varsigma) = 1\,. \tag{4.50}$$

Comparison of the exponents in Eq. (4.49) and Eq. (4.46) gives the value of the oscillator parameter for the center-of-mass oscillation as $\varsigma = v\sqrt{A}$.

With the same strategy, one can approach the calculation of the reaction $A+A \to 2A+\pi^+$ extracting all exponential factors. Corresponding values of the overlaps F_n,G_l and $H_{n\,l}$ may be rewritten, defining new polynomials f_n, g_l and $h_{n\,l}$:

$$F_n = \eta^{3(2Z-1)/2} \times \begin{cases} \exp\left(-\eta v w\left[Z(\mathbf{R}-\mathbf{r})^2 + (Z-1)(\mathbf{R}-\mathbf{r}')^2\right]/4\right)\ f_n & n \le Z\,, \\ \exp\left(-\eta v w\left[(Z-1)(\mathbf{R}-\mathbf{r})^2 + Z(\mathbf{R}-\mathbf{r}')^2\right]/4\right)\ f_n & n > Z\,; \end{cases} \tag{4.51}$$

$$G_l = \eta^{3(2N)/2} \exp\left(-N\eta v w\left[(\mathbf{R}-\mathbf{r})^2 + (\mathbf{R}-\mathbf{r}')^2\right]/4\right)\ g_l\,,$$

$$H_{nl} = \eta^{3/2} \exp\left(-\frac{(\mathbf{R}-\mathbf{r})^2 v^2 w^2 + \mathbf{k}^2 + 2i\mathbf{k}\cdot(\mathbf{R}v^2 + \mathbf{r}w^2)}{2(v^2+w^2)}\right)\ h_{nl} \qquad (\text{if } n > Z,\ r \Leftrightarrow r')\,.$$

It is useful to notice here that all the polynomials are functions of distances between the nuclei $(\mathbf{r}-\mathbf{R})$ and $(\mathbf{r}'-\mathbf{R})$ that we will denote as $\mathbf{x}$ and $\mathbf{y}$ respectively. Considering integration in Eq. (4.16) over variables $\mathbf{x}$, $\mathbf{y}$ and $\mathbf{R}$ we observe from Eq. (4.51) that the oscillating phase has the form

$$\exp\left(\frac{-i\mathbf{k}\cdot(\mathbf{R}v^2 + \mathbf{r}w^2)}{(v^2+w^2)} + i\mathbf{p}(\mathbf{r}-\mathbf{r}') - i\mathbf{p}_f\cdot\mathbf{R}\right)$$
$$= \exp\left(i\mathbf{p}\cdot(\mathbf{x}-\mathbf{y}) - \frac{i\mathbf{k}\cdot\mathbf{x}w^2}{v^2+w^2} - i(\mathbf{k}+\mathbf{p}_f)\cdot\mathbf{R}\right)\,,$$

and integration over $\mathbf{R}$ gives a momentum preserving δ-function that requires $\mathbf{k} = -\mathbf{p}_f$. For convenience we split the sum in Eq. (4.16) over $n \le Z$ and $Z < n \le 2Z$

and substitute F, G and H from Eq. (4.51)

$$\langle F|H|I\rangle = \frac{1}{\mathcal{N}_i\mathcal{N}_f}\int \frac{V}{\sqrt{2\omega V}}\frac{1}{2m}\eta^{3A}\, e^{-Avw\eta(x^2+y^2)/4}\, e^{-k^2/2(v^2+w^2)}$$

$$= \left(e^{-i\mathbf{k}\cdot\mathbf{x}\eta w/2v} \sum_{i\le Z,\, j} (-1)^{i+j} f_i g_j h_{ij} + e^{-i\mathbf{k}\cdot\mathbf{y}\eta w/2v} \sum_{i>Z,\, j} (-1)^{i+j} f_i g_j h_{ij} \right) e^{-i\mathbf{p}\cdot(\mathbf{x}-\mathbf{y})} d^3x d^3y\,. \tag{4.52}$$

The terms $\sum f_i g_j h_{ij}$ are again some polynomials of $\mathbf{x}$ and $\mathbf{y}$ proportional to $|k|$ and containing parameters v and w. The final integration can be performed with the help of Eq. (4.35), the corresponding parameters a and b being

$$a = A\eta vw/4 \quad , \quad b = \pm\, p - k\eta w/2v \quad . \tag{4.53}$$

As a result, we arrive at the formula (4.17) with polynomials

$$P(k,p) = \frac{1}{|\mathbf{k}|}\left[\sum_{i\le Z,\, j} (-1)^{i+j} f_i g_j h_{ij}\right] \left(-i\,\frac{\mathbf{p}+\mathbf{k}\eta w/2v}{\sqrt{A\eta vw}}\,,\, \frac{i\mathbf{p}}{\sqrt{A\eta vw}} \right)\,,$$

$$Q(k,p) = \frac{1}{|\mathbf{k}|}\left[\sum_{i>Z,\, j} (-1)^{i+j} f_i g_j h_{ij}\right] \left(\frac{-i\mathbf{p}}{\sqrt{A\eta vw}}\,,\, i\,\frac{\mathbf{p}-\mathbf{k}\eta w/2v}{\sqrt{A\eta vw}} \right)\,, \tag{4.54}$$

where the first argument is the transformation of elements of vector $\mathbf{x}$ and the second that of vector $\mathbf{y}$. From here it is also seen that if before transformation there existed a symmetry between $\mathbf{x}$ and $\mathbf{y}$, i.e. the nuclei were in an identical state, then $P(\mathbf{k},-\mathbf{p}) = \pm Q(\mathbf{k},\mathbf{p})$.

4.7.3 Toward a complete analytical answer, the reaction $A + A \to 2A + \pi^0$

As it was pointed out in the main text, the amplitude of the pionic process is approximately proportional to the amplitude of the fusion reaction. One can study the properties of the determinants arising in a fusion reaction in a quite general way, separately considering the four types of particles distinguished by spin and isospin in

the reaction of fusion of the type $A + A \to 2A$. This leads to the following form of a single-particle overlap matrix

$$2A \left\{ \left(\begin{array}{cc} \langle(\vec{\beta}_1;\mathbf{R})|(\vec{\alpha}_1;\mathbf{r})\rangle \cdots & \cdots \langle(\vec{\beta}_1;\mathbf{R})|(\vec{\alpha}_A;\mathbf{r}')\rangle \\ \vdots & \vdots \\ \underbrace{\langle(\vec{\beta}_A;\mathbf{R})|(\vec{\alpha}_1;\mathbf{r})\rangle \cdots}_{\text{first } A \text{ nucleons}} & \underbrace{\cdots \langle(\vec{\beta}_A;\mathbf{R})|(\vec{\alpha}_A;\mathbf{r}')\rangle}_{\text{second } A \text{ nucleons}} \end{array} \right) \right. . \tag{4.55}$$

Without loss of generality, $\mathbf{R}$ can be set to zero. A second important feature is that in the nuclei under consideration all inner shells are filled. Therefore, the resulting determinant is a function of the nucleon number A and extra parameters arising from different ways to distribute the particles in the outer shells.

It is interesting to present the exact result for the one-dimensional case where the problem is uniquely defined. We consider two oscillators with single-particle states from 0 till $A-1$ overlapping with one larger oscillator with occupied states from 0 up to $2A-1$, see Eqs. (4.41) and (4.42),

$$\begin{vmatrix} P_{0\,0}(x;v,w) & \cdots & P_{0\,A-1}(y;v,w) \\ \vdots & \ddots & \vdots \\ P_{2A-1\,0}(x;v,w) & \cdots & P_{2A-1\,A-1}(y;v,w) \end{vmatrix}$$

$$= \frac{(-1)^A (w(x-y))^{A^2} \sqrt{(2\,A)!}}{2^{\frac{(A-1)\,A}{2}} \sqrt{A!} \left(\prod_{i=1}^{A} \frac{(2\,i)!}{i!}\right)} \eta^{(2A-1)A} = \frac{1}{\gamma} (w(x-y))^q \eta^{\mathcal{Q}} \quad , \tag{4.56}$$

$$\gamma(A) = \frac{(-1)^A \sqrt{A!}}{\sqrt{(2A)!}} 2^{(A-1)\,A/2} \left(\prod_{i=1}^{A} \frac{(2\,i)!}{i!}\right) . \tag{4.57}$$

The result is just a single term which depends only on the distance between the two initial oscillator locations raised to the power equal to the difference in total number of quanta between initial and final systems, $q = A^2$. The term $\eta = 2vw/(v^2+w^2)$ comes in the power of total number of quanta in the final nucleus, $\mathcal{Q} = (2A-1)A$. This remains true only for Fermi systems in the ground state, i.e. if there are no gaps in the harmonic oscillator single-particle level occupation. The situation for a three-dimensional oscillator is similar. The required polynomial is still given by one

term that has a form of the product

$$\frac{1}{\gamma}(x_x - y_x)^{q_x}(x_y - y_y)^{q_y}(x_z - y_z)^{q_z} w^{q_x+q_y+q_z}\, \eta^{\mathcal{Q}_f} \quad , \tag{4.58}$$

where integers q_x, q_y and q_z are differences of the number of quanta between the final and initial systems in the x, y and z directions, respectively. A specific three-dimensional complication arises from the following aspect. The lowest energy state is, in general, degenerate as for non-magic nuclei one has the freedom of placing several particles into $(n+1)(n+2)/2$ degenerate levels of the n-th shell. The numerical parameter γ depends in this case also on the way the particles are placed in the outer shell of each nucleus. The harmonic oscillator symmetries in the problem often prohibit the transition.

The polynomials in Eq. (4.52) acquire a form of a product of four components, each of the form of Eq. (4.58) for each type of nucleons, times the sum of terms $(\vec{\sigma}\cdot\mathbf{k})$ acting on every pair of interacting nucleon species. Using the integrals from Eq. (4.39) and writing the action of $(\vec{\sigma}\cdot\mathbf{k})$ between initial and final spin parts of the wave function as a matrix element $\tilde{M}$ we arrive at the expression for the polynomial in Eq. (4.22)

$$P_{q_x,q_y,q_z}(k=0,p) = \frac{1}{\gamma}\left(\frac{2(v^2+w^2)}{Av^2}\right)^{(q_x+q_y+q_z)/2} \eta^{\mathcal{Q}_f} \times \left((q_x-1)!!\,(q_y-1)!!\,2^{\frac{q_z}{2}} T_{q_z}\left(ip\sqrt{\frac{2}{A\eta v w}}\right)\right)\tilde{M} \quad . \tag{4.59}$$

In the above expression we have redefined γ as a product of γ's for all four types of nucleons.

Chapter 5

Exploring the nuclear pion dispersion relation through the anomalous coupling $\gamma \rightarrow \gamma' \pi_0$

5.1 Introduction

Pions are expected to interact strongly with nuclear matter due to the mixture of pionic and delta-hole states. The mixture is especially strong when the momentum of the pionic mode approaches 300 MeV/c. In this momentum range the energy of the pionic mode, $(k^2 + m_\pi^2)^{1/2}$, crosses the energy of the delta-hole mode, $(k^2 + M_\Delta^2)^{1/2} - M_N$, and the energy of the pionic branch should lower due to level repulsion. This topic drew a great deal of attention in the late 1970s when it was thought that the pionic mode might be pushed below zero energy at sufficient nuclear density, which would result in pion condensation. An extensive review of pionic excitations and condensation in nuclear matter was published by Migdal [101], and recently, kaon condensation has been the subject of several investigations [102]. Since such novel behavior requires higher densities, the discussions are often in the context of neutron

stars [103], although relativistic heavy ion collisions were also once proposed as a mechanism for producing sufficient density for condensation.

Despite theoretical efforts in this area, experimental evidence of large in-medium corrections to the pion dispersion relation is sparse. The most promising information is from recent charge-exchange measurements from light ions scattered off heavy nuclei. The cross-sections appear enhanced for channels where pion-exchange is expected to dominate. This enhancement is consistent with the lowering of the energy of the pionic branch, which reduces the amount by which the exchanged pion is off-shell[104]. The interpretation of this experiment suffers only from the fact that the probe is hadronic and must traverse the surface of the heavy nucleus before interacting. Heavy-ion collisions, which can produce matter at three to four times nuclear density, were expected to create environments where the dispersion relation was extremely distorted. However, experimental signals, such as measuring pion spectra[105] or dilepton pairs[106, 107], of pionic properties in the interior of these regions proved difficult to extract.

In this work we study the inelastic scattering of photons off heavy nuclei as a means to create the pionic excitations within the medium. The anomalous coupling of a neutral pion to two photons, which is responsible for the decay of the π^0, can be used to excite a pionic mode in a heavy nucleus. The photon provides a clean probe for entering and exiting the interior of the nucleus. Unfortunately, this has the same drawback as the charge-exchange experiment mentioned in the previous paragraph — only space-like excitations can be investigated. However, in-medium effects are expected to lower the energy of the pionic branch, perhaps to the point that it crosses into the space-like region, $|\vec{k}_\pi| > \omega_\pi$. Thus, the reaction $\gamma \to \gamma' + \pi^0$, which is kinematically forbidden in free space, is allowed in the nuclear medium. Furthermore, the measurements of such a branch would provide direct evidence of

in-medium correction to the pion dispersion relation.

This chapter is organized into five parts. The next section briefly reviews the in-medium corrections to the pion dispersion relation. The following section shows the contribution to the cross section from the anomalous coupling to the π^0, outlines the procedure one must follow to map out the pion dispersion relation, and presents a discussion of how gauge-invariance constrains the cross-section to disappear at the space-like-to-time-like boundary. Due to this constraint, the contribution from the anomalous coupling is reduced in the region of interest, which allows background processes to pose a major problem. The bulk of the work is comprised of estimates for background processes which are presented in section 5.4, where non-pionic delta-hole channels are shown to provide most of the background. Given the possibility of using free-electron lasers to supply high-energy photons with 100% polarization, we also discuss the use of polarization measurements to eliminate background. We conclude that the only chance to defeat the background is to perform a difficult exclusive measurement, which would require a more sophisticated theoretical treatment.

5.2 The pion dispersion relation

The delta-hole and nucleon-hole both contribute to the in-medium correction to the self-energy of the pion in nuclear matter. The coupling to the nucleon-hole raises the energy of the pionic mode, while the coupling to the delta-hole state significantly lowers the energy, especially for momenta approaching 300 MeV/c. Numerous theoretical works in this direction [105] have focused on the correction to the pionic mode in perturbative pictures[108, 101]. Sophisticated treatments of the pion self energy were performed by Xia, Siemens and Soyeur[109], and Korpa and Malfliet[110]. There, self-consistent corrections to the delta's self energy and width were included.

In this section we present a simple model to illustrate the modifications of the

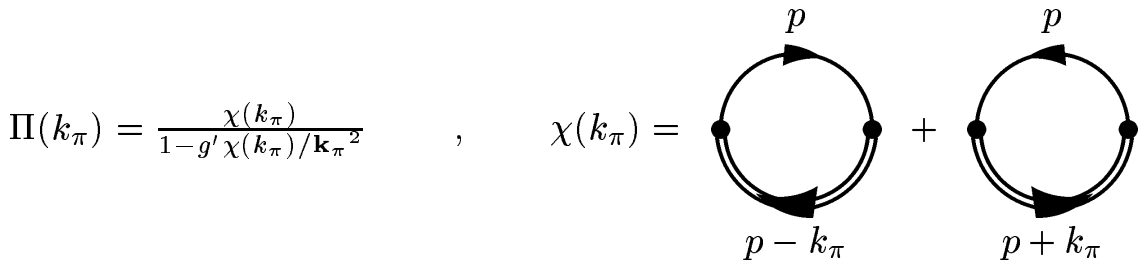

Figure 5.1: Delta-hole contributions to the pion self-energy.

pion dispersion relation in nuclear matter. We will forgo such lengthy calculations, as we wish to discuss how to experimentally observe the resulting dispersion relation, rather than how to better calculate in-medium corrections.

Self energy corrections can be written diagrammatically as shown in Figure 5.1. Vertex renormalization due to the effective four-point interaction between deltas and nucleons is incorporated through the phenomenological constant g'. Nucleon-hole contributions can also be considered but are much less important for $\vec{k}_\pi$ approaching 300 MeV/c.

Assuming an interaction Lagrangian density of the form,

$$\mathcal{L}_{\pi N\Delta} = \frac{g_{\pi N\Delta}}{m_\pi}(\overline{\Delta}^\mu \psi \partial_\mu \pi + h.c.) \ , \tag{5.1}$$

we obtain the self-energy correction for the pion propagator shown in Figure 5.1.

The delta propagator is assumed to have a Rarita-Schwinger form [111] for all the calculations in this section, in which the width is inserted by substitution $M_\Delta \rightarrow M_\Delta - i\Gamma_\Delta/2$ [112].

$$G_\Delta^{\mu\nu}(q) = \frac{i}{\not{q} - M_\Delta}\left[-g^{\mu\nu} + \frac{1}{3}\gamma^\mu\gamma^\nu + \frac{2}{3M_\Delta^2}q^\mu q^\nu - \frac{1}{3M_\Delta}\left(q^\mu\gamma^\nu - \gamma^\mu q^\nu\right)\right] \tag{5.2}$$

The nucleon propagator in the presence of nucleons filled to the Fermi momentum p_f has a correction given by:

$$G_N(p) = \frac{i}{\not{p} - M_N + i\varepsilon} + 2\pi(\not{p} - M_N)\delta(p_0^2 - E^2(p))\Theta(p_f - |\vec{p}|). \tag{5.3}$$

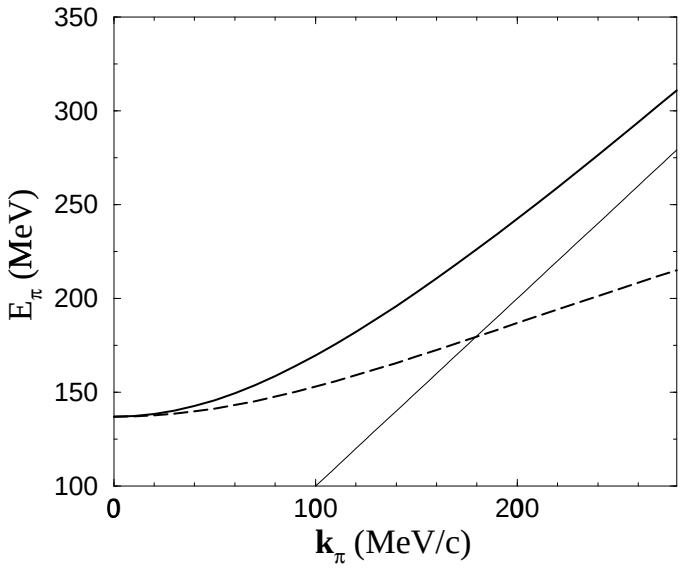

Figure 5.2: The pion dispersion relation is shown for both the vacuum case (solid line) and with an effective coupling $g_{\pi N\Delta}$=2.0 and g'=0.8 (dashed line) in Figure 5.1. The thin straight line shows the space-like-to-time-like boundary.

With the obtained self-energy term a dispersion relation could be inferred by finding a pole of the corresponding "dressed" pion propagator. Using these equations and assuming the coupling strengths, $g_{\pi\Delta N} = 2.0$ and $g' = 0.8$, we obtain the pion dispersion relation presented in Figure 5.2.

The value of the effective in-medium coupling constant is not precisely known although vertex corrections have been extensively studied. Many parameters used in more sophisticated analyses[109, 110] are still rather uncertain. For instance the delta's mass and width as well as the nucleon's mass in matter are somewhat uncertain, as are the coupling constants $g_{\pi N\Delta}$ and g'.

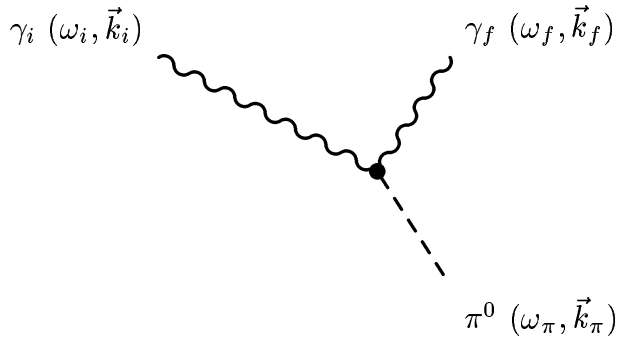

Figure 5.3: Pion production diagram.

5.3 Pion production through the anomalous coupling

We consider production of a neutral pion through an effective photon "decay" inside nuclear matter as shown in Figure 5.3.

This process can only occur if the resulting pion is space-like,

$$k_\pi^2 = (k_i - k_f)^2 = -2k_i \cdot k_f = -2\omega_i\omega_f(1 - \cos\theta) \leq 0\,, \tag{5.4}$$

where k_i and k_f are the incoming and outgoing momenta of the photon, and the outgoing photon leaves at an angle θ. An interaction that has a gauge invariant and parity conserving form is $\mathcal{L}_{\gamma\gamma\pi} = \alpha/(4\pi f_\pi) F^{\mu\nu}\widetilde{F}_{\mu\nu}\pi^0$, where α is the electromagnetic fine coupling constant, and the pion decay constant is $f_\pi = 93\,\mathrm{MeV}$. The transition amplitude $\tau_{i\to f} = \langle f, \pi|\mathcal{L}_{\gamma\gamma\pi}|i\rangle$ can be expressed in terms of the momenta and polarizations of the incoming and outgoing photons.

$$\begin{aligned} \tau_{i\to f} &= \frac{\alpha}{2\pi f_\pi} 2\epsilon_{\alpha\beta\gamma\delta} k_i^\alpha k_f^\beta \chi_i^\gamma \chi_f^\delta \\ &= \frac{\alpha}{2\pi f_\pi}(\vec{k}_\pi^{\,2} - {\omega_\pi}^2)\sin(\alpha_i - \alpha_f)\,, \end{aligned} \tag{5.5}$$

where k_i and k_f are the initial and final momenta of the photon and χ_i and χ_f are the corresponding polarizations. In the last line of Eq. (5.5) the transition

amplitude is written in terms of the momentum of the pion, and the incoming and outgoing polarization angles, α_i and α_f, as measured relative to the reaction plane. The principle difficulty in obtaining the goals of this study comes from the fact that the amplitude vanishes at the space-like-to-time-like boundary where the square of a pion four-momentum is zero, which is precisely the kinematic region of interest. This is a direct consequence of gauge symmetries involved in coupling two photons to a pseudoscalar. This result may be problematic since we investigate the area that is close to the space-like-to-time-like boundary, and therefore the cross sections obtained are quite small. The rate of this "decay" can be expressed in terms of the matrix element τ [113]:

$$dR = (2\pi)^4 \delta^4(k_f - p_i - k_i) |\tau_{i\to f}|^2 \frac{1}{2\omega_i} \frac{d^3k_f}{2\omega_f(2\pi)^3} \frac{d^3k_\pi}{2\omega_\pi(2\pi)^3} \,. \tag{5.6}$$

We will express our answer in terms of the energy and momentum transfer, $\omega_\pi \equiv \omega_i - \omega_f$ and $\vec{k}_\pi \equiv \vec{k}_i - \vec{k}_f$ respectively. Substituting a Lorentzian form in place of the energy preserving δ -function, allows the incorporation of a finite width to the pionic state

$$\delta(\omega - E) \to \frac{1}{\pi} \frac{2\omega^2\Gamma}{(\omega^2 - E^2)^2 + \omega^2\Gamma^2} \,. \tag{5.7}$$

In general the complicated form of the in-medium pion self-energy makes the above parameterization somewhat arbitrary. Nevertheless Eq. (5.7) follows from the choice of $-\omega_\pi\Gamma$ being equal to the imaginary part of the self-energy. For our numerical calculations presented below we used a fixed value of the pion width $\Gamma = 50$ MeV, which in the region of interest agrees well with the calculations presented in Sec. 5.2 and with the results of more sophisticated calculations [109, 110]. The decay rate into a pionic mode of energy ω_π and momentum $\vec{k}_\pi$ can be expressed as:

$$\frac{dR}{dw_\pi d|\vec{k}_\pi|} = \frac{\alpha^2}{(2\pi)^2 f_\pi^2} \frac{|\vec{k}_\pi|(\vec{k}_\pi^2 - \omega_\pi^2)^2}{2\omega_i^2} \sin^2(\alpha_i - \alpha_f) \frac{\omega_\pi\Gamma}{(\omega_\pi^2 - E_\pi^2)^2 + \omega_\pi^2\Gamma^2} \,. \tag{5.8}$$

To estimate the pion production cross section in the physical reaction of inelastic

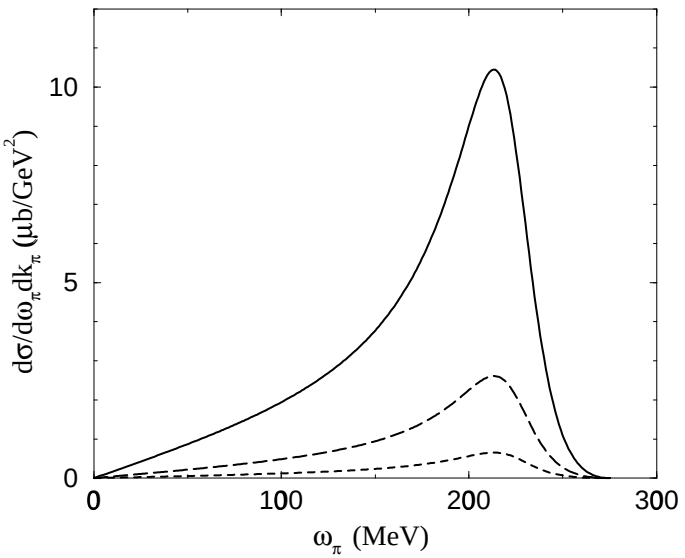

Figure 5.4: Neutral pion production through the anomalous coupling $\gamma \to \gamma' + \pi^0$. The on-shell energy is 225 MeV, the momentum transfer $|\mathbf{k}_\pi|$ is 275 MeV/c, and the pion's width is 50 MeV. Cross sections are shown for three incoming photon energies: 500 MeV (solid line), 1.0 GeV (long dashes) and 2.0 GeV (short dashes).

photon scattering from a heavy nucleus one must multiply the result in Eq. (5.8) by the nuclear volume. Examples of cross sections for the $\gamma \to \gamma' + \pi^0$ process calculated for a photon scattering off a Pb nucleus for different incoming photon energies are shown in Figure 5.4. In the calculations the on-shell energy of the pion is assumed to be 225 MeV and momentum transfer $|\vec{k}_\pi|$ is fixed at 275 MeV/c. Figure 5.5 shows the dependence of the peak location and height with respect to the on-shell energy. If the on-shell energy is not more then 25 MeV less than $|\vec{k}_\pi|$, the peak is probably too small to be observed.

The fact that the cross section is inversely proportional to the incoming photon energy suggests the use of lower energies for a greater signal. Lower energies also allow a more confident prediction of the background as very massive and not well

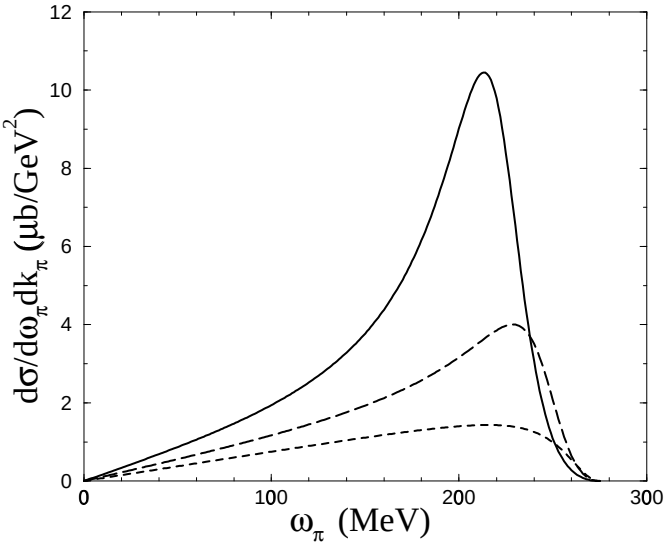

Figure 5.5: Neutral pion production through the anomalous coupling $\gamma \to \gamma' + \pi^0$. On-shell energies are 225 MeV (solid line), 250 MeV (long dashes) and 275 MeV (short dashes). The momentum transfer $|\mathbf{k}_\pi|$ is 275 MeV/c, and the pion width is 50 MeV. The incoming photon has an energy of 500 MeV.

understood nucleonic resonances do not contribute. Incoming photons with energies between 400 and 600 MeV are satisfactory for our purposes given the above considerations and the experimental ease with which they can be created. Lower-energy photons would be difficult to deal with since the final photon could be confused with those from nuclear processes such as giant-dipole decays.

For a 5 mm (a radiation length) lead target, one would need on the order of 10^{14} photons to investigate the peak in the region of interest. This estimate was ascertained by requiring 100,000 final-state photons to correspond to pion momenta between 225 and 275 MeV and pionic energies within 75 MeV of the momentum. This number of photons is within the realm of current experimental constraints, although the elimination of background to be discussed in the next section will push the viability of these measurements. The role of the width is important, as for vanishing widths the shape of the differential cross section in Eq. (5.6) becomes a sharp spike which would be more easily observed. A confident calculation of the width is not trivial, since the mixture of the pion and the delta-hole might represent a significant contribution. The off-shell behavior of the $\pi_0\gamma\gamma'$ vertex superimposes an additional effect. From the calculations in Ref. [114] it follows that in the the region of interest $k_\pi^2 = \omega_\pi^2 - |\vec{k}_\pi|^2 > -0.03$ GeV^2 , the reduction of the coupling strength is smooth and is on the level of one percent, which is negligible.

5.4 Calculating background processes

We consider two processes that might overwhelm the $\gamma \to \gamma' + \pi^0$ reaction, namely ordinary Compton scattering, that could also proceed through an intermediate Δ resonance, see Figure 5.6, and reactions that produce a Δ-hole (which decays into πN) as a final state, see Figure 5.8. These reactions are the same order in α as $\gamma \to \gamma' + \pi^0$. One might expect these background processes to be smaller than the

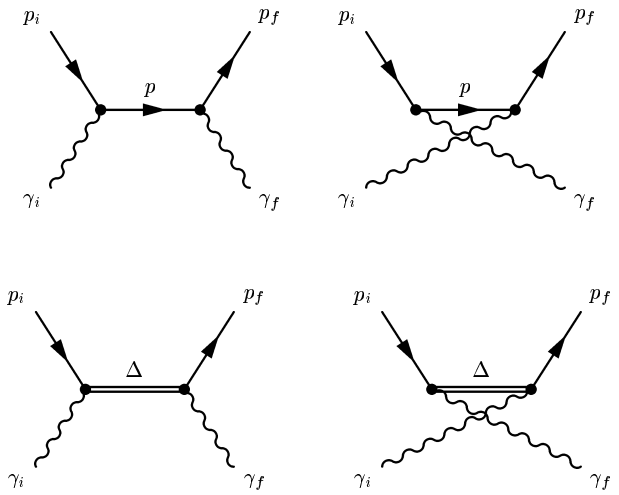

Figure 5.6: Feynman diagrams for the background Compton-like processes $\gamma + N \rightarrow \gamma' + N'$.

simple π_0 production process since they are further off-shell in the kinematic region we are exploring. However, even though $\gamma \rightarrow \gamma' + \pi^0$ might be nearly on-shell, a gauge constraint forces the matrix element to zero at the $k_\pi^2 = 0$ boundary and allows other channels to compete. We also report on our investigation of using polarization measurements to project the signal from the background. Unfortunately, our estimate of the background processes is done without the benefit of an experimental measurement of relevant processes in vacuum, e.g. $\gamma + p \rightarrow p' + \gamma' + \pi^0$. Certainly such measurements are possible and would greatly increase the confidence with which we present the background.

First, we discuss our estimate of normal Compton scattering as illustrated in Figure 5.6. We consider the intermediate state to be either a delta or a proton. The diagrams with the delta as an intermediate state provide the dominant contribution. The photon is assumed to interact with the baryon via the following couplings [115, 116, 117]:

$$\mathcal{L}_{p\gamma p} = e\overline{\psi}\gamma_\mu A^\mu \psi$$

$$\mathcal{L}_{\gamma N\Delta} = e\left\{\frac{G_1}{M_N}\overline{\Delta}^{\mu}\gamma^{\nu}\gamma_5\psi F_{\mu\nu} + \frac{G_2}{M_N^2}\partial^{\nu}\overline{\Delta}^{\mu}\gamma_5\psi F_{\mu\nu} + h.c.\right\} \quad (5.9)$$

We observed that the contribution from the second term proportional to G_2 is small, and we neglected it in our analyses.The value of $G_1 = 2.63$ has been determined from experiments[118, 119]. The regular Compton process was also small, and thus did not warrant including more sophisticated coupling, e.g. through magnetic moments.

The result for the cross section is shown in Figure 5.7. Again, we have assumed that the photon lost a momentum $|\vec{k}_\pi| = 275$ MeV/c. The form would be a sharp peak at low energy if it were not for our replacing the final delta function in the cross-section by a Lorentzian, giving the nucleon an effective width of 25 MeV. Since an on-shell nucleon with 275 MeV/c of momentum has only 50 MeV of energy, there is little contribution in the kinematic region of interest, where ω_π approaches $|\vec{k}_\pi|$. Since the kinematics were effectively smeared by the Fermi motion, changing the nucleon's width had little effect.

The primary contribution to the background derives from production of a delta-hole in the final state. Since this is precisely the process that mixes with the pion due to its kinematic proximity to the pionic mode, it is not surprising. Even though the delta-hole should be 50 MeV in energy higher than the pionic branch of the dispersion relation, its contribution is not constrained to go to zero when $|\vec{k}_\pi|$ equals ω_π. This lack of a constraint derives from the fact that a spin 3/2 delta and a spin 1/2 nucleon-hole do not necessarily form a pseudo-vector, and couple to $\partial\pi$, but can also couple to $J = 2$. Furthermore, the delta will decay into a nucleon and a pion. If the pion is charged, it can radiate photons readily since it is light and moves quickly. We find that only by gating on the presence of the π_0 and by requiring the target nucleus to be left in it's ground state, can one confidently translate the measurement into information regarding the nuclear pion dispersion relation.

The diagrams used for calculating the contributions for a delta-hole being in the

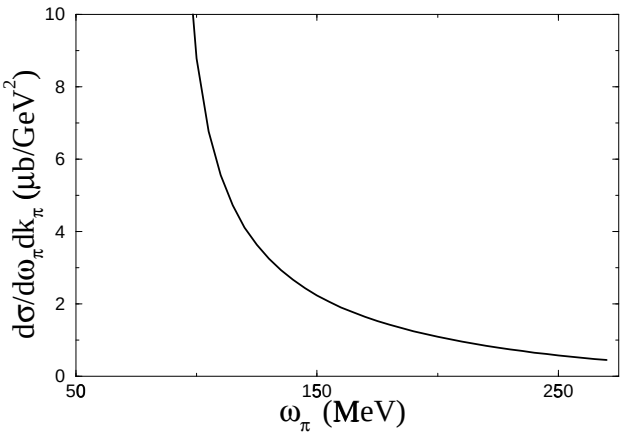

Figure 5.7: The contribution from $\gamma + N \rightarrow \gamma' + N'$ assuming the outgoing nucleon has a width of 25 MeV. This component is negligible for energy transfers greater than 200 MeV.

final state are shown in Figure 5.8. In order to maintain gauge invariance, the decay of the delta into pions is included. This decay is also crucial as Bremsstrahlung off the light charged pion is important. The coupling of the electromagnetic field to the delta is accomplished via minimal substitution.

One might also consider a diagram where the photon decays into a second photon and a pion, with the pion interacting and exciting the nucleon hole. However, this excitation is part of the signal rather than the background as it represents a truly pionic excitation that would disappear at the space-like-to-time-like boundary.

The Lagrangian for the delta that results in the Rarita-Schwinger form of the propagator is:

$$\mathcal{L}_\Delta = -\overline{\Delta}^\alpha \left\{ (i \not{\partial} - M_\Delta) g_{\alpha\beta} - (\gamma_\alpha i \partial_\beta + i \partial_\alpha \gamma_\beta) + \gamma_\alpha i \not{\partial} \gamma_\beta + M_\Delta \gamma_\alpha \gamma_\beta \right\} \Delta^\beta \qquad (5.10)$$

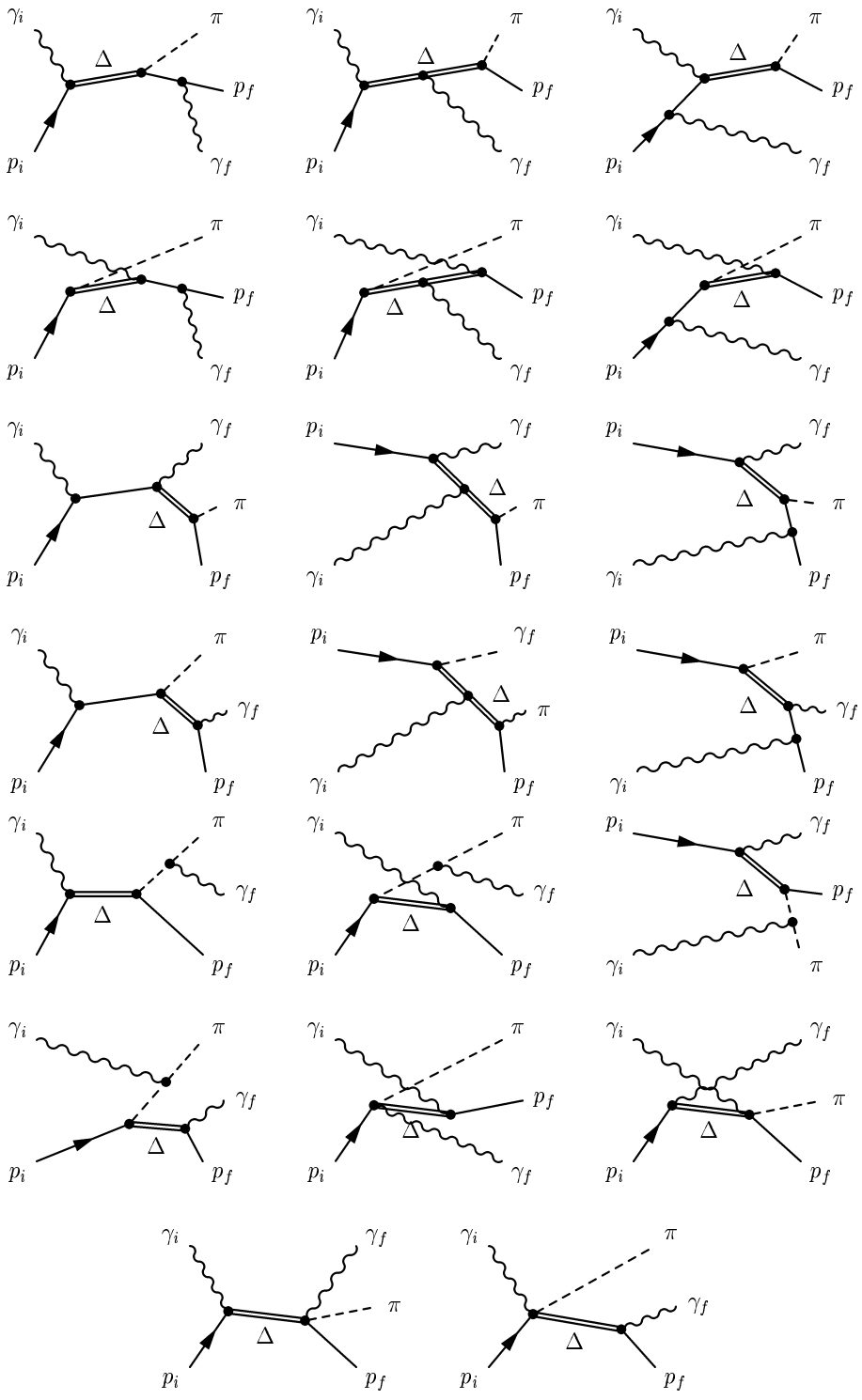

Figure 5.8: Matrix elements for calculating background processes where a pion, photon and excited nucleon are in the final state. These diagrams can be thought of as processes where a delta-hole (which subsequently decays) is created.

The associated coupling of a delta to a photon, through minimal substitution, is:

$$\mathcal{L}_{\Delta\Delta\gamma} = e\overline{\Delta^\alpha}\left\{g_{\alpha\beta}\gamma^\mu - g^\mu_\alpha\gamma_\beta - g^\mu_\beta\gamma_\alpha + \gamma_\alpha\gamma^\mu\gamma_\beta\right\}\Delta^\beta A_\mu \tag{5.11}$$

Due to the derivative nature of the $\pi N\Delta$ coupling shown in Eq. (5.1), minimal substitution requires a four point coupling of the photon to the $\pi N\Delta$ vertex.

$$\mathcal{L}_{\gamma\pi N\Delta} = ie\frac{g_{\pi N\Delta}}{m_\pi}\Delta^\mu A_\mu\psi\pi + h.c. \tag{5.12}$$

Minimal substitution from the interaction term in Eq. (5.9) also results in a four-point coupling, which we will neglect since G_2 is set to zero.

The 20 terms necessary for creating a nucleon, a photon and a pion in the final state are shown in Figure 5.8. A fixed width was used for the delta, which although is not realistic, simplified self-consistency checks regarding gauge invariance and the Ward-Takahashi identity. Since the delta-hole is not far off-shell, the answer should not vary greatly by incorporating an energy and density dependent width.

Transition elements were calculated for specific linear polarizations, α_i and α_f of the incoming and outgoing photons. The scattering plane of the photons defines the angles. For our signal, $\gamma \to \pi_0\gamma'$, the dependence is proportional to $\sin^2(\alpha_i - \alpha_f)$ as shown in Eq. (5.5). Since the final states illustrated in Figure 5.8 are three-body states with large widths from the delta decay, the final three particles could be assumed to be on-shell. Numerical integrations were performed over all final-state variables except for the photon polarizations and the energy and momentum lost by the photon, ω_π and $|\vec{k}_\pi|$.

The cross sections for the background are shown in Figure 5.9. The upper graph shows the background for charged pions, while the lower graph presents the background for the case where a neutral pion is created. The creation of a charged pion overwhelms the signal by more than an order of magnitude. This strength comes from the radiation off the light, fast-moving, charged particle.

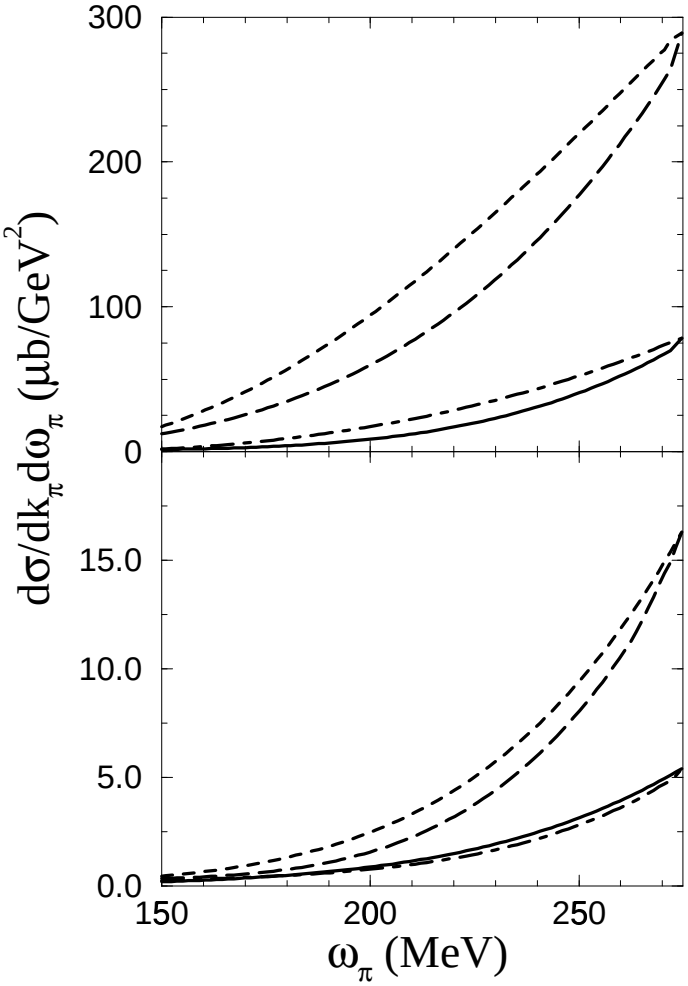

Figure 5.9: The cross section for the background process where a charged pion is created is shown in the upper panel. By requiring the created pion to be neutral, the background is greatly reduced as shown in the lower panel. Polarization projections are shown for $\alpha_i = 0,\ \alpha_f = 0$ (solid line),$\alpha_i = 0,\ \alpha_f = \pi/2$ (short dashes), $\alpha_i = \pi/2,\ \alpha_f = 0$ (long dashes), $\alpha_i = \pi/2,\ \alpha_f = \pi/2$ (dot-dashes).

Polarization does not significantly ameliorate the background as shown in Figure 5.9. The signal is proportional to $\sin^2(\alpha_i - \alpha_f)$ which has the same shape as part of the spin-2 delta-hole state.

By gating on neutral pions, one can reduce the background by an order of magnitude as shown by comparing the upper and lower panels of Figure 5.9. Although this background is now comparable to the signal, it is still possible that a charged pion could be created and undergo a charge exchange with the medium, resulting in a neutral pion.

The intractability of the background derives from the gauge invariance constraint that requires the cross section to disappear at the space-like-to-time-like boundary for pseudoscalar channels. Since the delta-hole state can couple in other ways than pseudoscalar modes, the background becomes problematic. We briefly discuss the idea of using an exclusive measurement to eliminate the background in the conclusion.

5.5 Conclusions

The subject of in-medium hadron masses has been historically inconclusive. The pion's in-medium properties are unique in that the dispersion relation may dip down into the space-like region at normal nuclear density. This permits the consideration of simple scattering experiments, such as the process proposed here, to investigate pionic modes.

Unfortunately, background processes where a delta-hole is produced in the final state with quantum numbers different than the pion overwhelms the pseudoscalar mode of interest here. Even polarization measurements were not adequate to focus in on the channel of interest. The only means to defeat such a problem is to eliminate the delta-hole channel (that which does not have the quantum numbers of a pion) from consideration. The delta-hole channel decays into a pion and a nucleon hole.

By requiring the nucleus to remain in it's original ground state, one could in principle eliminate the background. However, such a requirement would also eliminate much of the signal as a pionic mode can also decay by exciting the nucleus. Before proposing such a difficult exclusive measurement, one should perform an optical model calculation to realistically model the escape of the pion from the center of the nucleus. That is beyond the scope of the current work, where our aim is to investigate the inclusive measurement.

Chapter 6

Multiple pion production from an oriented chiral condensate

6.1 Introduction

Pions have always played an important role in heavy ion reactions. With their relatively strong coupling to nuclei and very small mass, pions can be produced in large quantities and can carry important detectable information about the state of nuclear matter during the reaction. Large fluctuations in the ratio of charged to neutral pions have been observed in cosmic ray experiments [120] and have recently been a subject of many discussions. The major interest in this direction is motivated by an almost decade-old idea [121, 122, 123] that at high enough energies the pion-sigma ground state symmetry breaking condensate can be destroyed. In the latter process of sudden cooling there is a chance of the formation of disoriented chiral domains, given that the terms responsible for the explicit breaking of chiral symmetry are small. The formation of this disoriented chiral condensate (DCC) is presumably responsible for the observed discrepancy in the ratio of pion species. Further enthusiasm about these ideas is generated by the fact that it may be possible to achieve an environment

capable of producing disoriented chiral domains in relativistic heavy ion collisions. In that case the large fluctuations in pion types can be a signal of a DCC.

There exist a number of theoretical works investigating the production and development of DCCs in heavy ion collisions. The assumption of a random equiprobable orientation of the pionic isovector leads [122] to the probability of observing a fraction of neutral pions $f \equiv N_{\pi^0}/(N_{\pi^+} + N_{\pi^-} + N_{\pi^0})$ being

$$\mathcal{P}(f) = \frac{1}{2\sqrt{f}}\,. \tag{6.1}$$

This result is consistent with the slowly varying classical pionic field as a solution of the non-linear σ-model [124]. It can also be obtained as a limiting large N distribution in the coherent single-mode pion production by an isoscalar operator [125, 126, 127]

$$\left(\vec{a}^{\,\dagger} \cdot \vec{a}^{\,\dagger}\right)^{N/2} = \left(a_x^\dagger a_x^\dagger + a_y^\dagger a_y^\dagger + a_z^\dagger a_z^\dagger\right)^{N/2}\,.$$

The formation and the nature of domain structures is an important question in itself [128, 129]. In the case of many small domains or in the absence of a DCC, one would expect a Gaussian distribution $P(f)$, following from the central limit theorem. More complicated methods of quantum and classical field theory applied to this problem with different assumptions of formation, evolution [130, 131] and dissociation of DCCs [132, 133] lead to different results. Pionic mode mixing and final state interaction may also greatly change the observed forms of these probability distributions [127, 124, 134].

Most of the existing theoretical works consider pion production from DCC domains formed in the dynamical process of symmetry restoration and later sudden relaxation into a non-symmetric vacuum which is some times called a quench [135]. The word "disoriented" also describes the theoretical foundation of the DCC approach which is based on introducing an effective disoriented current-type term in the Lagrangian. The advantage of this formalism is in the simplicity of the solution, as a current-type interaction can always be solved with a coherent state formalism [136]. In

contrast to that the linear sigma model, a well-established effective theory based on chiral symmetry, naturally leads to a quadratic pion field term in the Lagrangian. The goal of the present work is to consider an "oriented" chiral condensate with a chirally symmetric Lagrangian that to the lowest order is quadratic in the pion field. Throughout all this paper we are going to deal with the wave equation for pions in the form

$$\frac{\partial^2 \vec{\pi}}{\partial t^2} - \nabla^2 \vec{\pi} + m_{\rm eff}^2(\mathbf{x}, t)\, \vec{\pi} = 0\,. \tag{6.2}$$

This is the equation of motion deduced from a quadratic Lagrangian. Equation (6.2) contains an effective mass $m_{\rm eff}(\mathbf{x}, t)$ which is due to a mean field from non-pionic degrees of freedom. This term produces a parametric excitation of the pionic field, and, if $m_{\rm eff}^2 < 0$, may lead to amplification of low momentum modes and the formation of a chiral condensate. The chiral condensate in this picture is "oriented"; as opposed to the usual picture of a DCC. The scalar mean field (effective mass) introduced here does not break the symmetry properties of pion fields in any way. The quantum problems formulated by equations of the form (6.2) address a variety of physical issues, and can be encountered in different areas of physics. In general, such non-stationary quantum problems cannot be solved exactly. Even studies with approximate methods like perturbation theory, impulse approximations, adiabatic expansions and many others often require sophisticated approaches. We will address those rare occasions when exact solutions may be obtained. The significance of the analytical solution should not be underestimated. The exact results could exhibit the unperturbative features of the solutions, like phase transitions and condensates, as well as point the way to a good approximate theory.

The paper is structured as follows. We start with a short introduction to the linear sigma model and show that effectively it leads to Eq. (6.2) for a pion field. In the next section we discuss an exact solution of Eq. (6.2). First, we show that

from the classical solution a quantum solution can be built exactly. Then, based on the general form of the evolution matrix, we obtain and discuss possible forms of the multiplicity distribution. The bulk of the paper is concentrated in Sec. 6.4. where we further analyze the properties of the solutions to Eq. (6.2). By considering a simpler model of space-independent but variable-in-time effective mass we clearly define the exponentially growing "condensate" momentum modes. Depending on the number and strength of the condensate modes we obtain different distributions for a particle number and distributions over pion species. We emphasize the limits when Eq. (6.1) is recovered or when $\mathcal{P}(f)$ becomes Gaussian. In the following part of Sec. 6.4 we consider a full field equation with a time- and space-dependent mass parameter and address the exactly solvable case of a mass parameter abruptly changing and returning to normal. We show that in this picture the condensate modes are still identifiable and they still have a characteristic momentum distribution. Final summary and conclusions are given in Sec. 6.5.

6.2 The linear sigma model

Below we give a short review of the linear sigma model, point out the origin of Eq. (6.2) in the context of pion fields and deliberate the possible form of the effective mass term. We assume the usual linear sigma model Lagrangian of the pion and sigma fields [137]

$$\mathcal{L}_{L.S.} = \frac{1}{2}\left(\partial_\mu \vec{\pi}\right)\cdot\left(\partial^\mu \vec{\pi}\right) + \frac{1}{2}\left(\partial_\mu \sigma\right)\,\left(\partial^\mu \sigma\right) - \frac{\lambda}{4}\left(\left(\vec{\pi}^2+\sigma^2\right)-v_0^2\right)^2 + \epsilon\sigma\,, \tag{6.3}$$

where explicit symmetry breaking is introduced by the parameter ϵ. The sigma field has a non-zero vacuum expectation value f_π that is set by the Goldberger-Treiman relation and is related to the above mentioned symmetry breaking parameter as

$$v_0^2 = f_\pi^2 - \frac{\epsilon}{\lambda f_\pi}\,.$$

The Lagrangian of Eq. (6.3) produces the following masses of the pion and sigma mesons

$$m_\pi^2 = \frac{\epsilon}{f_\pi}\,, \qquad m_\sigma^2 = 2\lambda f_\pi^2 + \frac{\epsilon}{f_\pi}\,.$$

Equations of motion for each isospin component of the pion field π_τ have the form

$$\frac{\partial^2 \pi_\tau}{\partial t^2} - \nabla^2 \pi_\tau + \lambda \left((\vec{\pi}^2 + \sigma^2) - v_0^2 \right) \pi_\tau = 0\,. \tag{6.4}$$

In the mean field approximation non-pionic degrees of freedom, like the sigma field, are approximated by their expectation value. Then the dynamics of the pionic field can be viewed as a field equation of type (6.2), with a time- and space-dependent mass parameter

$$m_{\rm eff}^2(\mathbf{x}, t) = \lambda \left(\langle \vec{\pi}^2 + \sigma^2 \rangle - v_0^2 \right)\,.$$

As in the application to chiral condensates, we would like to solve Eq. (6.4) in the formalism of quantum field theory with reasonable expectation values $\langle \vec{\pi}^2 + \sigma^2 \rangle$. We do not solve the problem self-consistently because $m_{\rm eff}(\mathbf{x}, t)$, being generated by other degrees of freedom, is placed in by hand as a mean field. Before and long after the reaction the fields are in their ground state so that $\langle \pi_\tau \rangle = 0$ and $\langle \sigma \rangle = f_\pi$, which is equivalent to

$$m_{\rm eff}^2(\mathbf{x}, t = -\infty) = m_{\rm eff}^2(\mathbf{x}, t = +\infty) = m_\pi^2\,.$$

During the reaction, the behavior of the effective mass is unknown, and in our case would be an input to the model. When chiral symmetry is restored the expectation of the σ field tends to zero, while the effective squared pion mass is positive. A sudden return of the effective potential to its vacuum form (quenching) can strand the σ mean field near zero with a large negative value of the effective pion mass squared, which in the extreme limit would reach $m_{\rm eff}^2 = -\lambda v_0^2 \approx -m_\sigma^2/2$. A negative value of $m_{\rm eff}^2$ would lead to an exponential growth of the low momentum pion modes and long range correlations, i.e., the creation of a chiral condensate [138], see Fig. 6.1.

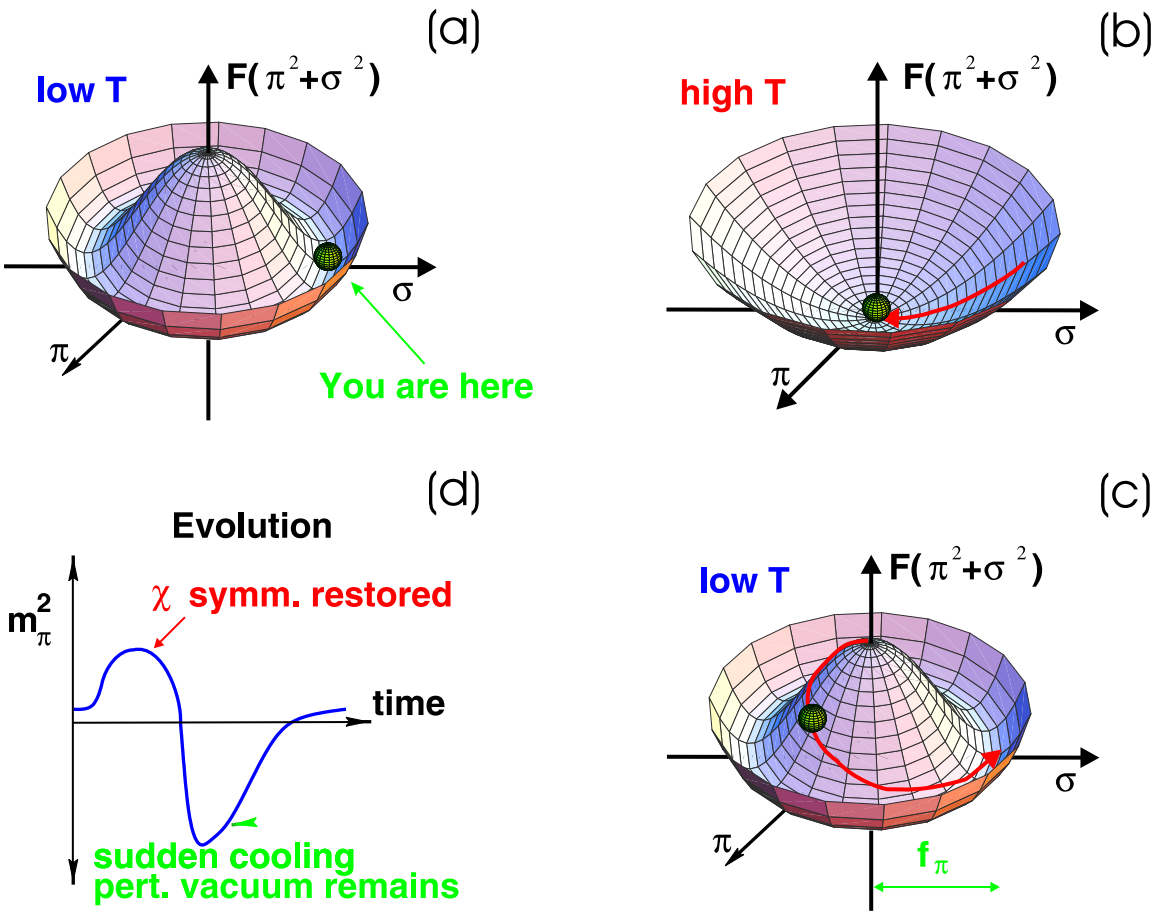

Figure 6.1: Illustration of the "quench" process. Panel (a) shows the normal $\pi - \sigma$ vacuum at low temperature. Panel (b) shows the restoration of chiral symmetry when the system is heated in the nuclear collision, and panel (c) demonstrates the "quench", the sudden restoration of the vacuum to its normal low temperature shape. In the process (a)-(b)-(c) the expectation values of $\langle\pi\rangle$ and $\langle\sigma\rangle$ change which is illustratively shown by the classical motion of a small ball. The curvature in the π direction is associated with the pion mass and the evolution of this quantity is schematically shown in panel (d).

6.3 From classical to quantum solutions

The generic form of the Lagrangian density of the field ψ that has field terms up to the second order in its potential energy part is

$$\mathcal{L} = \frac{1}{2}\left(\partial_\mu \psi\right)\left(\partial^\mu \psi\right) - J(\mathbf{x},t)\,\psi - \frac{1}{2}m^2(\mathbf{x},t)\,\psi^2\,. \tag{6.5}$$

To clarify the approach, we consider here a bosonic isoscalar field ψ. This does not limit the consideration and will be generalized later. It is known that the linear terms $J(\mathbf{x},t)$, often called a current or force, can always be removed from consideration [139]. The time-dependent current term is responsible for the creation of coherent states with a Poissonian distribution of particles. Intensive studies of a DCC produced by linear-type coupling of the pions to the disoriented mean field have been performed [134]. Unfortunately, many problems cannot be easily reduced to this linear approximation. As mentioned in the Introduction, for the chiral condensate this would require the introduction of a symmetry breaking isovector current $\vec{J}(\mathbf{x},t)$, whereas introducing a scalar effective mass (a quadratic term in the Lagrangian) preserves intrinsic symmetries.

There is one important feature of the problem with a quadratic perturbation in the Lagrangian. The equations of motion for the field, like Eq. (6.2), are linear for the Lagrangian (6.5); therefore they are identical for the classical fields and the corresponding operators in the Heisenberg picture. Thus, an exact classical solution is related to the solution to the quantized version of the problem. The step from classical to quantum treatment will be considered next.

6.3.1 Parametric excitation of a harmonic oscillator

The parametric excitation of a quantum harmonic oscillator has been extensively considered in the literature starting from refs. [140, 141, 142]. This corresponds to

our problem in the case of no spatial dependence of the effective mass. The presence of translational symmetry in this case leads to the conservation of linear momentum. The quantum number of momentum, k, can be used to label the normal modes. Each mode is just a simple oscillator with the time-dependent frequency. The simple Fourier transformation from x to k transforms the Hamiltonian, that corresponds to the Lagrangian in Eq. (6.5), into a sum over modes (for simplicity we keep one-dimensional notations)

$$H = \frac{1}{2}\int dx \, \Big(\dot{\psi}(x,t)^2 + \nabla^2\psi(x,t) + m_{\rm eff}^2(t)\psi^2(x,t)\Big) = \frac{1}{2}\sum_k \Big(\dot{\psi_k}^{\,2} + k^2\,\psi_k^2 + m_{\rm eff}^2(t)\psi_k^2\Big)\,. \tag{6.6}$$

With this reduction we arrive at the problem of the independent development of a large number of quantum oscillators. With the notation $\omega_k^2(t) = m_{\rm eff}^2(t) + k^2$, we have a classical equation of motion for each mode k

$$\ddot{\psi_k} + \omega_k^2(t)\psi_k = 0\,. \tag{6.7}$$

After the quantization, the ψ_k and the corresponding momenta become operators. Assuming a particular normal mode k below we omit this subscript.

Even for the problem of a simple oscillator, the relation between the classical and quantum solution is quite subtle; not to mention that classically Eq. (6.7) is analogous to a standard problem in quantum mechanics of scattering from a potential $-\omega^2$ that is known to have only a limited number of cases with exact analytical solutions, see the illustration in Fig 6.2.

Classically, the S-matrix would be defined if we assume that a solution of Eq. (6.7) with the asymptotics in the remote past corresponding to the frequency ω_- ,

$$\psi(t) = e^{-i\,\omega_- t} \quad \text{at} \quad t \to -\infty\,, \tag{6.8}$$

has evolved with time to a final general form of the solution with the frequency ω_+ ,

$$\psi(t) = \sqrt{\frac{\omega_-}{\omega_+}}\Big(u\,e^{-i\,\omega_+ t} + v^*\,e^{+i\,\omega_+ t}\Big) \quad \text{at} \quad t \to +\infty\,. \tag{6.9}$$

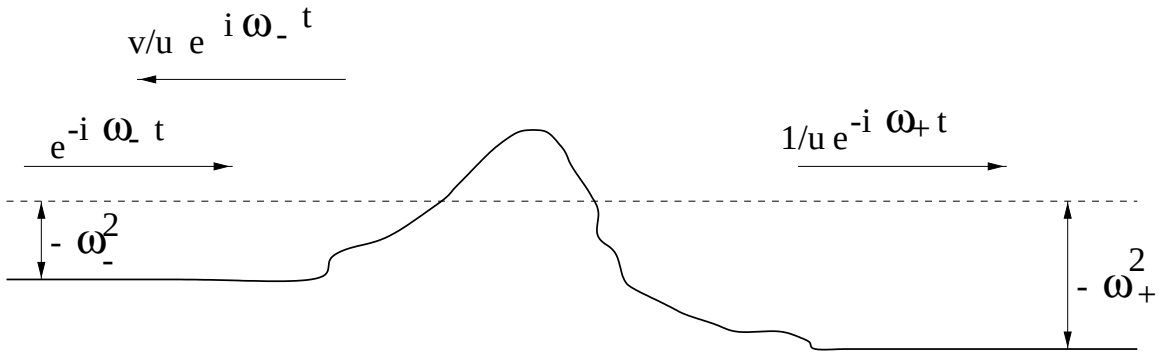

Figure 6.2: Illustration showing the scattering from the quantum problem of scattering. Mathematically this is the same problem as the problem of parametric excitation of classical harmonic oscillator.

It is clear that the complex conjugate to Eq. (6.8) will develop into a corresponding complex conjugate version of Eq. (6.9). Furthermore, the unitarity, i.e. conservation of probability applied to Eq. (6.7), results in a restriction posed on u and v

$$|u|^2 \, - \, |v|^2 \, = \, 1 \, . \tag{6.10}$$

In order to analyze the quantum version of the problem we use the language of secondary quantization, introducing creation and annihilation operators for a single harmonic oscillator. The time dependence of a quantized field coordinate $\psi(t)$ in the Heisenberg representation as $t \, \rightarrow \, -\infty$ is

$$\psi(t) \, = \, \frac{1}{\sqrt{2\omega_-}} \left(a \, e^{-i \, \omega_- t} \, + \, a^\dagger \, e^{i \, \omega_- t} \right) \, , \tag{6.11}$$

where the operators a and $a^\dagger$ do not depend on time and define the "in" state of the system. We will define the "out" state using operators b and $b^\dagger$ as

$$\psi(t) \, = \, \frac{1}{\sqrt{2\omega_+}} \left(b \, e^{-i \, \omega_+ t} \, + \, b^\dagger \, e^{i \, \omega_+ t} \right) \quad \text{at} \quad t \, \rightarrow \, +\infty \, . \tag{6.12}$$

Being supported by the fact that the field $\psi(t)$, even in its quantum form, satisfies Eq. (6.7), and with our assumptions about the classical solution (6.8, 6.9) we can

relate operators a and $a^\dagger$ with b and $b^\dagger$,

$$b \,=\, \left(u\,a + v\,a^\dagger\right)\,, \quad b^\dagger \,=\, \left(u^*\,a^\dagger + v^*\,a\right)\,, \tag{6.13}$$

with the same parameters u and v as in the classical solution. As seen (6.13) the "in" and "out" states are related by a Bogoliubov transformation. The condition that the commutation relation

$$[b, b^\dagger] \,=\, (|u|^2 - |v|^2)\,[a, a^\dagger] \,=\, 1$$

is preserved coincides with Eq. (6.10) .

It is possible to build an S-matrix corresponding to the transformation in Eq. (6.13), however the solution is very technical, and of limited use. We can use Eq. (6.13) directly to answer simple but relevant questions. The probability amplitude to have n final quanta if there was vacuum in the initial state is given by

$$C_n \,=\, {}_a\langle n|S|0\rangle_a \,=\, {}_a\langle n|0\rangle_b\,,$$

where the S-matrix is a transition matrix from the "in" state to the "out" state. Then

$$|0\rangle_b \,=\, \sum_{n=0}^{\infty} C_n|n\rangle_a\,,$$

and recursion relation for the coefficients C_n

$$C_{n+2} = -\frac{v}{u}\sqrt{\frac{n+1}{n+2}}\,C_n \tag{6.14}$$

may be found from the definition of the vacuum and Eq. (6.13):

$$b|0\rangle_b \,=\, \sum_{n=0}^{\infty} C_n\,\left(u\sqrt{n}\,|n-1\rangle_a + v\,\sqrt{n+1}\,|n+1\rangle_a\right) \,=\, 0\,.$$

Finally, normalized to unity, the transition probability from a vacuum to a state with $2n$ bosons is expressed by

$$|C_{2n}|^2 \,\equiv\, P(2n) \,=\, \frac{(2n)!}{2^{2n}\,(n!)^2}\,\rho^n\,\sqrt{1-\rho}\,, \tag{6.15}$$

where the parameter $\rho = |v/u|^2$ represents the reflection probability for Eq. (6.7) if it is viewed as a Schrödinger equation for scattering at zero energy off a potential $-\omega^2$. Conservation of probability, Eq. (6.10), limits the values of ρ to the region $\rho \in [0, 1)$. The distribution of particles produced from vacuum Eq. (6.15) peaks at zero and the average number of particles produced is

$$\overline{n} \;=\; \sum_{n=0}^{\infty} 2n\, P(2n) \;=\; \frac{\rho}{1-\rho}\,. \tag{6.16}$$

It is seen from the above expression that the number of particles diverges as ρ approaches one. This will be a region of interest in our later studies of chiral condensates.

A rigorous and detailed discussion of all the features in the transition from classical solutions of Eq. (6.7) to a problem of a quantum oscillator with a time-dependent frequency can be found in [140, 141, 142]. The corresponding Schrödinger equation for the wave function of the quantum oscillator is ($\hbar = 1$)

$$i\,\frac{\partial \Phi(x,t)}{\partial t} \;=\; -\,\frac{1}{2}\,\frac{\partial^2 \Phi(x,t)}{\partial x^2} + \frac{1}{2}\,\omega^2(t)\,x^2\,\Phi(x,t)\,, \tag{6.17}$$

where coordinate x originates from the field "coordinate" ψ, Eq. (6.7). Let some function $\psi(t)$ be a solution to classical Eq. (6.7) with $\omega(t = -\infty) = \omega_-$ and $\omega(t = +\infty) = \omega_+$. This function $\psi(t)$ can be written in terms of the real part $r(t)$ and phase $\gamma(t)$ so that $\psi(t) = r(t)\, e^{i\gamma(t)}$. With a direct substitution it can be shown that

$$\Phi(x,t) = \frac{1}{\sqrt{r(t)}}\,\exp\left(i\frac{\dot{r}x^2}{2r}\right)\chi(y,\tau) \tag{6.18}$$

is a solution to the quantum equation (6.17). Here a rescaled length y and time τ are introduced as $y = x/r(t)$, $\tau = \gamma(t)/\omega_-$. The function $\chi(x,t)$ is a standard solution of the Schrödinger equation for the oscillator with a constant frequency ω_-,

$$i\,\frac{\partial \chi(y,\tau)}{\partial \tau} \;=\; -\,\frac{1}{2}\,\frac{\partial^2 \chi(y,\tau)}{\partial y^2} + \frac{1}{2}\,\omega_-\,y^2\,\chi(y,\tau)\,. \tag{6.19}$$

The initial conditions for the solution $\chi(y,\tau)$ should be set at $t \to -\infty$ by the known conditions on $\Phi(x,t)$. Equation (6.15) can be generalized utilizing this more general

technique. It can be shown that the probability for a transition from the state with m quanta into the final state of n quanta is given by

$$\frac{\min(m,n)!}{\max(m,n)!}\sqrt{1-\rho}\left|P^{|m-n|/2}_{(m+n)/2}(\sqrt{1-\rho})\right|^2 , \tag{6.20}$$

where P^{μ}_{ν} are the associated Legendre polynomials and n and m have to be of the same parity. The established bridge between classical and quantum solutions is a remarkable achievement, but unfortunately analysis of Eq. (6.18) does not present a pleasant task.

6.3.2 Infinite number of mixed modes

General canonical transformation

The situation becomes more complicated if we return to the general field equation given by the Lagrangian density of Eq. (6.5), and assume that the modes cannot be separated. We keep assuming $J(x,t) = 0$ which is relevant to our particular problem but in general this factor can be included back in the discussion without much complication. The problem of the system of coupled oscillators has been discussed in great detail in [143]. The transformation analogous to Eq. (6.13) now takes an N-dimensional symplectic form, where N is the number of coupled modes [144],

$$b_k = \sum_{k'=1}^{N}\left(u_{k\,k'}\,a_{k'} + v_{k\,k'}\,a^{\dagger}_{k'}\right) , \quad b^{\dagger}_k = \sum_{k'=1}^{N}\left(u^{*}_{k\,k'}\,a^{\dagger}_{k'} + v^{*}_{k\,k'}\,a_{k'}\right) , \tag{6.21}$$

It is convenient to regard the operators a_k as components of an N-dimensional vector, and the numbers $u_{k\,k'}$ and $v_{k\,k'}$ as $N \times N$ matrices. Eq. (6.21) in matrix notation takes the form

$$b = S^{-1}\,a\,S = u\,a + v\,a^{\dagger} , \quad b^{\dagger} = S^{-1}\,a^{\dagger}\,S = u^{*}\,a^{\dagger} + v^{*}\,a . \tag{6.22}$$

Using the properties of the matrices u and v shown below, it is straightforward to check that the inverse transformation is given by

$$a = S\,b\,S^{-1} = u^{\dagger}\,b - v^{T}\,b^{\dagger}\,, \quad a^{\dagger} = S\,b^{\dagger}\,S^{-1} = u^{T}\,b^{\dagger} - v^{\dagger}\,b\,, \tag{6.23}$$

where u^{*}, $u^{\dagger}$ and u^{T} have their usual meanings of complex conjugate, hermitian conjugate and transpose matrices, respectively. Further, we will also use an inversion denoted as u^{-1}. Similarly to the one-mode example of Eq. (6.10), matrices u and v are subject to conditions that arise from the fact that the commutation relations have to be preserved. It follows from Eq. (6.22) that

$$u\,u^{\dagger} - v\,v^{\dagger} = 1\,, \quad u\,v^{T} - v\,u^{T} = 0\,, \tag{6.24}$$

and from the inverse transformation, Eq. (6.23)

$$u^{\dagger}\,u - v^{T}\,v^{*} = 1\,, \quad u^{\dagger}\,v - v^{T}\,u^{*} = 0\,. \tag{6.25}$$

Transitions between coherent states

In the case of many mixed modes it is still possible to obtain recursion relations similar to the single-mode situation of Eq. (6.14) but they become difficult to analyze. Next we will discuss the approach found in [143] with a different technique that uses the transitions between coherent states. We define a single-mode coherent state $|\alpha\rangle$ in the usual way as

$$|\alpha\rangle = e^{-|\alpha|^{2}/2} \sum_{n=0}^{\infty} \frac{\alpha^{n}}{\sqrt{n!}} |n\rangle\,. \tag{6.26}$$

In mathematics sums as in Eq. (6.26) are often called generating functions. It is convenient to introduce states with a different normalization [145] as

$$||\alpha\rangle = e^{|\alpha|^{2}/2}\,|\alpha\rangle = e^{\alpha\,a^{\dagger}}\,|0\rangle\,. \tag{6.27}$$

When applied to the states (6.27), the creation operation is equivalent to the derivative,

$$a^{\dagger}\,||\alpha\rangle = \frac{\partial}{\partial\alpha}\,||\alpha\rangle\,. \tag{6.28}$$

We continue to use the notation $|\alpha\rangle$ for a multidimensional coherent state, which should be interpreted as a product of the single-mode states. Here α is a vector and the derivative $\partial/\partial\alpha$ is understood as a gradient in N-dimensional space of modes. We are interested in finding the matrix elements of the evolution matrix S that implements the unitary transformation between initial and final states of the system. The evolution of the initial state is quite complicated and unless $v = 0$ the coherent state does not stay coherent as in general it evolves into a so-called "squeezed" state [146, 147]. Nevertheless it is possible to obtain an analytic expression for the matrix elements of the evolution operator S between coherent states. To proceed in this direction we will consider the action of the matrix S on the creation and annihilation operators given by Eqs. (6.22, 6.23), that actually serve here as the definition of the evolution matrix. By acting on the complex conjugate form of the first equation in Eq. (6.22) with $\langle\beta\,||S$ from the left and with $||\,\alpha\,\rangle$ from the right, and utilizing Eq. (6.28) we arrive at the following differential equation

$$\left(\beta^* \,-\, u^* \,\frac{\partial}{\partial\alpha} \,-\, v^*\,\alpha\right) \langle\beta||S||\alpha\rangle \,=\, 0\,. \tag{6.29}$$

In a similar manner from the first equation of Eq. (6.23) we obtain

$$\left(\alpha \,-\, u^\dagger \,\frac{\partial}{\partial\beta^*} \,+\, v^T\,\beta^*\right) \langle\beta||S||\alpha\rangle \,=\, 0\,. \tag{6.30}$$

The solution to the differential equations (6.29,6.30) determines the transition amplitude up to a normalization constant $C(u,v)$:

$$\langle\beta||S||\alpha\rangle \,=\, C(u,v)\,\exp\left(\beta^\dagger\,(u^\dagger)^{-1}\,\alpha \,+\, \frac{1}{2}\,\beta^\dagger\,v\,(u^*)^{-1}\,\beta^* \,-\, \frac{1}{2}\,\alpha^T\,(u^*)^{-1}\,v^*\,\alpha\right). \tag{6.31}$$

This solution can be checked directly by substitution into Eqs. (6.29,6.30) and utilizing the observation which follows from Eqs. (6.24, 6.25) that matrices $v\,(u^*)^{-1}$ and $(u^*)^{-1}\,v^*$ are both symmetric. The normalization constant may be obtained using the

completeness of coherent states [144],

$$C(u,v) = \left(\det(uu^\dagger)\right)^{-1/4} . \tag{6.32}$$

The evolution matrix given in the form of Eq. (6.31) can be transformed via a Taylor expansion in the particle number basis using the definitions in Eqs. (6.26, 6.27)

$$\langle\beta||S||\alpha\rangle = \sum_{\{n_k\}\{n'_l\}} \langle n_k|S|n'_l\rangle \prod_k^N \frac{\beta_k^{*n_k}}{\sqrt{n_k!}} \prod_l^N \frac{\alpha_l^{n'_l}}{\sqrt{n'_l!}} . \tag{6.33}$$

In general it is quite complicated to give a finite expression for the coefficients of the Taylor series arising from the multi-variable Gaussian. Expansions of two-variable Gaussians are known to be of the form of Legendre polynomials which give rise to Eq. (6.20). Nevertheless, the algorithm for the expansion is straightforward. First, the exponent should be expanded in terms of its argument and then each term can be expanded into a final sum with a generalized binomial expansion.

By considering a transition from the vacuum state we set all terms with α to zero in Eq. (6.31). In this case everything is completely determined by the matrix $v\,(u^*)^{-1}$. For the question of multiplicity distributions in the one-mode case, we note that the relative phase between u and v was of no importance, a single parameter ρ determined everything. We will further see that a similar picture holds in the general case, and only one matrix $vv^\dagger$ is needed to find the particle distributions. With the help of Eqs. (6.24, 6.25) it can be seen that the matrices $uu^\dagger$ and $vv^\dagger$ can be diagonalized simultaneously and that the eigenvalues of $vv^\dagger(uu^\dagger)^{(-1)} = v\,(u^*)^{-1}(v\,(u^*)^{-1})^\dagger$ form a set of parameters $\rho_k = |v_k/u_k|^2$ which are different for each mode.

Multiplicity distributions

Despite the complicated form of a general expression (6.31) one may calculate the moments of multiplicity distributions in a straightforward manner. Let the initial state $|i\rangle$ be characterized by a diagonal density matrix $\hat{n}^\circ$, a set of numbers of quanta

$\{n_k^\circ\}$ in each mode k on the diagonal. The average number of quanta in a final state $|f\rangle$ is determined by

$$\overline{n}_k \;=\; \langle f|a_k^\dagger\, a_k|f\rangle \;=\; \langle i|b_k^\dagger\, b_k|i\rangle\,.$$

With the above assumptions and Eqs. (6.22, 6.23), the density matrix $\hat{n}$ of a final state is

$$\hat{n} \;=\; u\hat{n^\circ}u^\dagger + v\hat{n^\circ}v^\dagger + vv^\dagger\,. \tag{6.34}$$

Throughout the rest of the work we will concentrate on the situation of a particular interest when particles are created from the vacuum and the first two terms in Eq. (6.34) are identically zero. The average total number of particles in this case may be expressed in a simple matrix form

$$\overline{n}_{\rm total} \;=\; \sum_k n_k \;=\; {\rm Tr}(v^\dagger v)\,, \tag{6.35}$$

which is consistent with Eq. (6.16). Higher moments of the particle distributions can be calculated in the same manner. Unfortunately, the calculation of an arbitrary moment requires path integration techniques while using Wick's theorem in the normal ordering of operators. Low order moments can be directly calculated, for example

$$\overline{n^2}_{\rm total} \;=\; \overline{n}^2_{\rm total} \;+\; 2\overline{n}_{\rm total} \;+\; 2\,{\rm Tr}\left((vv^\dagger)^2\right)\,, \tag{6.36}$$

$$\overline{n^3}_{\rm total} \;=\overline{n}^3_{\rm total}+6\overline{n}^2_{\rm total}+4\overline{n}_{\rm total}+6\overline{n}_{\rm total}\,{\rm Tr}\left((vv^\dagger)^2\right)+12{\rm Tr}\left((vv^\dagger)^2\right)+8{\rm Tr}\left((vv^\dagger)^3\right)\,. \tag{6.37}$$

Equation (6.36) can be identified as a super-Poissonian distribution of particle pairs. It follows from the above expressions that particle production is determined by the matrix $vv^\dagger$ which is related in a simple way to $uu^\dagger$, Eq. (6.10). As was mentioned before, the hermitian matrix $vv^\dagger$ can always be diagonalized with diagonal elements being average numbers of particles $\overline{n_q}$ in each eigenmode q. This diagonalization allows us to view particle production as a production from independent modes. A

connection can be established to the one-oscillator case, previously considered, by defining a set of parameters ρ as $\rho_q = \overline{n_q}/(1+\overline{n_q})$, that are the eigenvalues of $vv^\dagger uu^\dagger$. Considering the number of particles produced in each eigenmode we can restrict ourselves by the modes with $\rho_q \to 1$, that dominate the particle production. We will later refer to these modes as condensate modes. In the following section, it will be shown that the distinct physical feature of these modes is that they produce an exponentially large number of particles.

Next we consider a number of condensate modes with equal parameters ρ_q. For one mode the answer is in Eq. (6.15). For the case with several condensate modes one needs to know the distribution for the total sum of the particles, which is given by the convolution of the corresponding probabilities. As for the Fourier transformation, a convolution of several distributions results in a product of their generating functions. The generating function for the distribution (6.15) is

$$\tilde{P}(y) \;=\; \sum_{n=0}^{\infty} P(2n)\, y^n \;=\; \frac{\sqrt{1-\rho}}{\sqrt{1-\rho y}}\,.$$

We obtain total probabilities of particle production for any combination of species or any number of modes convoluted together, as a Fourier expansion of a product of corresponding generating functions. Suppose we are looking for a distribution $P_l(2n)$ that gives a probability to observe $2n$ particles appearing in l single-mode distributions (6.15). The Taylor expansion of $(1-\rho y)^{-l/2}$ gives

$$P_l(2n) \;=\; \frac{(l+2(n-1))!!}{2^n\, n!\, (l-2)!!}\, \rho^n\, (1-\rho)^{l/2}\,, \tag{6.38}$$

where the double factorial should be understood appropriately for odd and even l .

According to the central limit theorem, only the distributions corresponding to a small number of condensate modes have a shape that is very different from a Gaussian, see Figure 6.3 below. If parameters $\{\rho_q\}$ for the condensate modes are very different then only the important modes that produce many particles can be isolated

reducing the problem back to the case of several almost degenerate modes. The method of generating functions is also convenient in discussions of distributions over species. For example, the distribution for the total number of pions, regardless of the isospin projection, can be obtained as a distribution of the sum of three species, via convolution. Alternatively, one can think of the total condensate modes for pions as just a sum of numbers of condensate modes for all species.

As an example we apply Eq. (6.38) for one mode and three pion species. The probability of having $2n$ neutral pions is

$$P^0(2n) \;=\; P_1(2n) \;=\; \frac{(2n)!}{2^{2n}\,(n!)^2}\,(1-\rho)^{1/2}\,\rho^n\,, \tag{6.39}$$

the probability for observing $2n$ charged pions is

$$P^+(n) \;=\; P^-(n) \;=\; P^{\rm charged}(2n) \;=\; P_2(2n) \;=\; (1-\rho)\rho^n\,, \tag{6.40}$$

and finally the probability of having total $2n$ pions is

$$P^{\rm tot}(2n) \;= P_3(2n) \;=\; \frac{(2n+1)!}{2^{2n}\,(n!)^2}\,(1-\rho)^{3/2}\,\rho^n\,. \tag{6.41}$$

We note the convolution of three distributions in Eq. (6.39) that give rise to Eq. (6.41) produces a peaked curve with maximum at particle number

$$n_{\rm max} \;=\; \frac{3\rho-2}{1-\rho}\,.$$

The probability distributions (6.39, 6.40, 6.41) are shown in Fig. 6.3 with solid line, long dashed line and short dashed line, respectively. The figure displays a critical situation when parameter ρ is 0.999. This corresponds closely to the first mode in the example of a square perturbation considered in the next section.

Now we can return to the original questions: What is the probability to observe a certain fraction of neutral pions given the total number of pions detected? Is it possible to use this distribution for the detection of chiral condensate? In the one-mode approximation, given a total number of pions produced $2n_t$, the normalized

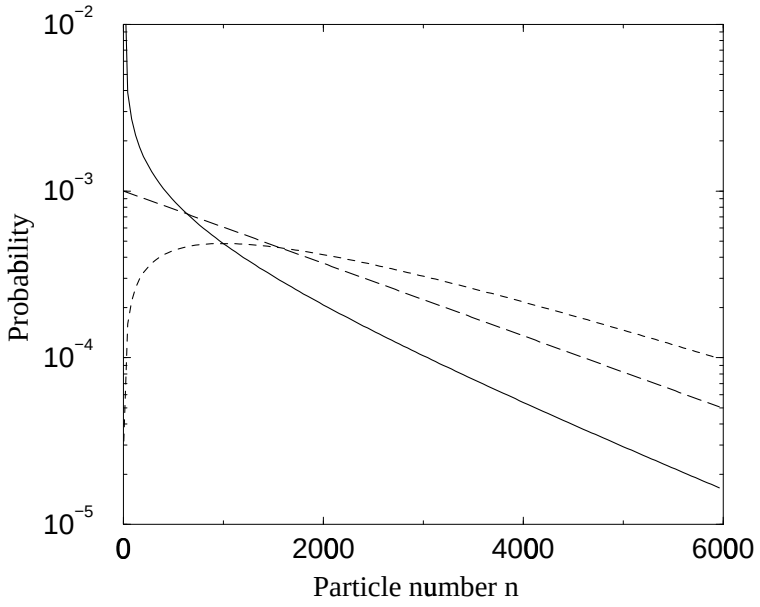

Figure 6.3: The particle number distribution for neutral pions (solid line), charged pions (long dashes), and for all pions (short dashed line). All curves are normalized to unity; note that the total number of pions and number of neutral pions both are always even, while any integer number of charged pions appearing in pairs is allowed. The parameter $\rho = 0.999$.

probability of observing $2n$ neutral particles is

$$\mathcal{P}\left(f=\frac{n}{n_t}\right) \;=\; \frac{P^0(2n)\,P^{\rm charged}(2n_t-2n)}{P^{\rm tot}(2n_t)} \;=\; \frac{(2n)!}{(2n_t)!}\left(\frac{n_t!}{n!}\right)^2 2^{2n_t-n}\,. \tag{6.42}$$

Finally, if both n and n_t are large, which is a good approximation in almost all regions, Stirling's formula may be used, and one finds

$$\mathcal{P}(f) \;=\; \frac{1}{(2n_t+1)\sqrt{f}}\,, \tag{6.43}$$

which coincides with Eq. (6.1) if the normalization over n_t+1 discrete points between zero and one is switched to the integral over $f\in[0,1]$.

Unfortunately, this result does not hold for all situations when several modes are participating together. The single-mode result (6.43) may be invalid when the largest eigenvalue of the matrix $vv^\dagger$ is exactly or almost degenerate. Physically, this may be due to some symmetry for example. One- and two-mode cases have their probability peaked at zero, this is no longer true for the convolution of three or more modes, Fig. 6.3. Eq. (6.38) can be applied to give a result for any number of modes j participating in the condensate, assuming they all have equal strength ρ. The distribution of neutral pions is given by

$$\mathcal{P}_j\left(f=\frac{n}{n_t}\right) \;=\; \frac{P_j(2n)\,P_{2j}(2n_t-2n)}{P_{3j}(2n_t)}\,. \tag{6.44}$$

With a Stirling's formula and the assumption $n\gg j$, Eq. (6.44) can be simplified to

$$\mathcal{P}_j(f) \;=\; \frac{(3j/2-1)!}{(j/2-1)!\,(j-1)!}\,f^{j/2-1}\,(1-f)^{j-1}\,. \tag{6.45}$$

For comparison, the probability distributions for one, two, and three modes in the condensate are shown in Fig. 6.4. The distributions of Eq. (6.45) have maxima, average and widths as follows

$$f_{\rm max} \;=\; \frac{j-3}{3j-4}\,,\;\; \overline{f}=1/3\,,\;\; \overline{f^2}-\overline{f}^2 \;=\; \frac{4}{27j+18}\,,$$

where the first equation can be applied with the restriction $j>2$. It follows from the central limit theorem that for a large number of modes one should expect a

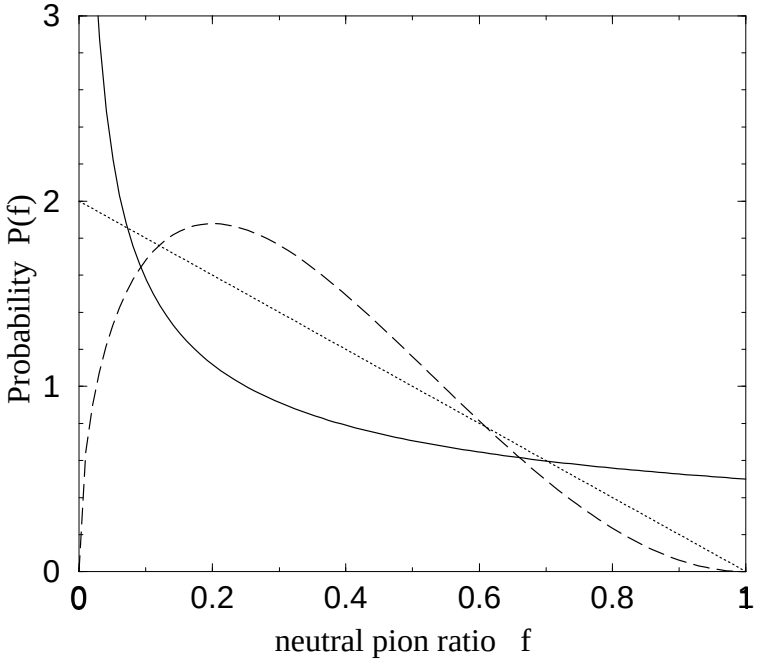

Figure 6.4: The probability $\mathcal{P}(f)$ that a given neutral pion fraction f is observed. The three curves display cases of one condensate mode (solid line), two energy-degenerate modes (dotted line), and three modes (dashed line).

Gaussian distribution that tends to a δ-function. Thus, as the number of modes in the condensate grows, there is a fast transition from a $1/\sqrt{f}$ type behavior to a sharp peak at $f = 1/3$.

Dynamics of matrices u and v

As some final remarks about the link between classical and quantum solutions to the wave equation arising from the Lagrangian in Eq. (6.5), we would like to discuss the technical question of constructing matrices u and v. Unfortunately, Eq. (6.2) has no general analytic solution even classically. The Green's function formalism reduces the problem to a Fredholm type integral equation. The exact solution can be obtained only in special cases, for a separable kernel [139], or in the sudden perturbation limit to be considered in the next section. However, numerical studies of Eq. (6.2) seem to offer a great chance of success.

It would be good to obtain equations for u and v that are still exact but written in the form convenient for numerical work. Let us quantize the field at every intermediate stage with bare particles [139] so that

$$\psi(x,t) = \sum_k \frac{1}{\sqrt{2\,\omega_k\,L}} \left(b_k(t)\, e^{i\,k\,x - i\omega_k\,t} \;+\; b_k^\dagger(t)\, e^{-i\,k\,x + i\omega_k\,t} \right) , \tag{6.46}$$

where $b_k(t)$ is now a time-dependent annihilation operator. Eq. (6.46) is written in an interaction representation, the explicit time dependence of the free field is given by the exponents, whereas creation and annihilation operators absorb the remaining non-trivial time dependence. In Eq. (6.46) the variable $\omega_k = \left(k^2 + m_{eff}^2(t \to -\infty) \right)^{1/2}$ is the initial time-independent frequency, thus there is no problem if at any point in time the effective mass goes through zero. As time goes to infinity $\psi(x,t)$ becomes the final "out" state, with operators b and $b^\dagger$ defined as before. For one-dimensional case L is the quantization length. For further simplicity we to denote

$$m_{eff}^2(x,t) \;=\; m_{eff}^2(t \to -\infty) \;+\; \Pi(x,t)\,, \tag{6.47}$$

this allows the separation of the interaction Hamiltonian. The perturbed Hamiltonian from Eq. (6.6) expressed in terms of $b(t)$ and $b^\dagger(t)$ is

$$H^{int}(t) = \sum_{k\,k'} \left\{ \Omega_{k\,k'}(t) \left(b_k^\dagger(t)\, b_{k'}(t) + \frac{\delta_{k\,k'}}{2} \right) + \right.$$

$$\left. \frac{1}{2}\, \Lambda_{k\,k'}(t)\, b_k^\dagger(t) b_{k'}^\dagger(t) + \frac{1}{2}\, \Lambda^*_{k\,k'}(t)\, b_k(t) b_{k'}(t) \right\}, \tag{6.48}$$

where the matrices Ω and Λ are determined as follows:

$$\Omega_{k\,k'}(t) \;=\; \frac{1}{2L\sqrt{\omega_k \omega_{k'}}}\, \Re \left(\Pi(k-k',\, t) e^{i(\omega_{k'} - \omega_k)t} \right) ,\;\; \Lambda_{k\,k'}(t) \;=\; \frac{\Pi(-k'-k,\, t)}{2L\sqrt{\omega_k \omega_{k'}}}\, e^{i(\omega_{k'} + \omega_k)t} . \tag{6.49}$$

In the above expression $\Pi(k,t)$ is a Fourier image of $\Pi(x,t)$, determined as

$$\Pi(k,t) \;=\; \Pi^*(-k,t) \;=\; \int \Pi(x,t)\, e^{i\,k\,x}\, dx\,,$$

and $\Re$ denotes a real part of the expression. Utilizing the Hamiltonian equation of motion in the interaction picture,

$$i\,\frac{d}{dt}\, b(t) \;=\; [b(t), H^{int.}(t)] \;=\; \Omega\, b(t) \;+\; \Lambda\, b^\dagger(t)\,,$$

it is possible to show that if $b(t)$ is defined through the initial operators a and $a^\dagger$ as

$$b(t) \;=\; u(t)\, a \;+\; v(t)\, a^\dagger\,, \tag{6.50}$$

where u and v must satisfy the matrix equations

$$i\,\frac{d}{dt}\, u(t) \;=\; \Omega(t)\, u(t) \;+\; \Lambda(t) v^*(t)\,, \tag{6.51}$$

$$i\,\frac{d}{dt}\, v(t) \;=\; \Omega(t)\, v(t) \;+\; \Lambda(t) u^*(t)\,. \tag{6.52}$$

At infinitely large times when the perturbation Π goes to zero, the right hand sides of Eqs. (6.51, 6.52) vanish and u and v become time-independent. In order to obtain matrices u and v for Eq. (6.22) one has to solve the above equations with initial conditions $u = 1$ and $v = 0$.

6.4 Application to chiral condensates

6.4.1 Separable modes, space-independent effective masses

To illustrate the machinery developed in the previous section we start with simple cases when the classical solution is known analytically. The first example is the space-independent field $\Pi(\mathbf{x},t) \equiv \Pi(t)$, see Eq. (6.47), i.e. the situation when the perturbation is uniform in a box to which the entire pion field is confined. The wave vector $\mathbf{k}$ is a good quantum number. Particles get produced independently in each mode labeled with $\mathbf{k}$, and production is determined by the classical reflection probability $\rho_{\mathbf{k}} = |v_{\mathbf{k}}|^2/|u_{\mathbf{k}}|^2$, Eq. (6.15). The distribution of particles for a single mode, Eq. (6.15), is a decaying function that has a maximum at zero. Its behavior can be approximated with Stirling's formula as

$$P(2n) \sim \frac{\rho^n}{\sqrt{n}},$$

where $P(2n)$ denotes the probability of creating $2n$ particles from the vacuum. The distribution in Eq. (6.15) for a value of $\rho = 0.999$ is shown in Fig. 6.3 as a solid line; some additional discussion is given below. The average number of particles produced in Eq. (6.16) is generally quite small unless we are in the condensate region when $\rho \to 1$. With the assumption of independent modes Eq. (6.4) reduces to

$$-d^2\pi_\tau/dt^2 - \Pi(t)\pi_\tau = (m_\pi^2 + k^2)\pi_\tau\,. \tag{6.53}$$

Eq. (6.53) is written in a form of the Schrödinger equation for scattering from a potential barrier of height $-\Pi$ at "energy" $m_\pi^2 + k^2$. The parameter ρ we are looking for, which links classical and quantum pictures, is the reflection coefficient for this scattering process.

Let the effective pion mass change and then return back to normal in a step function manner. This corresponds to the scattering off a rectangular potential barrier.

The situation when the tunneling is involved, is relevant to the case of a low momentum mode being amplified as the index of reflection is rapidly increasing. We assume that the perturbation $\Pi(t)$ has a non-zero value Π only for the time interval $t \in [0, T]$. The reflection probability for this scattering potential is

$$\rho_{\mathbf{k}} = \frac{|v_{\mathbf{k}}|^2}{1 + |v_{\mathbf{k}}|^2},$$

and the average number $\overline{n}_{\mathbf{k}}$ of particles created in the mode $\mathbf{k}$ is given by

$$\overline{n}_{\mathbf{k}} = |v_{\mathbf{k}}|^2 = \frac{\Pi^2}{4\,(m_\pi^2 + \mathbf{k}^2)\,|m_\pi^2 + \mathbf{k}^2 + \Pi|} \left| \sin\left(T\sqrt{m_\pi^2 + \mathbf{k}^2 + \Pi}\right)\right|^2, \quad (6.54)$$

Another form of the perturbation $\Pi(t)$ for which an exact analytical solution exists is the Eckart potential [148]

$$\Pi(t) = \frac{\Pi}{\cosh^2(t/T)},$$

where $\Pi = \Pi(0)$ is the minimum value of $\Pi(t)$ and T is the time scale of perturbation. The resulting form of the reflection probability is

$$\rho_{\mathbf{k}} = \left| \frac{1 + \cos\left(\pi\sqrt{4\,\Pi\,T^2 + 1}\right)}{\cosh\left(2\,\pi\,T\sqrt{m_\pi^2 + \mathbf{k}^2}\right) + \cos\left(\pi\sqrt{4\,\Pi\,T^2 + 1}\right)} \right|$$

Both forms of the perturbation $\Pi(t)$ with parameters that we use below for our numerical estimates are plotted in Fig. 6.5, right side shows the Eckart potential, rectangular barrier is on the left. Fig. 6.6 shows the average number of particles produced in the two models described above. For our estimate we made the following choice of parameters. The effective mass drops to the value of $m_{\text{eff}}^2 = -m_\sigma^2/2$, correspondingly the parameter Π is chosen at -1 GeV^2 for both models. The time scale, given by parameter T, is 1 fm/c and 0.5 fm/c for the square barrier and the Eckart potential, respectively. It is important to notice that even though the graph is plotted over a continuous variable k, our finite size spatial box allows only discrete values of momentum in each direction. With the expected interaction region size of 2

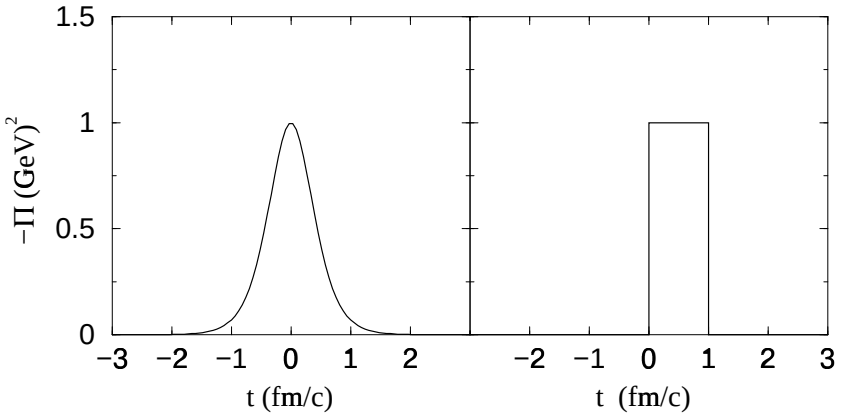

Figure 6.5: Eckart ($|\Pi| = 1$ (GeV)^2, $T = 0.5$ fm/c) and rectangular ($|\Pi| = 1$ (GeV)^2, $T = 1$ fm/c) perturbations are shown on the right and left panels, respectively.

fm, the lowest momentum in a cubic well of size L is $|\mathbf{k}| \approx \sqrt{3}\,\pi/L$, numerically this is about 540 MeV. According to Fig. 6.6, both models predict around several hundreds of particles. The next higher-lying modes, have significantly smaller numbers of particles. The picture presented shows that one can only hope to have very few modes that actually form the condensate, as the number of particles falls drastically for higher momenta. This is consistent with the argument that in order to get a noticeable condensate one should have the energy of the mode dipping below zero. The square barrier model provides a simple estimate for the number of particles produced if the mode just touches zero,

$$\overline{n} \;=\; -\frac{\Pi T^2}{4} \;\approx\; \frac{m_\sigma^2 T^2}{8} \;\approx 6\,,$$

where the sigma mass m_σ is taken 1.4 GeV and the interaction time T is around 1 fm/c .

For more complicated perturbations it is possible to use the WKB approximation in order to determine the reflection coefficient of classical Eq. (6.7) for tunneling.

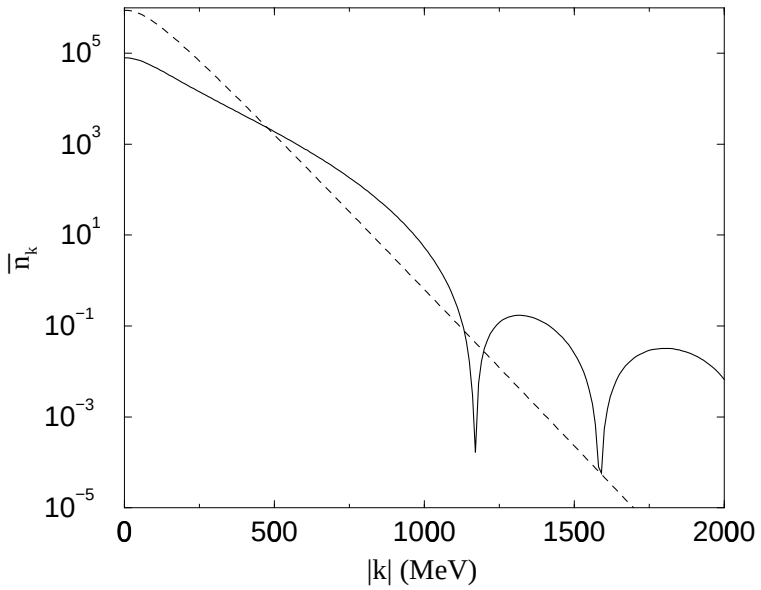

Figure 6.6: The average number of particles produced in the mode $\mathbf{k}$ as a function of k for square potential (solid line) and Eckart potential (dashed line). The parameters of the perturbation are chosen so that $\Pi = 1$ GeV^2 for both models, and T is 0.5 fm/c and 1.0 fm/c for Eckart and square potentials, respectively.

With the notation

$$\xi \;=\; 2\,\exp\left(\int_{-\infty}^{\infty} |\omega(t)|\,\Theta\left(-\omega^2(t)\right)\,dt\right)\,,$$

where the Heaviside theta-function limits the integration to the region of negative $\omega^2(t)$, we have the average number of particles given in the semiclassical limit of $\xi \gg 1$ by

$$\overline{n} \;=\; \frac{\xi^2}{4}\,. \tag{6.55}$$

Concerning the total particle distribution one has to add all particles from all modes and consider the distribution as a superposition. Based on the results of the above examples and Sec. 2 we can conclude the following. About a thousand neutral pions with momentum 540 MeV/c are produced by the lowest mode and are distributed according to $P_1(2n)$, Eq. (6.38). The distribution over species is $\mathcal{P}_1 \sim 1/\sqrt{f}$, Eq. (6.45). This is the single-mode result described by Eqs. (6.39, 6.40, 6.41) and shown in Fig. 6.3. Geometry is crucial here, as it determines the energies and degeneracies of other modes that may or may not compete with the lowest mode(s). Higher momentum modes in the box do not "condense" if, in the scattering picture, their energy is higher than the barrier and reflection is negligible. These modes, even jointly, may on average produce just several particles. The case of the non-condensate particle production will be considered with a better model in the next subsection.

These simple examples are still far from realistic. One of the major failures is that pions from the square box are not real pions and therefore all excitations that we obtain need to be projected onto final pion states given by the plane waves of the entire space. This projection will produce a momentum spread of the outgoing states, that will carry the characteristics of each condensate mode. Nevertheless, these models produced reasonable results and what is more important they have identified the physics of the process.

6.4.2 Time- and space-dependent perturbations

General solution for a step-like temporal perturbation

Here we will solve the perturbed Klein-Gordon equation for the pions in a more realistic case, where the effective pion mass is both space- and time-dependent,

$$\frac{\partial^2\pi}{\partial t^2} - \nabla^2\pi + \Big(m_\pi^2 + \Pi(\mathbf{x},t)\Big)\,\pi = 0\,. \tag{6.56}$$

Despite the fact that this dependence is put into the model by hand, the resulting features can be quite general. In order to keep our solutions analytic we choose the perturbation $\Pi(\mathbf{x},t)$ as a step function in time

$$\Pi(\mathbf{x},t) \;=\; \begin{cases} \Pi(\mathbf{x}) & \text{for} \quad t \in [0,T] \\ 0 & \text{otherwise} \end{cases} \quad .$$

This choice will allow us to solve Eq. (6.56) classically and to construct matrices u and v that control the evolution of a plane wave. For most of the discussion the form of $\Pi(\mathbf{x})$ is left as general, but in the last part for the numerical results we take it as a spherical square well.

The wave function $\pi(\mathbf{x},t)$ can be found in each of the time regions, and the solutions should be smoothly matched keeping $\pi(\mathbf{x},t)$ and the derivative $\partial\pi(\mathbf{x},t)/\partial t$ continuous. Introducing a separation of variables as $\pi(\mathbf{x},t) \;= \mathcal{X}(\mathbf{x})\,\mathcal{T}(t)$ we obtain equations of motion for $\mathcal{X}$ and $\mathcal{T}$ in all three time regions. In the perturbed region $t \in [0,T]$, Eq. (6.56) becomes

$$\begin{aligned} -\nabla^2\mathcal{X}(\mathbf{x}) + \Pi(\mathbf{x})\,\mathcal{X}(\mathbf{x}) \;&=\; \mathcal{E}\,\mathcal{X}(\mathbf{x})\,, \\ \frac{\partial^2\mathcal{T}(t)}{\partial t^2} + W^2\,\mathcal{T}(t) \;&=\; 0\,, \end{aligned} \tag{6.57}$$

where the dispersion relation is

$$W^2 = m_\pi^2 + \mathcal{E}\,. \tag{6.58}$$

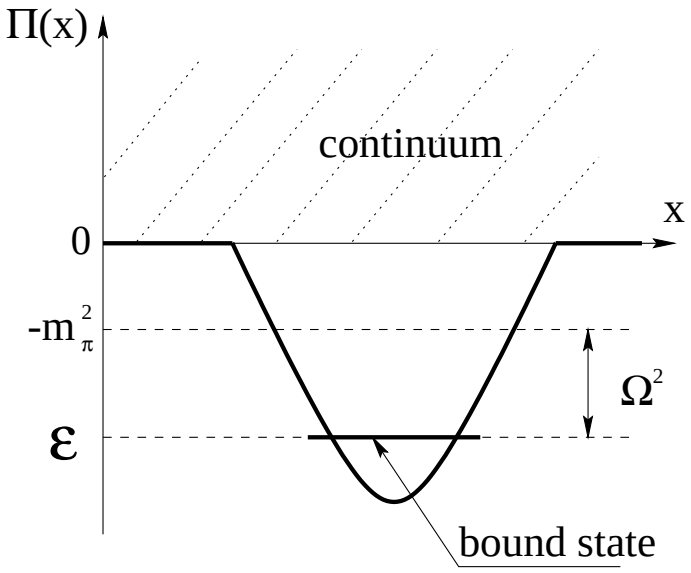

Figure 6.7: The schematic representation of the perturbation $\Pi(x)$, with one condensate bound state.

The unperturbed form of the free space wave equations at $t < 0$ or $t > T$ is

$$-\nabla^2 \mathcal{X}^\circ(\mathbf{x}) \;=\; |\mathbf{k}|^2\, \mathcal{X}^\circ(\mathbf{x})\,, \tag{6.59}$$
$$\frac{\partial^2 \mathcal{T}^\circ(t)}{\partial t^2} \;+\; \omega_{\mathbf{k}}^2\, \mathcal{T}^\circ(t) \;=\; 0\,,$$

with the usual relation

$$\omega_{\mathbf{k}}^2 = m_\pi^2 \;+\; |\mathbf{k}|^2\,.$$

Eq. (6.59) has simple plane wave eigensolutions that we denote as $|\mathbf{k}\rangle$ with positive eigenvalues $|\mathbf{k}|^2$. The perturbed Eq. (6.57) with negative Π may have negative energy bound states as well as the usual continuum states with positive energies, see Fig. 6.7. For such a bound state, W^2, Eq. (6.58), becomes negative and $W = i\Omega$ is imaginary. We denote the eigenstates of Eq. (6.57) as $|\kappa)$ and corresponding energy as $\mathcal{E}(\kappa)$. Here κ is a set of quantum numbers labeling the eigenstates. We also assume that both $|\mathbf{k}\rangle$ and $|\kappa)$ are properly normalized and form complete sets,

$$\langle \mathbf{k}|\mathbf{k}'\rangle \;=\; \delta_{\mathbf{k},\,\mathbf{k}'}\,, \quad (\kappa|\kappa') \;=\; \delta_{\kappa,\,\kappa'}\,, \quad 1 \;=\; \sum_{\mathbf{k}} |\mathbf{k}\rangle\,\langle\mathbf{k}| = \sum_{\kappa} |\kappa)\,(\kappa|\,.$$

To determine the Bogoliubov transformation matrices u and v we consider the evolution of the wave function

$$|\pi(t)\rangle \;=\; e^{-i\omega_{\mathbf{k}}t}\,|\mathbf{k}\rangle\,, \quad \text{for } t<0\,,$$

through an intermediate stage $t\in[0,T]$

$$|\pi(t)\rangle \;=\; \sum_{\kappa}\left(a_{\mathbf{k}\,\kappa}\,e^{-iW_\kappa t}\;+\;b_{\mathbf{k}\,\kappa}\,e^{iW_\kappa t}\right)\,|\kappa)\,,$$

into a final state

$$|\pi(t)\rangle \;=\; \sum_{\mathbf{k}'}\sqrt{\frac{\omega_{\mathbf{k}}}{\omega_{\mathbf{k}'}}}\,\left(u_{\mathbf{k}\,\mathbf{k}'}\,e^{-i\omega_{\mathbf{k}'}t}\;+\;v_{\mathbf{k}\,\mathbf{k}'}\,e^{i\omega_{\mathbf{k}'}t}\right)\,|\mathbf{k}'\rangle\,.$$

Continuity of the wave function and its derivative with respect to time allows the determination of the unknown coefficients $a_{\mathbf{k}\,\kappa}$ and $b_{\mathbf{k}\,\kappa}$ as well as the matrix elements of interest $v_{\mathbf{k}\,\mathbf{k}'}$ and $u_{\mathbf{k}\,\mathbf{k}'}$. The result is, both for real and imaginary W_κ,

$$u_{\mathbf{k}\,\mathbf{k}'} \;=\; \sqrt{\frac{\omega_{\mathbf{k}'}}{\omega_{\mathbf{k}}}}\,\frac{e^{i\omega_{\mathbf{k}'}T}}{2}\,\sum_{\kappa}\langle\mathbf{k}'|\kappa)(\kappa|\mathbf{k}\rangle\,\times$$
$$\left[\left(1+\frac{\omega_{\mathbf{k}}}{\omega_{\mathbf{k}'}}\right)\,\cos\left(W_\kappa\,T\right)\;-\;i\left(\frac{\omega_{\mathbf{k}}}{W_\kappa}+\frac{W_\kappa}{\omega_{\mathbf{k}'}}\right)\sin\left(W_\kappa\,T\right)\right]\,, \tag{6.60}$$

and

$$v_{\mathbf{k}\,\mathbf{k}'} \;=\; \sqrt{\frac{\omega_{\mathbf{k}'}}{\omega_{\mathbf{k}}}}\,\frac{e^{-i\omega_{\mathbf{k}'}T}}{2}\,\sum_{\kappa}\langle\mathbf{k}'|\kappa)(\kappa|\mathbf{k}\rangle\,\times$$
$$\left[\left(1-\frac{\omega_{\mathbf{k}}}{\omega_{\mathbf{k}'}}\right)\,\cos\left(W_\kappa\,T\right)\;-\;i\left(\frac{\omega_{\mathbf{k}}}{W_\kappa}-\frac{W_\kappa}{\omega_{\mathbf{k}'}}\right)\sin\left(W_\kappa\,T\right)\right]\,. \tag{6.61}$$

In order to see whether the condensate was formed we first address the question of the number of produced pions. Possible bound states in the solutions of Eq. (6.57) should be carefully treated. As seen below, bound states in Eq. (6.57) with the energy $\mathcal{E}$ below $-m_\pi^2$ produce an exponential growth of the particle number with time which is our starting criterion for the search of the condensate. The average number of particles may be then expressed using Eq. (6.35) as

$$\overline{n}=\sum_{\mathbf{k}\,,\,\mathbf{k}'}\,|v_{\mathbf{k}\,\mathbf{k}'}|^2=\frac{1}{4}\sum_{\kappa\,,\,\kappa'}\,\left\{A_{\kappa\,\kappa'}\,\cos\left(W_\kappa T\right)\cos\left(W_{\kappa'}T\right)+B_{\kappa\,\kappa'}\,\sin\left(W_\kappa T\right)\sin\left(W^*_{\kappa'}T\right)\right\}\,, \tag{6.62}$$

$$A_{\kappa\,\kappa'} = 2\left(I^{(-1)}_{\kappa\,\kappa'} I^{(1)}_{\kappa\,\kappa'} \;-\; \delta_{\kappa\,\kappa'}\right)\,,$$

$$B_{\kappa\,\kappa'} = \left(\frac{{I^{(1)}_{\kappa\,\kappa'}}^{\,2}}{W_\kappa W^*_{\kappa'}} - \left(\frac{W_\kappa}{W^*_{\kappa'}} + \frac{W^*_{\kappa'}}{W_\kappa}\right)\delta_{\kappa\,\kappa'} + {I^{(-1)}_{\kappa\,\kappa'}}^{2} W_\kappa W^*_{\kappa'}\right)\,,$$

where we assumed that the states are chosen in such a way that the amplitudes $\langle \mathbf{k}|\kappa)$ are real, and we introduced the notations

$$I^{(1)}_{\kappa\,\kappa'} = I^{(1)}_{\kappa'\,\kappa} \;=\; \sum_{\mathbf{k}} (\kappa|\mathbf{k}\rangle \omega_{\mathbf{k}} \langle \mathbf{k}|\kappa')\,,$$

and

$$I^{(-1)}_{\kappa\,\kappa'} = I^{(-1)}_{\kappa'\,\kappa} \;=\; \sum_{\mathbf{k}} (\kappa|\mathbf{k}\rangle \frac{1}{\omega_{\mathbf{k}}} \langle \mathbf{k}|\kappa')\,.$$

Depending on a particular level, W may be real or imaginary if in Eq. (6.58) the energy $\mathcal{E}$ is greater or less than m_π^2; nevertheless Eq. (6.62) works for both cases.

In practice it is convenient to express the overlap of $\langle \mathbf{k}|\kappa)$ using Eqs. (6.57, 6.59) for the states $|\kappa)$ and $|\mathbf{k}\rangle$. Multiplying Eq. (6.57) by $\mathcal{X}^\circ$ and Eq. (6.59) by $\mathcal{X}$ and subtracting results we obtain

$$(\mathcal{E} - \mathbf{k}^2)\mathcal{X}\,\mathcal{X}^\circ \;= \Pi(\mathbf{x})\mathcal{X}\,\mathcal{X}^\circ \;+\; \nabla(\mathcal{X}\nabla\mathcal{X}^\circ - \mathcal{X}^\circ\nabla\mathcal{X})\,. \tag{6.63}$$

Integration of Eq. (6.63) over all space produces a useful result

$$\langle \mathbf{k}|\kappa) = \frac{1}{\mathcal{E} - \mathbf{k}^2} \int d^3x\, \Pi(\mathbf{x})\mathcal{X}\,\mathcal{X}^\circ\,. \tag{6.64}$$

For the continuous spectrum, this expression contains an additional term with $\delta(\mathcal{E} - \mathbf{k}^2)$.

Due to large oscillations of the trigonometric factors in Eqs. (6.61) and (6.62), one should expect considerable particle production only in situations with imaginary W. This observation makes it natural to separate the sum in Eq. (6.62) into several contributions depending on the intermediate state $|\kappa)$. There are exponentially rising terms that involve transitions through the states with imaginary W; it is important that the bound states are discrete and that their number is finite. Another contribution is of all intermediate states that lie in the continuum. This second contribution is

always present for any perturbation even with no bound states. With a non-zero pion mass there maybe a number of discrete states that have real W but these states have negligible contributions compared to the states from the continuum. In the remaining part of this subsection we will mainly draw attention to the first two cases which we call "condensate" and "non-condensate" pion production.

Condensate pion production.

In the following picture we assume that there is one mode $|\kappa_0)$ with negative energy so that $W_{\kappa_0} = i\Omega$, and in the summation in Eq. (6.61) the term that involves this condensate state $|\kappa_0)$ is dominant. Thus, the distribution of particles and all other properties are the same as in the single-mode example, i.e. as for the parametrically excited single oscillator. According to Eqs. (6.35), (6.36), (6.37) and (6.24), the traces of $vv^\dagger$ and other higher powers of this matrix completely determine all moments of the particle distribution and thus the distribution itself. Therefore, it is sufficient to consider the eigenvalues of a hermitian matrix $vv^\dagger$.

Under the assumption that only one term in the sum in Eq. (6.61) is important, we can express the matrix element of $vv^\dagger$ as

$$\{vv^\dagger\}_{\mathbf{k},\,\mathbf{k}'} = a\frac{1}{\sqrt{\omega_{\mathbf{k}}\,\omega_{\mathbf{k}'}}} + b\,\sqrt{\omega_{\mathbf{k}}\,\omega_{\mathbf{k}'}} + c\,\sqrt{\frac{\omega_{\mathbf{k}}}{\omega_{\mathbf{k}'}}} + c^*\,\sqrt{\frac{\omega_{\mathbf{k}'}}{\omega_{\mathbf{k}}}}\,, \tag{6.65}$$

where the introduced coefficients are

$$a = \frac{1}{4}\left(I^{(1)}\cosh^2(\Omega T) + \Omega^2 I^{(-1)}\sinh^2(\Omega T)\right)\,, \tag{6.66}$$

$$b = \frac{1}{4}\left(I^{(-1)}\cosh^2(\Omega T) + I^{(1)}\sinh^2(\Omega T)/\Omega^2\right)\,, \tag{6.67}$$

$$c = \frac{1}{4}\left(i\left[I^{(1)}/\Omega + I^{(-1)}\Omega\right] - 1\right)\,, \tag{6.68}$$

and

$$I^{(-1)} = \sum_{\mathbf{k}} |\langle\mathbf{k}|\kappa_0)|^2\frac{1}{\omega_{\mathbf{k}}}\,, \quad I^{(1)} = \sum_{\mathbf{k}} |\langle\mathbf{k}|\kappa_0)|^2\omega_{\mathbf{k}}\,.$$

We wrote an element of the matrix $vv^\dagger$ in the form of Eq. (6.65) in order to show that it consists of only four factorizable terms. In accordance with a general theory of factorizable kernels, the only non-zero eigenvalues of the matrix $vv^\dagger$ are the eigenvalues of the following 4×4 matrix

$$\begin{pmatrix} aI^{(-1)} & b & c & bI^{(-1)} \\ a & bI^{(1)} & cI^{(1)} & c^* \\ aI^{(-1)} & b & c & bI^{(-1)} \\ a & bI^{(1)} & cI^{(1)} & c^* \end{pmatrix} . \tag{6.69}$$

Having the second two rows the same as the first two in the matrix (6.69) reduces the actual number of non-zero eigenvalues to two, and the secular equation for the eigenvalues λ

$$\lambda^2 - \lambda \,\mathrm{Tr}(vv^\dagger) + \frac{1}{16}(I^{(1)}\, I^{(-1)} - 1)^2 = 0\,. \tag{6.70}$$

The trace of the matrix $vv^\dagger$ in this expression is the same as the average number of particles produced by one condensate state $|\kappa_0)$,

$$\overline{n} = \mathrm{Tr}(vv^\dagger) = \frac{\cosh^2(\Omega\, T)}{2}\left(I^{(-1)}\, I^{(1)}\right) + \frac{\sinh^2(\Omega\, T)}{4}\left(I^{(-1)^2}\,\Omega^2 + \frac{I^{(1)^2}}{\Omega^2}\right) - \frac{1}{2}\,. \tag{6.71}$$

The result (6.71) can be also obtained directly from Eq. (6.62).

In the limit of $\exp(2\Omega T) \gg 1$, Eq. (6.71) becomes

$$\overline{n} \;=\; \frac{e^{2\Omega T}}{16}\left(I^{(-1)}\Omega \,+\, \frac{I^{(1)}}{\Omega}\right)^2 . \tag{6.72}$$

This approximation is relevant to our problem as we wish to determine the exponentially growing condensate modes and therefore we choose a physical environment for which this is true. The limitation $\exp(2\Omega T) \gg 1$ is then a criteria for the environment of a chiral condensate. As seen from Eq. (6.70), of the remaining two eigenvalues of the matrix $vv^\dagger$ one becomes exponentially large and the other one goes to zero. This is important because with only one nonzero eigenvalue we recover the single-mode

situation, discussed in the previous sections which leads to the distribution of particles of the form of Eq. (6.39) and a $1/\sqrt{f}$ form for the distribution over the pion species.

As a concluding statement we stress here that in principle just making the approximation $\exp(2\Omega T) \gg 1$ allows us to take one term in the sum of Eqs. (6.60, 6.61) from the very beginning, and the same approximation was used again in the end to purify the single mode. Therefore the condition $\exp(2\Omega T) \gg 1$ must be a clear indication of a condensate in the bound mode with relative energy Ω. If there are several bound condensate states with close energies Ω we would again recover the system of several modes that was discussed before.

Non-condensate pion production

To make the picture complete we have to estimate the number of particles that are produced from all the modes not involved in the condensate. The low-lying negative energy states that have energies above the pion mass do not make a considerable contribution. They may be estimated by the same method that was used for a condensate states just having oscillating exponents instead of exponential growth in Eq. (6.72),

$$\overline{n} \sim \frac{1}{16} \left(I^{(-1)}\Omega + \frac{I^{(1)}}{\Omega} \right)^2 . \tag{6.73}$$

This source does not produce many pions, as will be seen from the numerical example in the next section.

The contribution to the number of particles from the continuum is of a greater interest. First, as the number of states is infinite, unlike the previous case of bound states, we may have a significant contribution. Secondly, it is an important practical question because the continuum states always produce pions even if the condensate is absent. It follows from Sec. 6.3 that the charge distribution of pions from many modes

of almost equal strength is Gaussian. To perform a particle number estimate we again address Eq. (6.71). It is reasonable to assume that oscillating terms corresponding to different arguments W_κ and $W_{\kappa'}$ average out to zero and the contributing terms are those that are in phase, corresponding to the same κ. For these terms we take $\sin^2(WT) \approx \cos^2(WT) \approx 1/2$. Applying these approximations to Eq. (6.71) we obtain

$$\overline{n} = \frac{1}{2} \sum_{\kappa\,,\mathbf{k}} |\langle \mathbf{k}|\kappa)|^2 \frac{(\omega_{\mathbf{k}} - W_\kappa)^2}{\omega_{\mathbf{k}}\, W_\kappa} \,. \tag{6.74}$$

As seen from the structure of this equation, the arbitrary δ-contribution in Eq. (6.64) does not influence the result for $\overline{n}$.

6.4.3 The spherical square well

The spherical square well potential of finite depth is the simplest spatial perturbation $\Pi(\mathbf{x})$ that has an analytical solution. We assume that

$$\Pi(\mathbf{x}) = \begin{cases} -V & \text{for} \quad |\mathbf{x}| < R \\ 0 & \text{otherwise} \end{cases} \,.$$

The rotational symmetry makes angular momentum a good quantum number, and the remaining radial dependence can be expressed in terms of spherical Bessel functions. Due to the largest exponential enhancement the deepest level is expected to produce most of the contribution. Thus, we concentrate our attention on an s-wave bound ground state that will be a dominant condensate state in the process. By virtue of symmetry, all pions produced from this state will have a spherically symmetrical s-wave spatial distribution. Instead of plane waves it is convenient to quantize spherical waves in a large sphere of radius L. This leads to the substitution of the former basis $|\mathbf{k}\rangle$ by $|k, l, m\rangle$ where $k = |\mathbf{k}|$ and l and m are the orbital momentum and its projection, respectively. Needed overlaps between perturbed and non-perturbed states can be computed using the one-dimensional version of Eq. (6.64) where the

right hand side is obtained by integrating Eq. (6.63) from zero up to the size R giving

$$\langle \mathbf{k}|\kappa) = \frac{V}{\mathcal{E}-\mathbf{k}^2} \frac{(\mathcal{X}(r)\,\partial/\partial\, r\mathcal{X}^{\circ}(r) - \mathcal{X}^{\circ}(r)\,\partial/\partial\, r\mathcal{X}(r))}{\mathcal{E}-k^2+V}\Bigg|_{r=R}. \qquad (6.75)$$

In particular, for a bound ($\mathcal{E}<0$) s-state $|\kappa_0)$ Eq. (6.75) gives

$$(\kappa_0|k,0,0\rangle = \frac{2\alpha^2}{\sqrt{L}} \frac{\alpha\cot(\alpha R)\,\sin(kR) - k\cos(kR)}{\sin(\alpha R)\,(k^2-\alpha^2)\,(k^2+\alpha^2\cot^2(\alpha R))} \sqrt{\frac{\alpha}{\alpha R - \tan(\alpha R)}} \qquad (6.76)$$

where $\alpha = \sqrt{V-|\mathcal{E}|}$. This overlap is normalized to one as a sum over all momenta $k = \pi n/L$, where n is a nonnegative integer. Converting this sum into an integral over all positive k will remove the quantization radius L. The eigenenergies for s-states are given by the equation

$$\alpha\cot(\alpha R) + \sqrt{\mathcal{E}} = 0\,.$$

Within these results the matrices v and u can be evaluated via Eqs. (6.60, 6.61) and all the theory described above can be applied in a straightforward way.

As a realistic physical picture, we take the depth of the spherical well $V = 1$ GeV^2, radius $R = 1$ fm, and a lifetime of the condensate $T = 1$ fm/c. Then the lowest level is at a depth of $\mathcal{E}$ =(858 MeV)^2 which corresponds to $\Omega = \sqrt{|\mathcal{E}| - m_\pi^2} = 847$ MeV. These assumptions are probably exaggerated as the average number of pions of one particular type in this case is $\overline{n} \approx 2500$.

Figure 6.8 displays the behavior of the dimensionless variables $I^{(-1)}\Omega$, $I^{(1)}/\Omega$ and their sum $I^{(-1)}\Omega + I^{(1)}/\Omega$ shown in dashed, dotted and solid lines, respectively, as a function of the potential depth, left panel, and the potential size, right panel. The singularity of $I^{(1)}/\Omega$ at threshold corresponds to Ω approaching zero and does not have any physical significance because the approximation $\exp(\Omega T) \gg 1$ no longer holds. In general both plots are dominated by the behavior of Ω for the chosen parameters, whereas the integrals $I^{(-1)}$ and $I^{(1)}$ are weakly influenced by the form of $\Pi(\mathbf{x})$.

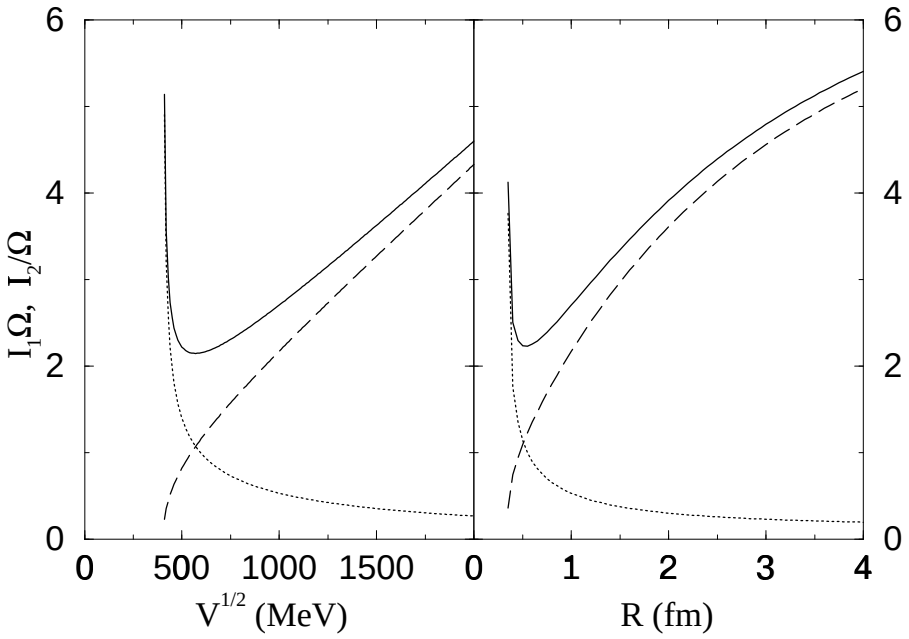

Figure 6.8: The behavior of the dimensionless variables $I^{(-1)}\Omega$, $I^{(1)}/\Omega$ and $I^{(-1)}\Omega + I^{(1)}/\Omega$ is shown in dashed, dotted and solid lines, respectively, as a function of the potential depth $\sqrt{V}$, left panel, and potential size R, right panel. A fixed size of 1 fm was used for the left panel and a fixed depth $\sqrt{V}$ =1 GeV was used for the plot in the right panel.

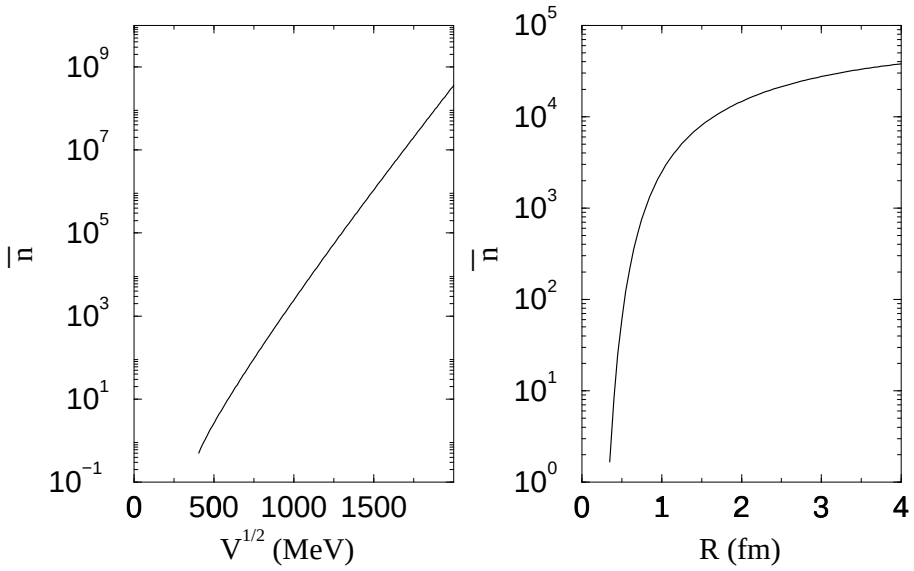

Figure 6.9: The average number of particles produced as a function of the depth of the potential field $\sqrt{V}$ is shown in the left panel, the size R was fixed at 1 fm. The right panel shows the number of particles produced as a function of size R given a fixed depth $V = 1$ GeV^2. The time length of the perturbation is set at T =1 fm/c.

Fig. 6.9 shows the average number of particles as a function of the well size, right panel, and depth of the perturbation, left panel. The average number of particles grows approximately exponentially with the potential depth (Fig. 6.9, left panel). This is simply related to the fact that in a deep well the ground state energy grows almost linearly with the depth having $\Omega \approx \sqrt{V}$. By making the potential wider the ground state approaches the bottom of the well, limiting Ω to a constant. This restrains the growth of particles shown on the right panel of Fig. 6.9. One should bear in mind that the conditions considered are quite extreme and were used here to emphasize the character of the condensate. Practically the time scale may be shorter and perturbation weaker, leading to a more pre-condensate picture with much fewer pions. The total energy available in a heavy ion reaction may provide a guideline to what the perturbation Π is and the realistic number of mesons produced are.

As a final part of this analysis we consider non-condensate pion production, which may be the main mechanism in most practical situations. Eq. (6.74) with the additional help of Eq. (6.75) results in the following form for s-wave pions from the continuum

$$\overline{n} = \frac{2V^2}{\pi^2} \int_0^\infty d\kappa \int_0^\infty dk \frac{(k \sin(\alpha R)\, \cos(kR) - \alpha\, \cos(\alpha R) \sin(kR))^2}{(\alpha^2 - k^2)^2 \omega_k W_\kappa \left(\omega_k + W_\kappa\right)^2}, \qquad (6.77)$$

where the parameter α is defined as $\alpha = \sqrt{\kappa^2 + V}$, $W_\kappa = \sqrt{\kappa^2 + m_\pi^2}$, and $\omega_k = \sqrt{k^2 + m_\pi^2}$ are the total energies of the corresponding modes. As expected, the number of particles produced with no condensate involved is quite small. The left panel in Fig. 6.10 shows the average number of non-condensate pions as a function of the potential depth for different spatial sizes R =0.5, 1, 2 fm. The right panel of the same figure displays the dependence on the size R for various values of V. The important conclusion here is that the number of non-condensate pions ranges from a few up to maybe a dozen for extreme cases. This number is completely negligible in the presence of a strong condensate that produces hundreds of mesons. However, present

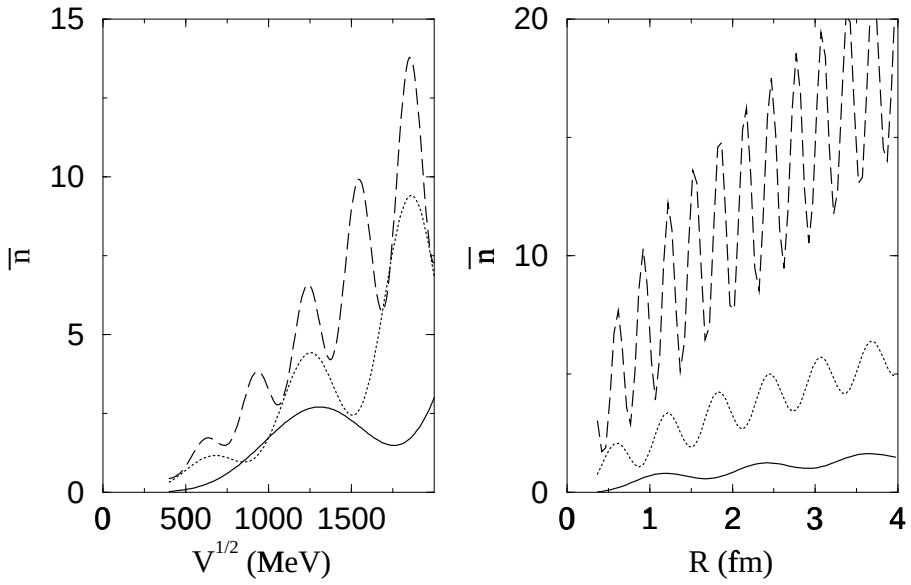

Figure 6.10: The left side shows the average number of pions of a particular type as a function of V, the depth of the perturbation. Curves displayed as solid, dotted and dashed lines correspond to the values of the radius R of 0.5, 1, and 2 fm, respectively. Plotted on the right hand side is the number of pions versus the radius R for values of $\sqrt{V}$ of 0.5, 1 and 2 GeV as solid, dotted and dashed lines, respectively.

experiments may just barely reach the point of the phase transition, and therefore the fraction of non-condensate pions is considerable, if not dominant. Moreover, other (conventional) mechanisms of pion production have to be taken into account.

6.5 Summary and conclusions

Our prime objective in this work was to study a mechanism of pion production in heavy ion and hadronic collisions related to the creation of a chiral condensate and to explore how pion distributions can signal the presence of a condensate. We studied

meson production by imposing a pion dispersion relation specific to the medium, i.e. with a space- and time-dependent effective mass.

In general, the problem of parametric excitation of the field quanta presents an interesting question as it is encountered in many branches of physics from condensed matter to high energy physics. The problem also exhibits a vast variety of solutions ranging from adiabatic to phase transitions and condensates.

We have conducted an extensive study of quantum field equations of a general form of Eq. (6.2). In our picture the parametric excitation of the field quanta is carried out by the externally given space- and time-dependent mass term. This term in the Lagrangian is quadratic in the field, and the states produced are often called "squeezed" [146, 147, 149, 150]. Some analogy can be drawn here from well studied linear current type terms that produce coherent states. However, the essential difference between coherent and squeezed states arises due to the fact that the latter correspond to the pairwise generation of quanta. In the case of pseudoscalar pions, this means that charge, isospin and parity are exactly preserved. We have emphasized the fact that the quantum solution can be built from the classical solution, and this important link was established via a canonical Bogoliubov transformation.

With our interest lying in the direction of chiral condensate we focused our attention on the potential of Eq. (6.2) to form a condensate with fast particle production and large correlations when the effective mass goes through zero. Along with a general formalism that can be used for numerical studies we have analytically solved the problem when the effective mass experiences sudden abrupt changes. Consideration of this particular temporal perturbation allowed us to clearly separate the exponentially rising collective pion condensate modes for any given spatial form of the perturbation in the effective mass. This produced conditions where the condensate and its signatures can be seen.

We have identified two basic channels of pion production. The first involves only a few discrete condensate modes and a large associated pion population. The second leads to the production of far fewer (non-condensate) particles with a broad phase space distribution. Mathematically these channels can be identified as production of mesons from bound and continuum states of a Schrödinger equation with a potential of the form of the perturbation itself, see Fig. 6.7. The bound states of negative energy are responsible for the characteristic features of the condensate.

Numerically, the number of non-condensed pions ranges from a few up to a dozen, and as expected is not very sensitive to the choice of the spatial and temporal form of the perturbation in the effective mass. In contrast, the condensate modes have an exponential sensitivity to the input parameters. As the abrupt changes in the effective pion mass grow in strength, a critical point is reached with the appearance of the condensate mode. The population of this mode increases dramatically from zero to thousands with a further slight change in the mass parameter. Due to this hyper-sensitivity of the number of condensed pions to the perturbation it is practically impossible to predict the effect quantitatively without specifying precisely the scenario of the process.

However, our results predict the number of non-condensate pions, thereby imposing a lower limit on the statistics needed to unambiguously detect the chiral condensate. Furthermore, we have shown that the condensate pions have a specific momentum distribution due to their common collective condensate mode. We have also shown that although the distribution over species starts from the famous $1/\sqrt{f}$ form for one mode it quickly becomes Gaussian with the appearance of successive modes. Therefore the presence of several modes complicates the detection of a chiral condensate. The number of modes present increases with energy. In addition, the mass parameter can be strongly perturbed in more than one region, each increasing

the number of modes. Tunneling and chaotic dynamics in the resulting multi-well potential might lead to another class of interesting problems.

This work can be extended in several directions. With the formalism presented here, large numerical studies of the effective pionic field in a hot medium can be conducted involving realistic and even self-consistent forms of the perturbation given by the σ field. Constraints on the perturbation of the mass parameter should be related more rigorously to observables. Further analysis of our results applied to phase transitions, zero-mass particle production, energy transfer and many other field theory problems would definitely be fruitful. We feel that this work may provide a step forward in the study and classification of field theories with parametric excitations and possibly clarify the nature of the produced squeezed states.

LIST OF REFERENCES

[1] M. Horoi, A. Volya, and V. Zelevinsky, Phys. Rev. Lett. **82** (1999) 2064.

[2] M. Horoi, A. Volya, and V. Zelevinsky, NSCL Annual Report 1997.

[3] A. Volya, S. Pratt, and V. Zelevinsky, Phys. Rev. C **59** (1999) 305.

[4] A. Volya, S. Pratt, and V. Zelevinsky, NSCL Annual Report, 1997.

[5] A. Volya, S. Pratt, and V. Zelevinsky, BAPS, **44** (1999) 257.

[6] A. Volya, K. Haglin, S. Pratt and V. Dmitriev, J. Phys. G **25** (1999) 2049.

[7] A. Volya, K. Haglin, S. Pratt and V. Dmitriev, NSCL Annual Report 1996.

[8] A. Volya, K. Haglin, S. Pratt and V. Dmitriev, BAPS, **43** (1998) 1178.

[9] A. Volya, S. Pratt, and V. Zelevinsky, Nucl. Phys. A **671** (2000) 617.

[10] A. Volya, S. Pratt, and V. Zelevinsky, NSCL Annual Report, 1999.

[11] A. Volya, S. Pratt, and V. Zelevinsky, BAPS, **44** No. 5 (1999) 38.

[12] S.T. Belyaev, Mat. Fys. Medd. Dan. Vid. Selsk. **31**, No. 11 (1959); in *Selected Topics in Nuclear Theory*, ed. F. Janouch (IAEA, Vienna, 1963) p. 291.

[13] A. Bohr and B. Mottelson, *Nuclear Structure*, Vol. II (Benjamin, New York, 1974).

[14] M. Hasegawa, S. Tazaki, Phys. Rev. C **47**, 188 (1993).

[15] A.L. Goodman, Adv. Nucl. Phys. **11**, 263 (1979).

[16] M. Barranco, S. Hernandez and R.M. Lombard, Z. Phys. **D 22**, 659 (1992).

[17] A. Bohr, B. Mottelson, *Nuclear Structure* , vol I (Benjamin, New York, 1974).

[18] D. R. Inglis, Phys. Rev. **96** (1954) 1059; Phys. Rev. **103** (1956) 1786.

[19] S.T. Belyaev. Mat. Fys. Medd. Dan. Vid. Selsk. **31** (1959) #11

[20] A.B. Migdal. Nuclear Physics **13** (1959) 655

[21] S. Belyaev, Nuclear Physics **24** (1961) 322

[22] Alex Brown, Vladimir Zelevinsky and Mihai Horoi, BAPS, **41** (1996) 854.

[23] V. Zelevinsky, *Introduction to Nuclear Theory* lecture course (Niels Bohr Institite, University of Copenhagen, 1995)

[24] J. Bardeen, L.N. Cooper and J.R. Schrieffer, Phys. Rev. **108**, 1175 (1957).

[25] B.R. Mottelson, Cours de l'Ecole d'Eté de Physique Théoretique des Houches 1958 (Dunod, Paris 1959), p. 283.

[26] G.E. Brown, *Unified Theory of Nuclear Models and Forces* (American Elsevier Publishing Co., Inc. - New York, 1971).

[27] N.N. Bogoliubov, JETP **34**, 58 (1958); Physica **26**, 1 (1960).

[28] A. K. Kerman, R. D. Lawson, Phys. Rev. **124**, 162 (1961).

[29] H. J. Lipkin, Ann. Phys. **31**, 528 (1960).

[30] Y. Nogami, Phys. Rev. **134B**, 313 (1964); Y. Nogami, I. J. Zucker, Nucl Phys. **60**, 203 (1964).

[31] S. Das Gupta and N. De Takacsy, Nucl. Phys. **A240**, 293 (1975).

[32] J. Bang and J. Krumlinde, Nucl. Phys. **A141**, 18 (1970).

[33] R. W. Richardson, Phys. Lett. **3**, 277 (1963); **5**, 82 (1963); **14**, 325 (1965).

[34] R. W. Richardson and N. Sherman, Nucl. Phys. **52**, 221 (1964).

[35] R. W. Richardson, J. Math. Phys. **6**, 1034 (1965); **18**, 1802 (1977).

[36] R. W. Richardson, Phys. Rev. **141**, 949 (1966); **144**, 874 (1966); **159**, 792 (1967).

[37] Feng Pan, J. P. Draayer, W. E. Ormand, Phys. Lett. B **422**, 1 (1998).

[38] G.D. Dang and A. Klein, Phys Rev **143** 735 (1966); Phys Rev **147** 689 (1966).

[39] G.D. Dang, R.M. Dreizler, A. Klein and C-S Wu, Phys Rev **172** 1022 (1968).

[40] S.T. Belyaev and V.G. Zelevinsky, Yad. Fiz. **16**, 1195 (1972).

[41] G. Racah, Phys. Rev. **62**, 438 (1942).

[42] B. A. Brown, Phys. Rev. C **58**, 220 (1998).

[43] E.P. Wigner, Ann. Math. **53**, 36 (1951); **62**, 548 (1955); **65**, 203 (1957); **67**, 325 (1958).

[44] F.J. Dyson, J. Math. Phys. **3**, 140, 157, 166 (1962).

[45] M.L. Mehta, *Random Matrices* (Academic Press, Boston, 1991).

[46] T.A. Brody, J. Flores, J.B. French, P.A. Mello, A. Pandey and S.S.M. Wong, Rev. Mod. Phys. **53**, 385 (1981).

[47] F. Haake, *Quantum Signatures of Chaos* (Springer, New York, 1991).

[48] *Statistical Theories of Spectra: Fluctuations*, ed. C.E. Porter (Academic Press, New York, 1965).

[49] C.M. Marcus *et al.*, Phys. Rev. Lett. **69**, 506 (1992).

[50] H.-J. Stöckmann and J. Stein, Phys. Rev. Lett. **64**, 2215 (1990); H.-D. Graf *et al.*, Phys. Rev. Lett. **69**, 1296 (1992); H. Alt *et al.*, Phys. Rev. Lett. **74**, 62 (1995).

[51] C. Ellegaard *et al.*., Phys. Rev. Lett. **75**, 1546 (1995); **77**, 4918 (1996).

[52] O. Bohigas and H.A. Weidenmüller, Annu. Rev. Nucl. Part. Sci. **38**, 421 (1988).

[53] V. Zelevinsky, Annu. Rev. Nucl. Part. Sci. **46**, 237 (1996).

[54] V.V. Flambaum, A.A. Gribakina, G.F. Gribakin and M.G. Kozlov, Phys. Rev. **A50**, 267 (1994).

[55] V. Zelevinsky, B.A. Brown, N. Frazier and M. Horoi, Phys. Rep. **276**, 85 (1996).

[56] V.G. Zelevinsky, Nucl. Phys. **A555**, 109 (1993).

[57] B. Lauritzen, P.F. Bortignon, R.A. Broglia and V.G. Zelevinsky, Phys. Rev. Lett. **74**, 5190 (1995).

[58] V.V. Flambaum, G.F. Gribakin and F.M. Izrailev, Phys. Rev. **E53**, 5729 (1996).

[59] B.A. Brown and B.H. Wildenthal, Annu. Rev. Nucl. Part. Sci. **38**, 29 (1988).

[60] G.F. Lang, C.W. Johnson, S.E. Koonin and W.E. Ormand, Phys. Rev. **C48**, 1518 (1993); S.E. Koonin, D.J. Dean and K. Langanke, Phys. Rep. **278**, 1 (1997).

[61] Y. Alhassid, D.J. Dean, S.E. Koonin, G. Lang and W.E. Ormand, Phys. Rev. Lett. **72**, 613 (1994).

[62] H. De Raedt and M. Frick, Phys. Rep. **231**, 107 (1993).

[63] M. Honma, T. Mizusaki and T. Otsuka, Phys. Rev. Lett. **77**, 3315 (1996).

[64] A. Novoselsky, M. Valliéres and O. La'adan, Phys. Rev. Lett. (1997).

[65] D. Mulhall, A. Volya, and V. Zelevinsky, LANL report nucl-th/0005014.

[66] Y.V. Fyodorov, O.A. Chubykalo, F.M. Izrailev and G. Casati, Phys. Rev. Lett. **76**, 1603 (1996).

[67] F.M. Izrailev, Phys. Rep. **196**, 299 (1990).

[68] V. Zelevinsky, M. Horoi and B.A. Brown, Phys. Lett. **B350**, 141 (1995).

[69] O.P. Sushkov and V.V. Flambaum, JETP Lett, **32**, 353 (1980); Sov. Phys. Usp. **25**, 1 (1982).

[70] H.L. Harney, A. Richter and H.A. Weidenmüller, Rev. Mod. Phys. **58**, 607 (1986).

[71] V.G. Zelevinsky, Nucl. Phys. **A553**, 125c (1993); **A570**, 411c (1994).

[72] N. Frazier, B.A. Brown and V. Zelevinsky. Phys. Rev. **C54**, 1665 (1996).

[73] C.A. Bertulani and V.G. Zelevinsky, Nucl. Phys. **A568**, 931 (1994).

[74] C.H. Lewenkopf and V.G. Zelevinsky, Nucl. Phys. **A569**, 183 (1994).

[75] J.B. French and K.F. Ratcliff, Phys. Rev. **C3**, 94 (1971).

[76] M. Horoi, B.A. Brown and V. Zelevinsky, Phys. Rev. **C50**, R2274 (1994).

[77] W.A. Richter, M.G. van der Merwe, R.E. Julies, and B.A. Brown, Nucl. Phys. **A523**, 325 (1991).

[78] G. Casati, B.V. Chirikov, I. Guarneri and F.M. Izrailev, Phys. Rev. **E48**, R1613 (1993).

[79] F. Woynarovich and H.-P. Eckle, J. Phys. **A20**, L97 (1987).

[80] D. Horn et al., Phys. Rev. Lett. **77**, 2408 (1996).

[81] Y. Le Bornec et al., Phys. Rev. Lett. **47**, 1870 (1981).

[82] M. Waters et al., Nucl. Phys. A**564**, 595 (1993).

[83] J. Miller et al., Phys. Rev. Lett. **58**, 2408 (1987).

[84] B. Erazmus et al., Phys. Rev. **C44**, 1212 (1991).

[85] P. Braun-Munzinger, P. Paul, L. Ricken, J. Stachel, P. H. Zhang, G. R. Young, F. E. Obenshain and E. Grosse, Phys. Rev. Lett. **52**, 255 (1984).

[86] T. Suzaki, et al., Phys. Lett. **B257**, 27 (1991).

[87] D. Vasak, H. Stöcker, B. Müller and W. Greiner, Phys. Lett. **93b**, 243 (1980).

[88] D. Vasak, B. Müller and W. Greiner, J. Phys. G: Nucl. Phys. **11**, 1309 (1985).

[89] G. Li, D. T. Khoa, T. Maruyama, S. W. Huang, N. Ohtsuka and A. Faessler, Nucl. Phys **A534**, 697 (1991).

[90] A. Bonasera, G. Russo and H. H. Wolter, Phys. Lett. B **246**, 337 (1990).

[91] C. Providência and D. Brink, Nucl. Phys. **A485**, 699 (1988).

[92] D. S. Koltun and A. Reitan, Phys. Rev. **141**, (1966) 1413.

[93] T. Sato, T.-S. H. Lee, F. Myhrer, and K. Kubodera, Phys. Rev. **C56**, 1246 (1997).

[94] T. Ericson and W. Weise, *Pions and Nuclei* (Clarendon Press, Oxford, 1988).

[95] E. K. Warburton and D. J. Millener, Phys. Rev. C **39**, 1120 (1989).

[96] S. Karataglidis, P. Halse, and K. Amos, Phys. Rev. C **51**, 2494 (1995).

[97] S. Karataglidis, P. J. Dortmans, K. Amos and R. de Swiniarski, Phys. Rev C **52**, 861 (1995).

[98] A. I. Baz, I. B. Zeldovich and A. M. Perelomov, *Scattering, reactions and decay in nonrelativistic quantum mechanics* (Jerusalem, Israel Program for Scientific Translations, 1969).

[99] H. De Vries et al., Atomic Data and Nuclear Data Tables, Vol **36**, 495 (1987).

[100] A. M. Sandorfi, J. R. Calarco, R. E. Rand and H. A. Schwettman, Phys. Rev. Lett. **45**, 1615 (1980).

[101] A. B. Migdal, Rev. Mod. Phys. **50**, 107 (1978).

[102] D.B. Kaplan and A.E. Nelson, Phys Lett. **B175**, 57 (1986).

[103] G.E. Brown, C-H. Lee, M. Rho and V. Thorsson, Nucl. Phys. **A567**, 1 (1994).

[104] V. Dmitriev. Nucl. Phys. **A577** 249c (1994).

[105] C. Fuchs, L.Sehn, E. Lehmann, J. Zipprich and A. Faesler LANL report, nucl-th/9610027.

[106] C. Gale and J. Kapusta, Phys. Rev. **C35**, 2107 (1987).

[107] C. L. Korpa and Scott Pratt, Phys Rev Lett. **64**, 1502 (1990).

[108] T. Ericson and W. Weise, *Pions and Nuclei*, Carendon Press Oxford (1988).

[109] L. Xia, P. J. Siemens, M. Soyeur, Nucl. Phys. **A578**, 498(1994).

[110] C.L. Korpa and R. Malfliet, Phys. Rev. C**52**, 2756 (1995).

[111] B. J. Read, Nucl. Phys. **B52**, 565 (1973).

[112] M. Jetter and H. W. Fearing, Phys. Rev. **C51**,1666 (1995).

[113] Claude Itzykson and Jean-Bernard Zuber "Quantum Field Theory", McGraw-Hill Inc.1980.

[114] M. R. Frank, K. L. Mitchell, C. D. Roberts, P. C. Tandy, Phys. Lett. B **359**, 17 (1995).

[115] L. Tiator, H. J. Weber and D. Drechsel, Nucl. Phys. **A306** , 468 (1978).

[116] H. F. Jones and M. D. Scadron, Ann. Phys. **81**,1 (1973).

[117] R. M. Davidson, Nimai C. Mukhopadhyay, and R. S. Wittman, Phys. Rev. D **43**, 71 (1991).

[118] F. de Jong, K. Nakayama, V. Herrmann and O. Scholten, Phys. Lett. **B333**, 1 (1994).

[119] H. Garcilazo and E. M. de Goya, Nucl. Phys. **A562**, 521 (1993).

[120] C. M. G. Lattes, Y. Fujimoto, and S. Hasegawa, Phys. Rep. **65** , 151 (1980).

[121] A. A. Anselm, Phys. Lett. B **217**, 169 (1989).

[122] A. A. Anselm, JETP Lett. **59**, 503 (1994).

[123] J. D. Bjorken, K. L. Kowalski, and C. C. Taylor, SLAC Report No. SLAC-PUB-6109, 1992 (unpublished).

[124] A. A. Anselm and M. G. Ryskin, Z. Phys. A **358**, 353 (1997).

[125] K. L. Kowalski, and C. C. Taylor, Case Western Reserve University Report No. CWRUTH-92-6, 1992 (unpublished).

[126] S. Pratt and V. Zelevinsky, Phys. Rev. Lett. **72**, 816 (1994).

[127] Z. Huang and M. Suzuki, Phys. Rev. D **53**, 891 (1996).

[128] Z. Huang, I. Sarcevic, and R. Thews, Phys. Rev. D **54**, 750 (1996).

[129] J. Randrup and R. Thews, Phys. Rev. D **56**, 4392 (1997).

[130] Y. Kluger, F. Cooper, E. Mottola, J.P. Paz, and A. Kovner, Nucl. Phys. A **590**, 581c (1995).

[131] F. Cooper, Y. Kluger, E. Mottola, and J. P. Paz, Phys. Rev. D **51**, 2377 (1995).

[132] M. A. Lampert and J. F. Dawson, Phys. Rev. D **54**, 2213 (1996).

[133] M. Asakawa, Z. Huang, and X. Wang, Phys. Rev. Lett. **74**, 3126 (1995).

[134] G. Amelino-Camelia, J. D. Bjorken, and S. E. Larsson, Phys. Rev. D **56**, 6942 (1997).

[135] K. Rajagopal and F. Wilczek, Nucl. Phys. B **404**, 577 (1993).

[136] D. Horn and R. Silver, Annals of Physics **66**, 509 (1971).

[137] V. Koch, International Journal of Modern Phys. E, Vol 6, No 2, 203 (1997)

[138] K. Rajagopal, *Quark-Gluon Plasma 2*, ed. R. Hwa (World Scientific, 1995).

[139] E. Henley and W. Thirring, *Elementary Quantum Field Theory* (McGraw-Hill, 1962).

[140] V. Popov and A. Perelomov, JETP **29**, 738 (1969).

[141] V. Popov and A. Perelomov, JETP **30**, 910 (1970).

[142] A. Baz, I. Zeldovich, and A. Perelomov, *Scattering, Reactions and Decays in Nonrelativistic Quantum Mechanics* (Nauka, Moscow 1971).

[143] B. R. Mollow, Phys. Rev. **162**, 1256 (1967).

[144] J-P. Blaizot and G. Ripka, *Quantum theory of finite systems* (MIT Press, Cambridge, 1986).

[145] R. J. Glauber, Phys. Rev. **131**, 2766 (1963).

[146] B. Picinbono and M. Rousseau, Phys. Rev. **A1**, 635 (1970).

[147] W-M. Zhang, D. H. Feng, and R. Gilmore, Rev. Mod. Phys. **62**, 867 (1990).

[148] C. Eckart, Phys. Rev. **35**, 1303 (1930).

[149] F. DiFilippo, V. Natarajan, K. Boyce, and D. Pritchard, Phys. Rev. Lett. **68**, 2859 (1992).

[150] J. Aliaga, G. Crespo, and A. N. Proto, Phys. Rev. Lett. **70**, 434 (1993).